

**PHOTO-CATALYTIC DEGRADATION OF DYE BY
USING RAW AND PRE-TREATED ILMENITE**

LEE RU BIN

**INSTITUTE OF GRADUATE STUDIES
UNIVERSITY OF MALAYA
KUALA LUMPUR**

2018

**PHOTO-CATALYTIC DEGRADATION OF DYE BY
USING RAW AND PRE-TREATED ILMENITE**

LEE RU BIN

**DISSERTATION SUBMITTED IN FULFILMENT OF
THE REQUIREMENTS FOR THE DEGREE OF MASTER
OF PHILOSOPHY**

**INSTITUTE OF GRADUATE STUDIES
UNIVERSITY OF MALAYA
KUALA LUMPUR**

2018

UNIVERSITY OF MALAYA
ORIGINAL LITERARY WORK DECLARATION

Name of Candidate: LEE RU BIN

Matric No: HGA140027

Name of Degree: MASTER OF PHILOSOPHY

Title of Project Paper/Research Report/Dissertation/Thesis ("this Work"):

PHOTO-CATALYTIC DEGRADATION OF DYE BY USING RAW AND PRE-TREATED ILMENITE

Field of Study: ENVIRONMENTAL ENGINEERING

I do solemnly and sincerely declare that:

- (1) I am the sole author/writer of this Work;
- (2) This Work is original;
- (3) Any use of any work in which copyright exists was done by way of fair dealing and for permitted purposes and any excerpt or extract from, or reference to or reproduction of any copyright work has been disclosed expressly and sufficiently and the title of the Work and its authorship have been acknowledged in this Work;
- (4) I do not have any actual knowledge nor do I ought reasonably to know that the making of this work constitutes an infringement of any copyright work;
- (5) I hereby assign all and every rights in the copyright to this Work to the University of Malaya ("UM"), who henceforth shall be owner of the copyright in this Work and that any reproduction or use in any form or by any means whatsoever is prohibited without the written consent of UM having been first had and obtained;
- (6) I am fully aware that if in the course of making this Work I have infringed any copyright whether intentionally or otherwise, I may be subject to legal action or any other action as may be determined by UM.

Candidate's Signature

Date:

Subscribed and solemnly declared before,

Witness's Signature

Date:

Name:

Designation:

PHOTO-CATALYTIC DEGRADATION OF DYE BY USING RAW AND PRE-TREATED ILMENITE

ABSTRACT

Ilmenite is a natural mineral ore made up of TiO_2 and iron. Most of the commercial TiO_2 products are extracted and purified from ilmenite mineral. Recently, raw ilmenite has shown a great potential to be used as photo-catalyst for degradation of a harmful dye such as Reactive Black 5. However, the high concentration of Fe ions in ilmenite become the major drawbacks for dye photo-degradation because the presence of excessive Fe ion may lead to fast electron recombination rate. Therefore, pre-treatment on the ilmenite by reducing the content of Fe has been developed to increase the effectiveness for the photo-degradation of dye. Ilmenite has been pre-treated via single step chloride leaching process by using HCl as the leaching agent in order to remove an excessive amount of Fe ions. This is because chloride leaching process generates less waste as compared to sulphate leaching process and the by-product, iron chloride (FeCl_2 and FeCl_3) can be used for iron extraction. Comprehensive studies on different parameters, such as HCl concentration, temperature, time, and calcination temperature has been conducted in order to control the specific architecture of pre-treated ilmenite. Pre-treated ilmenite with low Fe content (0.76 - 7.15 atomic% of Fe) was successfully produced through chloride leaching process. It is interesting to observe that pre-treated ilmenite demonstrated complete (100%) dye degradation within 30 min but the raw ilmenite only able to achieve 40% of dye degradation efficiency. In this study, it was demonstrated that an appropriate low amount of Fe ions in pre-treated ilmenite plays an important role as an effective dopant by decelerate the recombination centre.

Keyword: ilmenite, chloride leaching, photodegradation, RB 5

**PENGURAIAN PEWARNA SECARA PEMANGKINAN FOTO
MENGUNAKAN ILMENIT SEMULA JADI DAN SELAPAS PRA-RAWATAN**

ABSTRAK

Ilmenit merupakan mineral asli yang mengandungi TiO_2 dan besi. Kebanyakan produk TiO_2 di dalam pasaran adalah diekstrak daripada ilmenit. Baru-baru ini, kajian terbaru mendapati ilmenit mempunyai potensi untuk dijadikan mangkin foto untuk menguraikan pewarna yang berbahaya seperti "Reactive Black 5". Walaubagaimanapun, secara semulajadi ilmenit mempunyai kepekatan ion Fe yang tinggi menjadi satu kelemahan utama dalam pemangkinan foto untuk menguraikan pewarna kerana penggabungan elektron akan berlaku dengan pantas. Oleh itu, pra-rawatan terhadap ilmenit perlu dilakukan untuk meningkatkan keberkesanan sebagai mangkin foto dengan mengurangkan kandungan Fe dalam ilmenit. Pra-rawatan ilmenit dijalankan melalui proses larutan klorida dengan menggunakan HCl sebagai agen pelarut. Ini adalah kerana proses larutan klorida akan menjana sisa yang lebih sedikit berbanding dengan proses larutan sulfat dan hasil sampingan iaitu besi klorida (FeCl_2 dan FeCl_3) boleh digunakan dalam pengekstrakan besi. Kajian-kajian komprehensif terhadap parameter berlainan seperti kepekatan HCl, suhu proses larutan klorida, tempoh masa proses larutan klorida dan suhu pengkalsinan telah dilakukan untuk mengawal struktur ilmenit selepas pra-rawatan. Pra-rawatan ilmenit dengan kandungan Fe yang rendah (0.76-7.15 atomik.% Fe) telah disintesis melalui proses larutan klorida. Pra-rawatan ilmenit menunjukkan 100% pewarna telah terurai dalam masa 30 minit manakala ilmenit tanpa rawatan hanya mampu mencapai lebih kurang 40% degradasi. Dalam kajian ini, didapati kepekatan ion Fe yang rendah menjadi penyumbang utama sebagai dopen yang berkesan memperlambatkan penggabungan semula elektron.

Kata Kunci: ilmenit, larutan klorida, foto-degradasi, RB 5

ACKNOWLEDGEMENTS

First and foremost, I have to thank my research supervisors, Associate Prof. Dr. Juan Joon Ching and Dr. Lai Chin Wei. Without their assistance and dedicated involvement in every step throughout my research project, this thesis would have never been accomplished.

Secondly, I would like to express my gratitude towards University of Malaya (UM) and Nanotechnology and Catalysis Research Centre (NANOCAT) for providing me with the opportunity to fulfil my research project under a conducive research environment with sufficient facilities.

Furthermore, I would like to thank Dr. Lee Kian Mun, all the academic, technical staffs of UM and NANOCAT and my postgraduate colleagues for their help, advice and assistance throughout my research project.

Last but not least, I would like to express my sincere gratitude to my parents and friends for their continuously support and encouragement along the year in this project. This accomplishment would not have been possible without them. Thank you.

TABLE OF CONTENTS

Abstract	iii
Abstrak	iv
Acknowledgements	v
Table of Contents	vi
List of Figures	ix
List of Tables.....	xi
List of Appendices	xiv
CHAPTER 1: INTRODUCTION.....	1
1.1 Introduction.....	1
1.2 Problem Statement.....	8
1.3 Objectives of research.....	9
1.4 Outline of research work	10
1.4.1 Synthesis and characterisation of pre-treated ilmenite.....	10
1.4.2 Photo-catalytic activity of Pre-treated ilmenite.....	10
1.5 Outline of thesis.....	11
CHAPTER 2: LITERATURE REVIEW.....	12
2.1 Introduction.....	12
2.2 Dye Removal Techniques.....	13
2.2.1 Membrane filtration.....	13
2.2.2 Coagulation-flocculation	16
2.2.3 Advanced oxidation process.....	19
2.3 Ilmenite and titanium dioxide properties.....	26
2.3.1 Ilmenite properties.....	26

2.3.2	Titanium dioxide properties	29
2.4	Ilmenite metallurgical process	32
2.4.1	Commercialised Ilmenite conversion process	32
2.4.2	Sulphuric acid leaching processes	34
2.4.3	Hydrochloric acid (HCl) leaching process	38
2.5	Potential application of doped TiO ₂ photo-catalyst.....	41
CHAPTER 3: METHODOLOGY		47
3.1	Introduction.....	47
3.2	Raw materials and chemical	48
3.3	Experimental procedures	49
3.3.1	Acid leaching procedure.....	50
3.3.2	Calcination temperature	51
3.4	Photo-catalytic activity testing of raw and pre-treated ilmenite.....	51
3.5	Catalyst characterisations	53
3.5.1	X-ray Diffraction.....	54
3.5.2	Raman Spectroscopy	55
3.5.3	Photoluminescence Spectroscopy	56
3.5.4	Field Emission Scanning Electron Microscopy	57
3.5.5	X-ray Photoelectron Spectroscopy.....	58
3.5.6	UV-vis Diffuse Reflectance Spectroscopy (DR-UV-Vis).....	58
3.5.7	Nitrogen adsorption-desorption measurement	59
3.5.8	Zeta Potential.....	60
3.5.9	Elementary analysis.....	61
CHAPTER 4: RESULTS AND DISCUSSION		62
4.1	Introduction.....	62

4.2	Raw ilmenite.....	62
4.2.1	Physiochemical properties of raw ilmenite	63
4.2.2	Photo-degradation process of RB5 using raw ilmenite.....	72
4.2.2.1	Effect of pH.....	72
4.2.2.2	Inorganic ions as hydroxyl radical scavengers.....	74
4.2.2.3	Catalyst loading in RB 5 solution	76
4.3	Physicochemical properties of pre-treated ilmenite at different HCl concentration	77
4.3.1	EDX analysis.....	77
4.3.2	Raman analysis.....	78
4.3.3	XRD analysis.....	80
4.3.4	XPS analysis.....	81
4.3.5	Nitrogen absorption-desorption analysis.....	82
4.3.6	FESEM.....	84
4.3.7	DR UV-Vis analysis.....	86
4.3.8	Photoluminescence analysis.....	87
4.3.9	Zeta potential analysis.....	88
4.4	Photo-catalytic activity of pre-treated ilmenite at different HCl concentration ...	90
CHAPTER 5: CONCLUSION.....		92
5.1	Conclusion.....	92
5.2	Suggestions and Recommendations	93
References.....		95
List of Publications and Papers Presented		121
Appendix A.....		122
Appendix B.....		123
Appendix C.....		124

LIST OF FIGURES

Figure 2.1: Schematic diagram of photo-catalytic process acting on the semiconductor photo-catalyst. (Hoffmann et al., 1995)	22
Figure 2.2: Structure of FeTiO ₃ (a) ball and stick model and (b) packed octahedral model in which FeO ₆ (light colour) and TiO ₆ (dark colour) (Wilson et al., 2005).....	27
Figure 2.3: The basic unit cell structure of rutile, brookite and anatase from left to right (Esch et al., 2014).....	30
Figure 2.4: RB 5 structure.....	43
Figure 3.1: Overview of research methodology.....	48
Figure 3.2: Detailed flow chart of pre-treated Ilmenite synthesis.....	50
Figure 3.3: Annealing profile of the calcination of pre-treated Ilmenite.	51
Figure 3.4: Schematic diagram of the photo-reactor set up for photo-degradation of RB 5 dye solution.	52
Figure 4.1: XRD pattern of raw ilmenite (R: rutile TiO ₂ ; I: raw ilmenite).....	64
Figure 4.2: Raman plot of raw ilmenite. (Fe: FeO, Fe*: Fe ₂ O ₃ , I: raw ilmenite)	64
Figure 4.3: XPS survey (a) spectrum of raw ilmenite and XPS spectra of (b) Ti 2p.....	66
Figure 4.4: Zeta potential of raw ilmenite, PZC of raw ilmenite is at pH 4.5.	68
Figure 4.5: (a) N ₂ adsorption-desorption BET isotherm for raw ilmenite (b) the BJH pore size distribution (from the desorption branch of the isotherms).	69
Figure 4.6: FESEM images of the raw ilmenite: a) raw ilmenite powder; b,c) a close up on the surface of raw ilmenite powder.....	70
Figure 4.7: Proposed schematic energy level of manmade iron doping TiO ₂ . (Daghrir et al., 2013).....	71
Figure 4.8: Photoluminescence data of raw Ilmenite.....	72
Figure 4.9: Effect of dye degradation at various pH value (a) absence of raw ilmenite (b) presence of raw ilmenite. (Dye concentration 5 ppm, catalyst loading 1g/L, 25°C)	74
Figure 4.10: Kinetic rate of dye degradation of raw ilmenite in the presence of different inorganic ion at pH 2 (dye concentration 5ppm, catalyst loading 1g/L, 25 °C).....	76

Figure 4.11: Effect of dye degradation at various catalyst loading at pH 2. (Dye concentration 5 ppm, temperature 25°C)	77
Figure 4.12: Raman plot of pre-treated Ilmenite with different HCl concentration	79
Figure 4.13: XRD pattern of pre-treated ilmenite prepared by chloride leaching process: (a) H-15, (b) H-20, (c) H-25, (d) H-30, (d) H-35.....	81
Figure 4.14: XPS survey spectrum of H-25 pre-treated Ilmenite sample.....	82
Figure 4.15: Nitrogen adsorption/desorption linear isotherm for all pre-treated ilmenite sample.	84
Figure 4.16: Surface morphology at magnification of 50,000× for (a) H-15, (b) H-25 and (c) H-35	85
Figure 4.17: Changes in band gap energy of pre-treated ilmenite sample by leaching raw ilmenite with different concentration of HCl	87
Figure 4.18: Photoluminescence spectrum of H-15, H-20, H-25, H-30 and H-35 pre-treated Ilmenite samples.....	88
Figure 4.19: Zeta potential of the pre-treated ilmenite in various acid concentration. ...	89
Figure 4.20: Dye degradation (C_t/C_0) of pre-treated ilmenite treated under different HCl concentration at pH 3. (Dye concentration 5 ppm, catalyst loading 1.0 g/L, 25°C)	91

LIST OF TABLES

Table 1.1: Characteristic of wastewater and major pollutant components from each stage of the textile manufacturing industry (Arumai Dhas, 2008; Verma et al., 2012).	3
Table 1.2: Standard requirement for Standard A and B in Malaysia (National Water Services Commission, 2009).....	4
Table 1.3: Characteristics of ilmenite	8
Table 2.1: Effectiveness of membrane filtration studied by different researchers for COD reduction and colour removal of textile wastewater.	15
Table 2.2: Effectiveness of different chemical coagulants studied by different researchers for COD reduction and colour removal of textile wastewater.	17
Table 2.3: Effectiveness of different AOPs studied by different researchers for COD reduction and colour removal of textile wastewater.	23
Table 2.4: Crystal structure date of TiO ₂ . (Cromer & Herrington, 1955; Mo & Ching, 1995)	30
Table 2.5: Commercialised process of Ilmenite conversion to TiO ₂ (Zhang et al., 2011).	33
Table 2.6: Various researches on optimisation of sulphate leaching process for direct leaching and purification.....	36
Table 2.7: Various researches on optimisation of chloride leaching process for direct leaching and purification.....	40
Table 2.8: Photo-degradation of RB 5 by using TiO ₂ and doped TiO ₂	43
Table 3.1: Raw materials and chemicals used for the synthesis of pre-treated ilmenite.	49
Table 3.2: The parameters investigated on the photo-catalytic activity of raw ilmenite	53
Table 4.1: Elementary analysis of RB 5 solution at pH 2 with catalyst loading 1.0 g/L under solar irradiation for 20 min.	73
Table 4.2: EDX of pre-treated ilmenite under different HCl concentration. (Temperature: 110 °C, reaction time: 24 h)	78
Table 4.3: The binding energy of Ti and O from H-25 pre-treated ilmenite sample.....	81
Table 4.4: pore size distribution of pre-treated ilmenite sample.....	84

LIST OF SYMBOLS AND ABBREVIATIONS

Al	:	Aluminium ions
AMN	:	Ammoniacal nitrogen
AOPs	:	Advanced oxidation processes
AOX	:	Absorbable organic halides
BOD	:	Biological oxygen demand
BOD ₅	:	5 days biological oxygen demand
Cl ⁻	:	Chloride ions
COD	:	Chemical oxygen demand
CO ₂	:	Carbon dioxide
eV	:	Electron volt
Fe	:	Iron ions
Fe ²⁺	:	Ferrous ions
Fe ³⁺	:	Ferric ions
FeCl ₂	:	Iron (II) chloride
FeCl ₃	:	Iron (III) chloride
FeTiO ₃	:	Ilmenite
FeSO ₄	:	Iron sulphates
g/L	:	Gram per litre
h	:	Hour
HCl	:	Hydrochloric acid
H ₂ O ₂	:	Hydrogen peroxide
H ₂ O	:	Water molecules
HO ₂ •	:	Hydroperoxyl radicals
M	:	Molar

Mg	:	Magnesium ions
m ³	:	Cubic meter
mg/L	:	Milligram per litre
min	:	minutes
NaOCl	:	Sodium hypochlorite
nm:	:	Nano meter
OH•	:	Hydroxyl radicals
O ₂ • ⁻	:	Superoxide radicals
ppm	:	Parts per million
RB 5	:	Reactive Black 5 dye
RO•	:	Alkoxy radicals
RM	:	Ringgit Malaysia
SS	:	Suspended solids
Si	:	Silicon ions
TDS	:	Total dissolved solids
Ti	:	Titanium ions
TiO ₂	:	Titanium dioxide
TiOCl ₂	:	Titanyl chloride
TiOSO ₄	:	Titanyl sulphates
TSS	:	Total suspended solids
USD	:	United States Dollar
UV	:	Ultraviolet light
W	:	Watts
ZnO	:	Zinc oxide
°C	:	Degree Celsius
µm	:	micro meter

LIST OF APPENDICES

- Appendix A: Complete dye degradation at 2.0g/L catalyst loading at pH 2. (Dye concentration 5 ppm, temperature 25°C) 122
- Appendix B: Dye degradation (C_t/C_0) of pre-treated Ilmenite treated (a) under different exposure temperature, (b) different exposure time, and (c) different calcination temperature at pH 3. (Dye concentration 5 ppm, catalyst loading 1.0 g/L, 25°C) 123
- Appendix C: Pore size distribution of pre-treated Ilmenite under different HCl concentration. 124

University of Malaya

CHAPTER 1: INTRODUCTION

This chapter consists of the overall discussion about the rise of textile wastewater issues and the use of titania base material as photo-catalyst for textile wastewater oxidation in which the research topic is concerned. The objectives, motivations as well as the outline of the research scope are also given.

1.1 Introduction

The Industrial Revolution brought new innovations in design, manufacturing and production of clothing, revolving the landscape of textile industry forever. According to the World Trade Statistical Review 2015 done by World Trade Organisation (WTO), just in the year 2015, the world textiles and apparel exports had the total value of \$ 291 billion USD and \$ 445 billion USD, respectively (WTO, 2016). Generally, textile fibres can be classified into natural and man-made fibres. Common natural textile fibres are cotton, linen, wool and silk while man-made fibres are viscose, cellulose acetate, polyester and etc. (Bechtold et al., 2004). Nevertheless, the textile industries do not just solely involved the textile fibres but the use of dye as colouring ingredient which provide bundles of artistic and aesthetic perspective to clothing. Currently, there are around 100,000 types of available dyes existing in the market with an annual production of 0.7 to 1 million tons worldwide (Gupta, 2009). Most of the total dyes produced are used in textiles (90%) and the remaining portion is used in other sectors such as leather, paper, plastic and chemical industry (Hameed et al., 2007). The forecast for the global demand of dyes and pigments is expected to increase with an average rate of 3.5% annually, with 2.3 million tons in 2013 (Freedonia, 2009). China emerged as the largest textile fibre producing country in 2009 and continues to produce around 0.9 million tons of dye and pigments annually (Freedonia, 2009; WTO, 2016).

In Malaysia, the textile industry has contributed to the economic growth in the East Coast of Peninsular Malaysia largely due to the handmade batik industry. Man-made textiles from Malaysia have contributed to about 1.03% of the world's production. In 2015 alone, Malaysia earned RM 13.2 billion from the export of textiles and ranked as the ten largest export earner (MIDA, 2015). Textile industries are one of the biggest users of water in various textile processing stages. Textile finishing wastewater accounts for 22% of the total volume of industrial wastewater generated in Malaysia and the daily water consumption in textile industry can reach up to 3000 m³ per day (Pang & Abdullah, 2013). Huge amounts of textile wastewater, especially liquid effluent, pose significant impacts to environmental quality if it does not treated prior release.

The textile mill can be classified into two processes; dry processing mills and wet processing mills. These two processing methods generate different types of waste and wastewater (Nagaraj & Couucil, 1992). Most of the waste from dry processing mills is made up of rejected cotton. Alternatively, the wet processing mills have several main processing stages which produce various types of wastewaters including cleaning wastewater, process wastewater, non-contact cooling wastewater and storm water. Table 1.1 displays the main process in wet processing mills together with the components of major pollutants generated from their respective stage. Huge quantities with diverse chemical constituents such as acids, alkali, enzymes, starch, dyes, solvents, oils etc. are consumed in these stages during textile processing and discharged as effluent after processing. Hence, textile wastewater contains suspended solids, highly recalcitrant organic pollutants and intense colour (Al-Kdasi et al., 2004; Bisschops & Spanjers, 2003; Ledakowicz et al., 2001; Savin & Butnaru, 2008; Verma et al., 2012). Textile wastewater can be classified by measuring biological oxygen demand (BOD), chemical oxygen demand (COD), colour, total suspended solids (TSS), dissolved solids (DS), BOD/COD ratio, Kjeldahl nitrogen, etc. Typical character of raw textile wastewater can be concluded

by a COD range from 150 to 12,000 mg/L, BOD range from 80 to 6,000 mg/L, BOD/COD ratio of around 0.25, TSS between 2,900 to 3,100 mg/L, total Kjeldahl nitrogen from 70 to 80 mg/L, wide range of pH, and high intensity of colour (Arumai Dhas, 2008; Bisschops & Spanjers, 2003; Savin & Butnaru, 2008; Verma et al., 2012).

Table 1.1: Characteristic of wastewater and major pollutant components from each stage of the textile manufacturing industry (Arumai Dhas, 2008; Verma et al., 2012).

Process	Constituents	Wastewater characteristics
Sizing	Yarn waste, unused starch-based sizes	High BOD, medium COD
Desizing	Enzymes, starch, waxes, ammonia	BOD (34-50% of total), high COD, temperature (70-80 °C)
Scouring	Disinfectants and insecticides residues, NaOH, surfactants, soaps	Oily fats, BOD (30% of total), high pH, temperature (70-80 °C), dark colour
Bleaching	H ₂ O ₂ , AOX, NaOCl, organics	High pH, TDS
Mercerisation	NaOH	High BOD, high pH, suspended solids
Dyeing	Colour, metals, sulphide, salts, acidity/alkalinity, formaldehyde	High toxicity, BOD (6% of total), high dissolved solids, high pH.
Printing	Urea, solvents, colour, metals	High toxicity, high COD, high BOD, high dissolved solids, high pH, strong colour
Finishing	Chlorinated compounds, resins, spent solvents, softeners, waxes, acetate	Low alkalinity, low BOD, high toxicity

The textile industries in Malaysia usually have their own wastewater treatment plant and the treated effluents are discharged into a drain instead of a centralised treatment system. Therefore, they are bound by legislative requirements to remove immensely polluted and coloured wastewater. However, some of the discharged effluents fail to meet the discharge limits set by the government (Idris et al., 2007). According to the Environmental Quality Act 1974, the minimum requirements on sewage industrial

effluent are classified into two standards; standard A effluent for the industrial areas located at upstream regions of the water reservoir and standard B effluent for the downstream region (Department of Environment Ministry of Natural Resources and Environment, 2010). The standard A and B requirement has been summarised in Table 1.2. The textile wastewaters possess huge amounts of pollutants that are dangerous to the environment if released without proper treatment. The release of textile wastewaters could block passage of sunlight to water, prevent the aquatic plant from carrying out photosynthesis, thus disturbing the ecosystem balance (Georgiou et al., 2003; Merzouk et al., 2010). Alternatively, textile wastewater contaminates ground water systems due to wastewater leaching through the soil (Namasivayam & Sumithra, 2005).

Table 1.2: Standard requirement for Standard A and B in Malaysia (National Water Services Commission, 2009)

Parameter	Standard A [mg/l]	Standard B [mg/l]
BOD ₅	10	20
COD	60	100
SS	20	40
AMN	5	10
Nitrate nitrogen	10	20

In 1974, the Ecological and Toxicological Association of the Dyestuffs Manufacturing Industry (ETAD) found that basic dyes and diazo direct dyes (-N=N- bond in structure) are the most toxic among 4,000 dyes tested (Robinson et al., 2001). Recent researches have shown several dyes and their decomposition derivatives may induce antagonistic and synergetic toxicological effects to aquatic life and even human health (Georgiou et al., 2003; Üstün et al., 2007). Moreover, various dye classes contain heavy metals such as copper, chromium, lead, cadmium, nickel, etc. for their role as textile colourants. The release of these metals and the persistent dyes structures are genotoxic and microtoxic towards human health and the ecosystem. Several animal studies reported the consumption of dyes has carcinogenic, genotoxic, mutagenic and teratogenic properties.

For example, triphenylmethane dyes promote tumour growth in some species of fish and are cytotoxic in mammalian cells (Hameed & El-Khaiary, 2008; Jadhav et al., 2012). In addition, sporadic and excessive exposure to coloured effluents have severe effects on human health, it causes irritations to the skin, eyes, allergic dermatitis, immune suppression, leukaemia, cyanosis, quadriplegia etc. (Foo & Hameed, 2010).

Conventional biological processes do not always provide satisfactory results, specifically in industrial wastewater treatment, as many organic substances from various industries are toxic and non-biodegradable (García et al., 2001; Lapertot et al., 2006; Pulgarin & Kiwi, 1996; Steber & Wierich, 1986). Thus, combined treatment becomes a feasible option for such biologically persistent wastewater. One of the options is the use of advanced oxidation process (AOPs), which is widely recognized as a highly efficient treatment for recalcitrant wastewater. Highly reactive hydroxyl radicals ($\text{OH}\cdot$) are generated in AOPs, which are non-selective to degrade organic pollutants (Balcioglu et al., 2001; Bhatkhande et al., 2002b; Chong et al., 2010; García-Montaña et al., 2006; Gaya & Abdullah, 2008; Reddy & Kim, 2015). By applying this chemical oxidation process in pre-treatment, i.e. converting the initially persistent organic compounds into more biodegradable intermediates, which would then be treated in subsequent biological processes, could yield promising results (Haberl et al., 1991; Hu & Yu, 1994; Kearney et al., 1988; Mantzavinos et al., 1999; Parra et al., 2000; Sarria et al., 2003). An enormous amount of studies dealing with partial pre-oxidation of dye wastewater involving AOPs, have been widely reported. Few investigations carried out in past few years include a biological system coupled with AOP pre-oxidation to complete the treatment of actual or synthetic textile wastewater (Damodar & You, 2010; Liu & Chiou, 2005; Reddy & Kotaiah, 2005; You et al., 2010).

In recent years, photo-catalysis systems have attracted great interest from the science community as the most promising way to solve environmental problems, especially degrading dyes pollutants from the wastewater stream. In this manner, a photo-catalysis system is considered to be the ideal environmental solution toward realizing a green economy future. Heterogeneous photo-catalytic oxidation processes employing catalysts such as TiO_2 , ZnO , etc. and UV light has demonstrated promising results in the degradation of persistent organic pollutants by producing more biologically degradable and less toxic substances (García-Ripoll et al., 2008; García et al., 2006; Maldonado et al., 2007). This process is largely dependent on the in-situ generation of hydroxyl radicals under ambient conditions which are capable of converting a wide spectrum of toxic organic compounds including non-biodegradable substances into relatively innocuous end products such as CO_2 and H_2O . The usage of TiO_2 in wastewater treatment began during 1970 and 1980s based on Heller's research and knowledge. It turned out that TiO_2 could break down organic compounds under sunlight irradiation (Chan et al., 2011; Wold, 1993). Since then, research on applying TiO_2 in wastewater treatment has been investigated.

TiO_2 is relatively inexpensive, highly stable chemically and the photo-generated holes are highly oxidizing. However, TiO_2 effectively functions under the UV region ($\lambda < 400$ nm) and only accounts for about 4-5% of UV rays from our solar energy. Thus, the efficient use of visible light from our solar energy is essential for effectively degrading organic dye. These drawbacks cannot be overcome by only optimizing the dimensions of TiO_2 itself. Therefore, considerable efforts have been exerted to solve these drawbacks by modifying TiO_2 with the addition of electron donors (hole scavengers), carbonates salts, metal ion doping, anion doping, and dye sensitization have been investigated. Several researches have revealed that doped TiO_2 with elements managed to reduce the valence band in TiO_2 , hence reducing photon energy required to excite electrons and

produce hydroxyl radicals (Adán et al., 2014; Barakat et al., 2014; Crişan et al., 2015; Ctibor et al., 2014; Thuy et al., 2012; Wan et al., 2011). Nevertheless, these modifications of TiO₂ with potential dopants remain several challenges and drawbacks, including the expensive in production, time-consuming and harmful chemical in use. Titanium (IV) isopropoxide is the titania based chemical often used in sol gel method has the negative impact in human health and acute toxic to human and environment.

In recent years, there are also a few researches which have successfully applied a more economical method by using ilmenite (FeTiO₃) or modified ilmenite to degrade the organic compounds (Moctezuma et al., 2011; Pataquiva-Mateus et al., 2016; Tao et al., 2013). In Moctezuma et al. (2011) study, ilmenite was capable to partially break down phenol into carboxyl acid and Pataquiva-Mateus et al. (2016) study proved ilmenite has the capability to completely degrade Orange II dye solution under acidic condition. Pataquiva-Mateus et al. (2016) suggested Fe from ilmenite dissolved into the solution thus homogenous Fenton reaction occurred to assist the Orange II dye degradation. On the other hand, Tao et al. (2013) synthesised rutile TiO₂ nanorod with low Fe concentration as impurities from ilmenite. In the study, the rutile TiO₂ nanorod successfully mineralised oxalic acid and the kinetic rate of photo-degradation is better than that of commercial rutile TiO₂.

In fact, ilmenite is a natural source of low titanium content TiO₂ (usually approximately 50-60%). ilmenite mineral is relatively cheap with a record of 140-165USD/metric tonnes (Sheffield, 2017) while the market price of pure TiO₂ has reached up to 2000 USD/metric tonnes (Leanne, 2016). Its deposits can be found on all five major continents (North and South America, Africa, Euro-Asia and Australia). According to recent estimates, the world's total reserves of ilmenite exceed 680 million tonnes and are sufficient for the preparation of 350-450 million tonnes of TiO₂ (Survey, 2015). Table 1.3

summarises the physiochemical properties of ilmenite (Giaquinta & Loye, 1994; Zhou et al., 2003). Based on Table 1.3, ilmenite has the band gap energy of 2.58 – 2.9 eV which means ilmenite could be a photo-catalyst that can generate •OH radicals for pollutant oxidation under visible light irradiation theoretically. Since there are abundant reserves and relatively cheap in cost of ilmenite, hence ilmenite could be a promising heterogeneous photo-catalyst to be used in wastewater treatment plant.

Table 1.3: Characteristics of ilmenite

Physical Properties	Iron black, 2.58-2.9 eV band gap
Crystallography	Trigonal-rhombahedral
Optical Data	Uniaxial
Chemical Properties	Iron titanium oxide, FeTiO ₃

1.2 Problem Statement

The exceptional chemical and physical properties of ilmenite have been long studied by geologists. Although the use of ilmenite in photo-degradation under a specific set of environment conditions has been reported (Moctezuma et al., 2011; Pataquiva-Mateus et al., 2016), it is still far from becoming a potential candidate for photo-degradation application. This is because the high concentration of Fe in the structure remains a great challenge. In addition, poor visible light absorption and rapid recombination of charge carriers limit the widespread use of ilmenite (Zhou et al., 2005). Thus to produce high efficient pollutant oxidation system using ilmenite as an efficient photo-catalyst candidate is challenging unless several issues have pointed out are addressed.

One of the ways to improve the photo-degradation performance of ilmenite is pre-treated ilmenite through acid leaching technique to form high purity of TiO₂ with nano-meter size and high surface area properties. This is because ilmenite mineral naturally has

low surface area and large grain size. Acid leaching technique is the most feasible method due to its high efficiency to remove most of Fe ions from ilmenite in short period. Moreover, acid leaching technique is relatively simple; it has been adopted for large-scale industrial production to produce high purity of TiO₂ (Zhang et al., 2011). However, in getting the right dimensions and morphologies, a controlled synthesis procedure for the production of pre-treated ilmenite must be investigated and optimized. Therefore, in the present study, considerable efforts have been devoted to the synthesis of pre-treated ilmenite that could increase the photo-degradation performance. In this study, pre-treated ilmenite fulfils several basic requirements for better charge separation efficiency, such as low Fe concentration than that of the raw ilmenite. In this manner, conduction band electrons from pre-treated ilmenite can be injected to the band of due to the internal electrostatic field from the interpretation of inter-band state between the iron and titanium (Crişan et al., 2015; Zhou et al., 2005). Such a mechanistic understanding is very important for the controlled growth of pre-treated ilmenite structures, which has potential application not only for heterogeneous catalysis and photo-catalysis but in electronics circuits, solar cell and etc.

1.3 Objectives of research

The aims of this research are listed as follow:-

- To study the physicochemical properties of raw ilmenite.
- To identify the most influencing factor in synthesis of pre-treated ilmenite using simple chloride leaching process and to study the physicochemical properties of pre-treated ilmenite.
- To investigate the efficiency of photo-catalytic activity of pre-treated Ilmenite as compared to raw Ilmenite under artificial light irradiation by using Reactive Black 5 dye.

1.4 Outline of research work

There are three main sections in this research project overall which include the synthesis of pre-treated ilmenite, material characterisation and photo-degradation of dye. These three well-organised work scopes will be investigated carefully in order to accomplish the objectives mentioned in Section 1.3.

1.4.1 Synthesis and characterisation of pre-treated ilmenite

In this stage, pre-treated ilmenite was primarily synthesised through single chloride leaching process technique. Basically, the raw ilmenite was leached with hydrochloric acid (HCl) and then ilmenite with high purity of Ti was precipitated by hydrolysis in chloride leaching process. The acid leaching was carried out with different concentration of hydrochloric acid, exposure time, temperature and calcination temperature. The physicochemical properties of the raw and pre-treated ilmenite were been conducted with Raman spectroscopy, X-ray diffraction analysis, field emission scanning electron microscopy, Nitrogen adsorption-desorption measurement, X-ray photo-electron spectroscopy, photoluminescence spectroscopy, UV-vis diffuse reflectance spectroscopy, energy-dispersive X-ray spectroscopy, zeta potential and elementary analysis. The detailed procedures used to prepare and characterise the raw and pre-treated ilmenite are discussed in Chapter 3- Research Methodology.

1.4.2 Photo-catalytic activity of Pre-treated ilmenite

The photo-catalytic activity of raw and pre-treated ilmenite was evaluated with a custom-made photo-reactor with Xenon 150 W lamp. The performance of the raw and pre-treated ilmenite in the photo-degradation of RB 5 dyes was analysed using UV-vis spectrophotometer.

1.5 Outline of thesis

This thesis is arranged into five chapters. Chapter 1 comprises the introduction of textile wastewater in this research work, problem statement, research objectives, and outline of research work. Chapter 2 covers the technologies in textile wastewater treatment, properties of ilmenite, and ilmenite metallurgical process and photo-degradation of RB 5 dye by various catalysts. In Chapter 3, research methodology, characterisation, and photo-catalytic testing used are described. Chapter 4 presents the results and discussions of the raw and pre-treated ilmenite for photo-catalysis degradation of Reactive Black 5 dye. At last, Chapter 5 concludes the study with several suggestions and recommendations for future work.

University of Malaya

CHAPTER 2: LITERATURE REVIEW

2.1 Introduction

The rise of environmental awareness among the public has increased the urgent need of fostering new development in the area of industrial wastewater treatment. The heterogeneous photo-catalysis is one of the most promising prospects for efficient industrial wastewater treatment. To bring the heterogeneous photo-catalysis technology to the point of commercial readiness and viability in term of performance and cost, substantial research on the development of heterogeneous photo-catalysis for industrial wastewater treatment is necessary.

Recent studies have indicated that TiO_2 has emerged as the leading candidate in heterogeneous photo-catalysis because of its chemical long-term stability, widespread availability, non-toxicity and cost effective (Anpo & Kamat, 2010; Macwan et al., 2011). In order to further improve the immigration of photo-induced charge carriers, considerable effort has to be exerted to further improve the TiO_2 performance under visible light illumination because the TiO_2 can fully utilise photon in UV regions only due to its large band gap energy thus limiting its practical application for sun light irradiation. One of the methods to overcome this disadvantage is coupling foreign elements or compounds with TiO_2 because these impurities can reduce the recombination rate of the photo-induced electron-hole pairs through trapping effects of photo-generated electron (Barakat et al., 2014; Chan et al., 2011; Crişan et al., 2015; Zarazúa-Morín et al., 2016). The ilmenite contains iron oxide species as foreign compounds in TiO_2 lattice structure naturally and ilmenite is the main mineral source to produce TiO_2 , yet the relationship between raw ilmenite and pre-treated ilmenite photo-catalyst as well as their photo-catalytic performance was still a matter of debate and remains unclear. Therefore, the development of pre-treated ilmenite photo-catalyst to reduce iron oxide concentration in ilmenite using acid leaching technique remains to be determined. In the subsequent

section, the current and emerging technologies in textile wastewater treatment, physiochemical properties of TiO₂ and ilmenite, techniques adopted for ilmenite improvement and works done by various researchers with regards to the pre-treated ilmenite, the iron-doped TiO₂ and its photo-degradation on azo dyes will be reviewed in detail.

2.2 Dye Removal Techniques

Textile wastewater contains very diverse chemical composition, ranging from organic products, polymers to inorganic compounds. Many dyes have complex structure, synthetic origin and structural varieties. Thus, the conventional sewerage system failed to decolourised and treated textile dye effluent (Robinson et al., 2001). Textile wastewater treatment can be classified into 3 groups, physical, chemical and biological. In this section, the current and promising physical (membrane filtration) and chemical (coagulation and photo-catalysis) treatment in dye removal will be reviewed in detail.

2.2.1 Membrane filtration

The use of membrane filtration (MF) technology shows a physical separation between waste and water, preventing unwanted particles from passing through a specially designed filter by applied different pressure as the driving force. The typical pore size in MF is in the range of < 1 nm to 0.1 µm, thus MF can be classified into a various group such as micro filtration, nano-filtration and reverse osmosis according to the target pollutant for removal and separation. Materials to make membranes can be an organic polymer or inorganic materials such as glass, metal or ceramic. MF mostly use in aqueous fluid treatment in order to fulfil three purposes: to reject impurities, to retain and concentrate the pollutants and to permeate and purify of the target component.

In textile wastewater treatment, the first two purposes are significant as through MF, dye and other foreign substance will be retained but allowing water to pass through. Most

of the time, MF normally coupled with biological or other advanced wastewater treatment in order to meet discharge effluent standard set by each country and to reduce the burden on MF. Many researchers reported highly effective dye removal from textile wastewater by using MF. Schoeberl et al. (2005) showed that COD and colour removal from textile wastewater was 89-94% and 65-91% respectively. Brik et al. (2006) had the similar observation on COD (60-95%) and colour (46-98.5%) reduction. In contrast, studies by Deowan et al. (2013) and Yurtsever et al. (2015) did not achieve similar efficiency in colour removal when only around 20-50% of colour reduction was observed; suggesting that different sources of textile wastewater effluent would affect the colour removal efficiency since some of the stages in textile operation generated different types of pollutants. Albeit Yurtsever et al. (2016) indicated almost decolourisation was achieved; however different type of bioreactor was used in this study, indicating that the type of microorganism in bioreactor play important role in membrane bioreactor. Moreover, Yigit et al. (2009) and Deowan et al. (2016) pointed out that the dye rejection happened in membrane bioreactor are mainly due to adsorption onto biomass or on sludge, thus this suggests that the certain types of dye may pass through membrane (Deowan et al., 2016; Yigit et al., 2009). Liu et al. (2011) compared the efficiency of reverse osmosis and nano-filtration membrane in the treatment of biologically-treated textile effluent. In the study, nano-filtration has better COD removal while reverse osmosis has better salinity reduction. Table 2.1 summarises some reported MF and their respective performances. It is interesting to point out that, researches solely studying MF filtration often use influents with lower COD and does not reflect the actual problem, because, in reality, textile wastewater influent normally has higher COD concentrations. Regardless of the efficiency, MF has several main drawbacks: high cost, membrane fouling and high concentrated dyebath production which requires proper treatment before disposal. In addition, mandatory pre-treatment units for removing suspended solids in wastewater

Table 2.1: Effectiveness of membrane filtration studied by different researchers for COD reduction and colour removal of textile wastewater.

Technique	Sample	Influent COD [mg/L]	COD removal [%]	Colour removal [%]	References
Membrane bioreactor	Synthetic textile wastewater	2000	80-85	>95	(Yurtsever et al., 2016)
Membrane bioreactor	Textile wastewater	2367±125	95±1	40-55	(Deowan et al., 2016)
Membrane bioreactor	Synthetic textile wastewater	1000	97	30-50	(Yurtsever et al., 2015)
Membrane bioreactor	Synthetic textile wastewater	2500	90	20-50	(Deowan et al., 2013)
Membrane bioreactor	Textile mill wastewater	600-1200	85-92	60-75	(Huang et al., 2009)
Membrane bioreactor	Textile wastewater	1380-6033	60-95	87	(Brik et al., 2006)
Membrane bioreactor	Dye house wastewater	1606-2997	93	80.5	(Schoeberl et al., 2005)
Membrane	Synthetic textile wastewater	300	-	>99.9	(Han et al., 2016)
Membrane	Synthetic textile wastewater	100-1000	80-90	-	(Ong et al., 2014)
Membrane	Synthetic textile wastewater	50	98	92-98	(Patel et al., 2012)
Membrane	Textile wastewater	708	80-100	>90	(Aouni et al., 2012)
Membrane	Textile wastewater	96-108	97	100	(Liu et al., 2011)

is required in order to prolong the life time of the membranes. (Akbari et al., 2006; Robinson et al., 2001).

2.2.2 Coagulation-flocculation

Colloidal particles, whether dissolved or suspended solids in wastewater, tend to sink and form a sludge, or not at all depending on the particles' surface electrical charges that either mutually attracts or repels each other. The addition of chemical coagulation and flocculation in wastewater would change the physical state of colloidal particles, neutralise the surface electrical charges of colloidal particles, cause the particles to agglomerate together to form floc and will be removed from wastewater through the sedimentation process. Chemical coagulation is a complicated phenomenon, involving different inter-related parameters, thus it is arduous to determine how well coagulation will work under pre-determined conditions. Common chemical coagulants include hydrolysing metallic salts such as calcium hydroxide/lime (Ca(OH)_2), aluminium sulphate/alum ($\text{Al(SO}_4)_3$), ferric chloride (FeCl_3) and ferrous sulphate ($\text{Fe}_2(\text{SO}_4)_3$) whereas polymers are used as flocculants (Annadurai et al., 2004; Semerjian and Ayoub, 2003). Various researches on coagulation and flocculation in textile wastewater treatment have been summarised in Table 2.2.

Tan et al. (2000) compared the colour removal efficiency between alum, magnesium chloride (MgCl_2) and poly-aluminium chloride (PACl). The result showed that MgCl_2 had the shortest settling times with the 88.40% of COD reduction and 97.90% of colour removal under the pH range from 10.5 to 11.0. Similar results were also reflected in Gao et al. (2007) and El-Gohary et al. (2009) work with comparable colour removal efficiency under mild alkaline conditions. Alternatively, Jiang et al. (1998) pointed out that pre-hydrolysed metallic salts, for example, poly-aluminium chloride (PACl), poly-ferric chloride (PFCl), poly-ferrous sulphate (PFS) and poly-aluminium sulphate (PAS)

Table 2.2: Effectiveness of different chemical coagulants studied by different researchers for COD reduction and colour removal of textile wastewater.

Coagulants	Sample	Influent COD [mg/L]	COD removal [%]	Colour removal [%]	References
Various inorganic salt	Synthetic dye wastewater	-	-	>95	(Han et al., 2016)
Aluminium sulphate	Textile wastewater	963	-	-	(Aquino et al., 2016)
Commercial coagulant (SICOAG C-21)	Textile wastewater	-	-	95.6	(López-López et al., 2016)
Zinc chloride	Textile wastewater	-	92±1.22	98±0.88	(Kadam et al., 2015)
Poly-aluminium chloride (PACl)	Multiple dye wastewater	1000	-	80	(Liang et al., 2014)
Ferrous sulphate	Synthetic dye wastewater	350-828	28.3-45.4	91.4-93.8	(Rodrigues et al., 2013)
Aluminium electrode	Textile wastewater	1357	85	80	(Merzouk et al., 2011)
Aluminium electrode	Synthetic dye wastewater	50	83	100	(Dalvand et al., 2011)
Iron electrode	Synthetic dye wastewater	-	-	98.1	(Chafi et al., 2011)
Magnesium chloride and alum	Textile wastewater	595±131	40-50	100	(El-Gohary & Tawfik, 2009)
Magnesium chloride and hydrated lime	Synthetic dye wastewater	-	-	98	(Gao et al., 2007)
Poly-aluminium chloride (PACl)	Textile wastewater	-	-	99.9	(Choo et al., 2007)
Magnesium chloride	Industrial dye wastewater	2040-3190	88.4	97.9	(Tan et al., 2000)

demonstrated better effectiveness than hydrolysed metallic salts (Jiang & Graham, 1998). In addition, Gregory et al. (2001) compared the effectiveness of various pre-hydrolysed coagulants for the treatment of wastewater and showed PACl had rapid flocculation and formed stronger flocs than that of alum at the equivalent dosage (Gregory and Rossi, 2001). This observation suggested that these pre-hydrolysed coagulants are pre-neutralised, reducing the effect of water pH on the coagulants and hence reducing the need of pH correction in the influent.

Another approach in coagulation and flocculation method is electro-coagulation. This technique uses a direct current source between metal electrodes which immersed in the solution, leading to the dissolution of metal electrodes into the solution as metal ions. These dissolved metal ions form as coagulated species and metal hydroxides under suitable pH condition, causing particle destabilisation and aggregation. Aluminium and iron are normally used as metal electrodes in electro-coagulation. Chafi et al. (2011) compared the effectiveness between iron and aluminium electrodes to remove a highly soluble acid dye. In the result, iron electrodes have better decolourisation yield than aluminium electrodes. Additionally, aluminium electrodes required higher current supplied to achieve similar decolourisation yield as iron electrodes. Chafi et al. suggested Al and Fe adopted different decolourisation mechanism to remove the acid dye.

The coagulation-flocculation process has been used as main treatment or pre-treatment due to its low capital cost (Anjaneyulu et al., 2005), but this technique generates a high volume of sludge which is harmful and highly toxic to the environment, therefore subsequent treatment is required in order to reduce the toxicity of sludge before disposal.

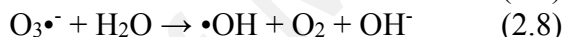
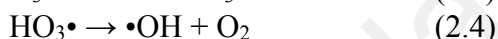
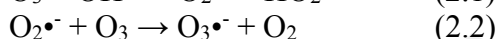
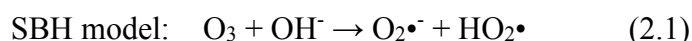
2.2.3 Advanced oxidation process

Advanced oxidation processes (AOPs) have gained attention from researchers in the research and development of wastewater treatment technologies because AOPs show excellent results in the removal or degradation of recalcitrant pollutants into biodegradable compounds that can subsequently be treated by conventional or biological treatment (Anjaneyulu et al., 2005; Lai et al., 2014). For example, Yanagisawa et al. (2008) reported that AOPs breakup the recalcitrant triazinic ring of cyanuric acid shows that AOPs has high efficient in destroying recalcitrant pollutants.

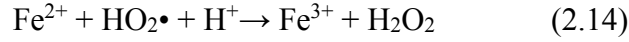
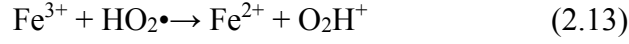
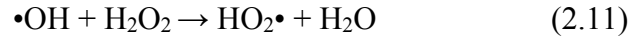
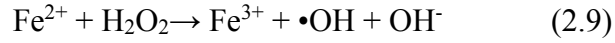
The efficacy of AOPs relies on the generation of reactive free radicals such as superoxide radical ($O_2^{\bullet-}$), hydroperoxyl radical (HO_2^{\bullet}), hydroxyl radical ($\bullet OH$) and alkoxy radical (RO^{\bullet}). These free radical species are atoms or molecules that possess one or more unpaired electrons. The $\bullet OH$ is the focus in AOPs for wastewater treatment due to its high standard potentials of 2.8 V, thus it is highly reactive and non-selective in oxidizing and decomposing numerous hazardous compounds to carbon dioxide and inorganic ions (Chong et al., 2010; Esplugas et al., 2002; Herrmann, 2010; Pera-Titus et al., 2004; Reddy & Kim, 2015). Common AOPs used to treat wastewater include ozone oxidation, Fenton process and photo-catalysis.

Ozone has standard reduction potentials of 2.07 V in acidic solution and 1.25 V in basic solution. Consequentially, the pH of the solution determines the oxidation mechanism of ozone because pH can affect the kinetics and pathways of the reaction (Hoigne & Bader, 1975; Hoigne & Bader, 1979; Pera-Titus et al., 2004; Wang & Xu, 2012). Direct ozonation is the predominant reaction pathway under acidic conditions whereas the indirect pathway prevails under basic conditions (Agustina et al., 2005; Pera-Titus et al., 2004). Two mechanisms of ozone oxidation have been proposed depending on the pH region; Staehelin-Bühler-Hoigné (SBH) model in neutral pH region and

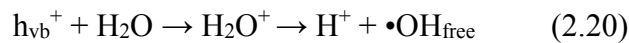
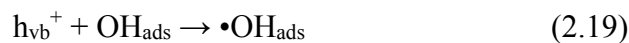
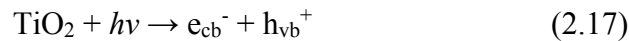
Tomiyasu-Fukutomi-Gordon (TFG) model for a higher pH range (Buehler et al., 1984; Nemes et al., 2000; Staehelin & Hoigne, 1985). Both models suggest that the decomposition of O₃ with hydroxide in water to produce •OH but TFG model corresponds to an oxygen atom transfer reaction at the beginning (Eq. 2.5). This phenomenon could associate with the hydroxide concentration in the solution since TFG model occurs under higher pH condition.



Homogeneous Fenton process is a number of cyclic reactions, whereby ferrous to ferric ions oxidation occurred to catalyse the decomposition of H₂O₂ to hydroxyl radicals in acidic medium (Eq. 2.9). Alternatively, Fe³⁺ ions reduced by excess H₂O₂ to regenerate back to Fe²⁺ ions and more radicals (Eq. 2.10). This reaction is called Fenton-like reaction but the reaction has slower reaction rate compare with Fenton process (Deng and Englehardt, 2006; Neyens and Baeyens, 2003). Besides that, the regeneration of Fe²⁺ happens when Fe³⁺ reacts with HO₂• (Eq. 2.13). (Brillas & Martínez-Huitle, 2015; Deng & Englehardt, 2006; Haber & Weiss, 1934; Nidheesh, 2015). Radical-radical reactions are reported to occur during the Fenton process as well (Eq. 2.11 & 2.15). Excess H₂O₂ will be decomposed to molecular oxygen and water when the absence of any organic molecule to be oxidised (Eq. 2.16). Equations 2.9 – 2.15 demonstrate the classical Fenton free radical mechanism in the absence of organic compounds (Brillas et al., 2009; Haber & Weiss, 1934; Kang et al., 2002b; Neyens & Baeyens, 2003).



In the heterogeneous photo-catalytic process, TiO_2 is the most widely studied semiconductor catalyst, and the $\bullet\text{OH}$ generation mechanisms of TiO_2 has been discussed extensively in literature (Chan et al., 2011; Daghrir et al., 2013; Habisreutinger et al., 2013; Low et al., 2012; Ni et al., 2007; Yu et al., 2010; Yu et al., 2014). Figure 2.1 displays the proposed photo-induced process acting on the TiO_2 under light irradiation. Electrons (e_{cb}^-) in TiO_2 are excited from the valence band into the conduction band when the absorbed irradiation energy ($h\nu$) is enough to overcome the band gap energy, leaving electron-deficient sites (“holes”) (h_{vb}^+) behind. The photo-generated holes react with surface adsorbed hydroxyl groups or water to form adsorbed $\bullet\text{OH}$ radicals ($\bullet\text{OH}_{ads}$), then the adsorbed $\bullet\text{OH}$ radicals leave the surface into solution to form free $\bullet\text{OH}$ radicals ($\bullet\text{OH}_{free}$) (Bhatkhande et al., 2002a; Chen et al., 2005; Hoffmann et al., 1995; L. Yang et al., 2008).



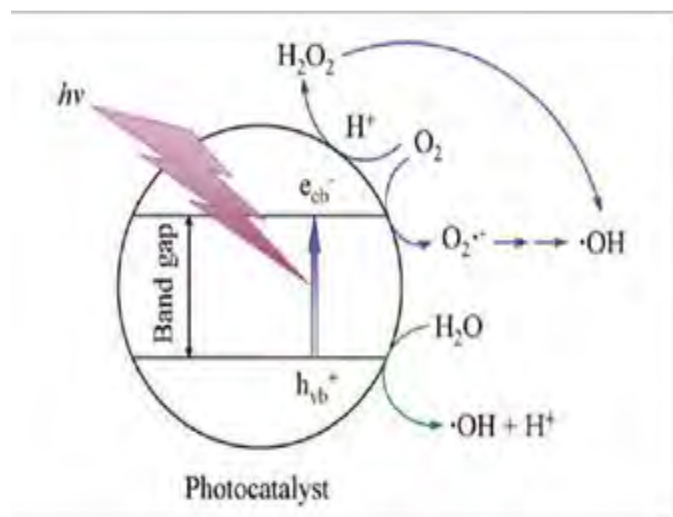


Figure 2.1: Schematic diagram of photo-catalytic process acting on the semiconductor photo-catalyst. (Hoffmann et al., 1995)

There are various reports on the degradation of the simulated textile mixture and real textile wastewater from industries using AOPs. Table 2.3 summarises some of the reported AOPs and their performance. Tehrani-Bagha et al. (2010) observed that ozone oxidation was able to achieve 100 % of colour removal of C.1. Reactive Blue 19, which is a persistent anthraquinone-based organic dye in less than 60 min. Qi et al. (2011) used ozone as pre-treatment for the secondary effluent from textile industry treatment plant before introduced into biological treatment. In the study, the integration of ozone and biological aerated filter (BAF) treatment had higher COD and colour removal than the separation of treatment. In addition, ozone did not impose any significant impact on the microorganism population in the BAF, but enhanced the efficiency of the biochemical treatment. Mezzanotte et al. (2013) pointed out that although ozone demonstrated high colour removal efficiency, however, the concentration of carbonyl by-product increased at the same time. The increasing concentration of carbonyl by-product can be related with the destruction of the aromatic ring by ozone, causing a ring opening and lead to a formation of carbonyl by-product.

Table 2.3: Effectiveness of different AOPs studied by different researchers for COD reduction and colour removal of textile wastewater.

Method	Sample	Influent COD [mg/L]	COD removal [%]	Colour removal [%]	References
Ozone oxidation	Textile wastewater	70 ± 30	-	100	(Mezzanotte et al., 2013)
Ozone oxidation	Synthetic dye wastewater	400	64.96	100	(Turhan et al., 2012)
Ozone oxidation	Textile wastewater	55-147.7	56.9	87.5	(Qi et al., 2011)
Ozone oxidation	Synthetic dye wastewater	800	55	100	(Tehrani-Bagha et al., 2010)
Fenton process	Textile wastewater	450	50	-	(GilPavas et al., 2017)
Fenton process	Textile wastewater	1132.6 ± 2.5	28	92.5	(Hayat et al., 2015)
Fenton process	Textile wastewater	2100	70	-	(Blanco et al., 2012)
Fenton process	Textile wastewater	564	91	100	(Karthikeyan et al., 2011)
Photo-catalysis	Textile wastewater	1125 ± 70	53	88	(Deveci et al., 2016)
Photo-catalysis	Textile wastewater	558.5 ± 5.05	70	97	(Souza et al., 2016)
Photo-catalysis	Textile wastewater	9500-11000	94	-	(Meenatchisundaram et al., 2014)
Photo-catalysis	Synthetic textile wastewater	-	-	70	(Rao et al., 2012)

Blanco et al. (2012) compared between Fenton and biological-Fenton coupled processes for textile wastewater treatment. The result showed that the stand-alone Fenton process achieved 70% COD removal, whereas the coupled process reached an increased COD removal of 86%. The biological-Fenton process was able to achieve the desired treatment goals using a reduced dosage of hydrogen peroxide and iron ions thus this suggested that introduction of biological treatment in AOPs could reduce chemical dosage and cost requirement for photo-degradation. Karthikeyan et al. (2011) coupled homogeneous and heterogeneous Fenton oxidation processes to treat textile wastewater. In this research, the homogenous Fenton process only substantially reduced the colour intensity of the textile wastewater whereas the coupled homogeneous and heterogeneous Fenton process achieved complete colour removal. The complete removal of colour in coupled Fenton process indicated the aromatic compounds and chromophoretic groups found in dye compounds were more effectively destroyed by hetero-catalytic oxidation since similar observation was not reflected in solely homogeneous Fenton process. In addition, Manenti et al. (2014) reported that photo-Fenton process improved the biodegradability index of textile wastewater for subsequent biological.

In the study of photo-catalyst in textile wastewater treatment, Deveci et al. (2016) proposed the integrated process of fungal membrane bioreactor and photo-catalytic membrane reactor for the treatment of industrial textile wastewater. ZnO and TiO₂ were chosen as photo-catalyst in the research and the photo-catalytic degradation of TiO₂ alone achieved 88% colour removal and 53% COD reduction efficiencies. By employing the proposed integrated system with TiO₂, 93% of colour and 99% of COD removal were observed since fungal biodegradation process cannot remove colour effectively. Deveci et al. pointed out TiO₂ has better efficiencies than that of ZnO for both colour and COD removal. A similar observation was reflected in Souza et al. (2016) study which compared the photo-catalytic activity of TiO₂, ZnO and niobium pentoxide (Nb₂O₅) in the photo-

degradation of textile wastewater (Lee et al., 2016). Commercial TiO₂ has the best photo-degradation efficiency with 97% colour removal and 70% COD reduction. This is because TiO₂ can perform well on wide range of pH whereas ZnO has good photo-catalytic activity under acidic environment. Rao et al. (2012) set up a TiO₂ coated pebble bed photo-catalytic reactor and evaluated the reactor efficiency for the decolourisation of selected reactive dye solution as well as synthetic dye house effluents. 70% of colour removal was accomplished for the photo-degradation of synthetic dye house effluents under sunlight irradiation. In addition, Meenatchisundaram et al. (2014) used TiO₂ as pre-treatment prior biodegradation treatment and observed 94% of COD removal efficiency whereas ozonation has 82% COD removal efficiency. Better biodegradation efficiency was recorded by using TiO₂ could be suggested that the adsorption of dye compounds on TiO₂ allowed •OH easily to oxidise adsorbed dye compounds.

Among ozonation, Fenton process and photo-catalysis, photo-catalysis has the best choice because TiO₂ has a wider range of pH stability in the term to generate •OH radicals whereas the Fenton process requires adjustment of pH of the effluent to the acidic condition prior the process and create high iron concentration sludge. Besides that, the ozonation process involves high installation, energy cost and short life span but photo-catalysis could fully utilise sunlight to treat the effluent. However, there are some problems that need to be solved before fully integrating the photo-catalysis process into a system, such as difficulties of separating the photo-catalyst from the treated effluent and narrowing the band gap energy of the semiconductor photo-catalyst since pure TiO₂ has high band gap energy thus it can only fully utilise photon in UV region.

2.3 Ilmenite and titanium dioxide properties

2.3.1 Ilmenite properties

Ilmenite is a black or steel-grey coloured mineral composed of titanium-iron oxide, FeTiO_3 , with weakly magnetic properties. Scientists have studied the magnetic behaviour of ilmenite for the interpretation of historical fluctuations in the Earth's magnetic field as rocks containing it displays self-reserved magnetisation (Robinson et al., 2002). An ionic or semi-ionic crystal made up of the ABO_3 composition has a tendency to adopt either one from two forms, perovskite form (high coordination if ionic packing is allowed) or sesquioxide structure (lower coordination). Figure 2.2 shows the common sesquioxide structures and the lithium niobate structures as these two structures are based on the higher symmetry corundum (B_2O_3) structure. In the corundum structure, the anion lattice is closely packed with cations in a hexagonal structure, occupying two-thirds of the available octahedral interstices such that the octahedral of AO_6 share edges in (001) planes in a honeycomb arrangement; the octahedral faces share atoms between adjacent planes. Ilmenite has two types of metal ions in the composition, and are arranged in alternating bilayers perpendicular to the c axis, -Fe-Ti-O-Ti-Fe- has arranged along the threefold axes, causing a reduction in the $\bar{R}3$ symmetry. Figure 2.2 shows that the Fe and Ti ions are arranged with O ions in octahedral form with three octahedral edges shared between cation octahedrals of the same type. Each octahedral cation site overlaps one octahedral face with a cation of the other type in an adjacent bilayer and at the same time, the opposite face is overlapped with an empty octahedral site. Ilmenite has two formula units in the crystallographic cell with ions at $\pm (0, 0, \text{Fe}_z)$, Ti ions at $\pm (0, 0, \text{Ti}_z)$ and oxygen ions at $\pm (\text{O}_x, \text{O}_y, \text{O}_z; -\text{O}_y, \text{O}_x - \text{O}_y, \text{O}_z; \text{O}_y - \text{O}_x, -\text{O}_x, \text{O}_z)$. On the other hand, the lithium niobate form of ilmenite differs by having mixed Fe Ti bilayers and a threefold axis ordering of -Fe-Ti-O-Ti-Fe-. As FeTiO_3 mostly formed under earth crust and in lava, thus the temperature and pressure affect the adoption of ilmenite, lithium niobate or

perovskite structures of FeTiO_3 in order to be the stable phase at ambient pressure (Wilson et al., 2005).

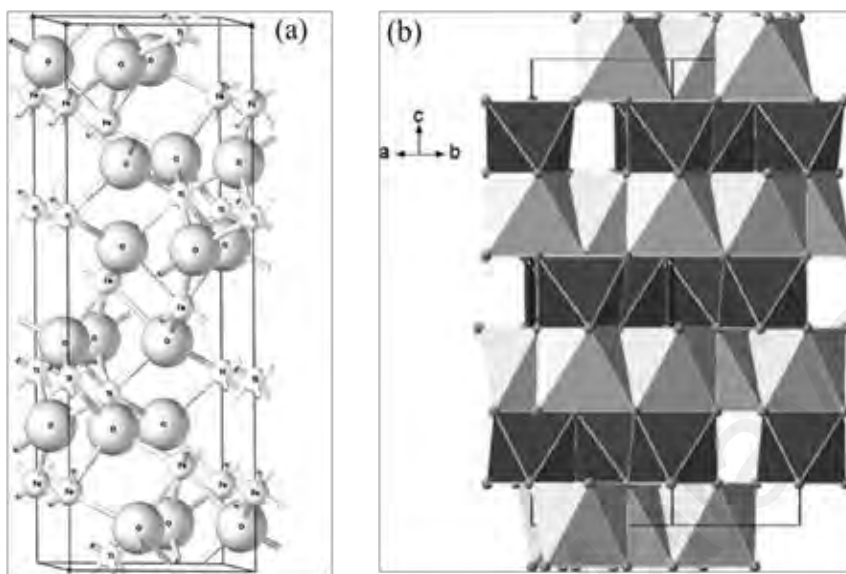


Figure 2.2: Structure of FeTiO_3 (a) ball and stick model and (b) packed octahedral model in which FeO_6 (light colour) and TiO_6 (dark colour) (Wilson et al., 2005).

The electronic properties of ilmenite have been actively investigated. For instance, Tao et al. (2011) investigated the potential of ilmenite minerals in the application of supercapacitors by modifying the morphology of ilmenite, reporting that the capacitance of ilmenite nano-flowers was 122 ± 14.5 F/g. In addition, the untreated ilmenite has the similar binding energy of the Fe $2p_{3/2}$ peaks with milled ilmenite (about 711.0 ± 0.2 eV), with a clear shake up satellite structure of Fe 2p core-level, a broad peak of O 1s and a sharp Ti 2p structure in XPS spectra of ilmenite, FeTiO_3 (Tao et al., 2011). When the Fe concentration is low in the iron titanate catalyst, the Fe 2p has the highest binding energy as titanium species has the inductive effect towards iron species, thus the electron cloud surrounding the Fe species has the severest deviation. As the Fe concentration increases, the binding energy of Ti 2p shifted towards the low energy direction, suggesting that the titanium species “pull” the electron cloud of iron species closer (Yu et al., 2009). FeTiO_3 has two distinct cation charge orderings consistent with O^{2-} anions, which are $\text{Fe}^{2+}\text{Ti}^{4+}$ and $\text{Fe}^{3+}\text{Ti}^{3+}$, thereby the local electronic configuration of the Fe^{2+} and Fe^{3+} states are d^6

and d^5 respectively. The charge transfer excitation between the above-mentioned two states is well known and has been studied in a number of Fe and Ti-bearing minerals (Sherman, 1987). Wilson et al. studied the electronic and the magnetic structure of ilmenite by using two most common treatment of electronic exchange and correlation to test ilmenite, which were Hartree-Fock (HF) and modified form of Becke's three parameter hybrid functional (B3LYP) theory. In the study, the HF approximation showed that the $Fe^{3+}Ti^{3+}$ state was found to be more stable than the $Fe^{2+}Ti^{4+}$ state, as Fe^{3+} possessed five unpaired electrons whereas Fe^{2+} has a doubly-occupied dz^2 orbital. The valence band of ilmenite is composed of O 2p and Fe 3d states while the conduction bands arise from the contribution of O 2p, Ti 3d and Fe 3d orbitals (Chen et al., 2013; Wilson et al., 2005).

The band gap of ilmenite measured by electrochemical measurements was reported to be between the values of 2.58 and 2.9 eV (Butler & Ginley, 1977; Ginley & Butler, 1977). Strens et al. (1979) measured the diffuse reflectance spectra of ilmenite and showed the absorption peaks of ilmenite at energies of about 1, 2.5 and 4 eV. The 1 eV transition was attributed to a $t2g-eg$ transition of octahedral Fe^{2+} , the 2.5 eV transition was attributed to a $Fe^{2+}-Ti^{4+}$ charge transfer and 4 eV transition attributed to an O-Ti charge transfer (Strens & Wood, 1979). However, the diffuse reflectance spectra measured by Strens et al. (1979) did not provide definitive measurements of band gaps.

Despite the abundance of ilmenite, only a handful of studies on the photo-catalytic activity of ilmenite has been reported. Moctezuma et al. (2011) mixed ilmenite with commercial TiO_2 powder to test the photo-degradation efficiency of phenol. In the research, ilmenite showed the capability to breakdown phenol into carboxylic acid and ilmenite accelerated the dispersed TiO_2 settling time (Moctezuma et al., 2011). Pataquiva-Mateus et al. (2016) showed that ilmenite has high photo-catalytic activity under acidic condition and achieved more than 95% dye removal efficiency.

2.3.2 Titanium dioxide properties

Titanium dioxide (TiO_2) is the naturally occurring oxide of titanium and exists as white in colour. It can be found in ilmenite and rutile mineral ore. Its unique characteristics such as non-toxicity, strong photo-catalytic activity, easy handling and stability against corrosion have attracted numerous studies in various application (Chen & Mao, 2007; Lai et al., 2015; Wold, 1993). TiO_2 has three crystalline polymorphs: rutile, anatase and brookite. Figure 2.3 shows the basic unit-cell structure of these three phases (Esch et al., 2014). Rutile and anatase TiO_2 have a tetragonal crystal structure, with 6 and 12 atoms per unit cell respectively. In both crystalline unit cells, each Ti atom is coordinated to 6 O atoms and each O atom is bonded to 3 Ti atoms. Both rutile and anatase have slight distortion in the TiO_6 octahedron where by two Ti-O bonds are slightly greater than the other four bonds, with some of the O-Ti-O bond angles are deviating from 90° . The distortion was found to be greater in anatase than rutile crystal structure. Brookite TiO_2 has a more complicated crystal structure, containing 8 O atoms and 16 Ti atoms in the orthorhombic cell. In spite of that, brookite has similar interatomic distance and the O-Ti-O bond angles with rutile and anatase. Yet, brookite has 6 different Ti-O bonds ranging from 1.87 to 2.04 Å, a significant distinction between brookite and another 2 crystalline polymorphs. In addition, brookite has 12 different O-Ti-O bonds with angles ranging from 77° to 105° whereas rutile and anatase have only two kind of Ti-O bonds and O-Ti-O bond angles (Landmann et al., 2012; Mo & Ching, 1995; Reyes-Coronado et al., 2008). A detailed crystal structure data of TiO_2 has been summarised in Table 2.4.

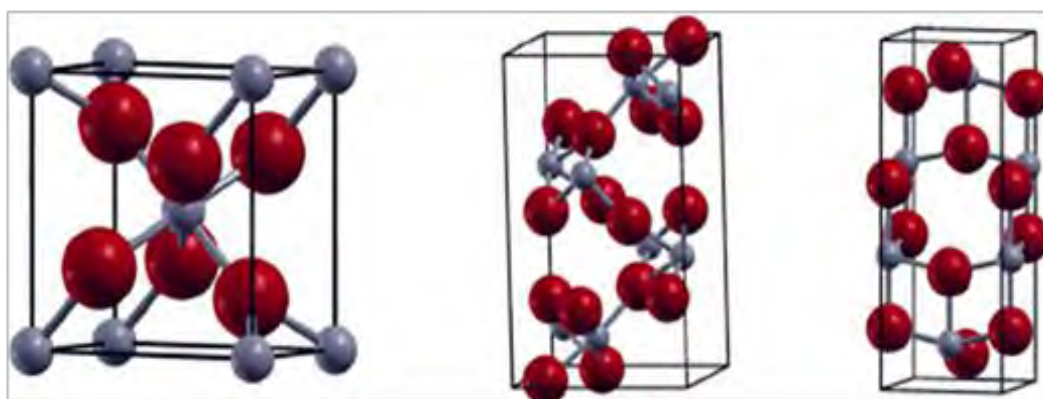


Figure 2.3: The basic unit cell structure of rutile, brookite and anatase from left to right (Esch et al., 2014).

Table 2.4: Crystal structure data of TiO₂. (Cromer & Herrington, 1955; Mo & Ching, 1995)

	Rutile	Anatase	Brookite
Crystal structure	Tetragonal	Tetragonal	Orthorhombic
Lattice constants (Å)	a= 4.5936 c= 2.9587	a= 3.784 c= 9.515	a= 9.184 b= 5.447 c= 5.145
Density (g/cm ³)	4.13	3.79	3.99
Ti-O bond length (Å)	1.949 (4) 1.980 (2)	1.937 (4) 1.965 (2)	1.87~2.04
O-Ti-O bond angle	81.2° 90.0°	77.7° 92.6°	77.0°~105°

The electronic properties of TiO₂ are as follows. The valence band of TiO₂ is made up of 2p orbitals of oxygen hybridised with 3d orbitals of titanium, with the sigma (σ) bonding higher than the pi (π) bonding in the valence band as the sigma bonding state of oxygen is located at lower energy region (Zallen & Moret, 2006). On the other hand, the π bonding state and ρ_{π} bonding state is in the middle and higher energy region of the valence band respectively (Chen & Mao, 2007). 3d orbitals of titanium occupy the conduction band and can be separated into two components, t_{2g} and e_g . The t_{2g} can be divided into three states, d_{yz} , d_{zx} , and d_{xy} . As the d_{xy} is located at the bottom of conduction band, thus anatase has metal-metal interaction distance of 5.35Å whereas 2.96Å in rutile (Hanaor and Sorrell, 2011).

TiO₂ has 3 different band gaps according to its crystalline structure: 3.05 eV in rutile phase, 3.23 eV in anatase phase and 3.26 eV in brookite phase (Lee & Yang, 2011; Reyes-Coronado et al., 2008). Optical absorption measurement shows the rutile and anatase phases are transparent in the visible region (Zallen & Moret, 2006). Anatase has higher band gap energy as the crystal momentum restrict the electron transition between the valence and conduction bands, thus anatase has only 1 indirect band gap (Asahi et al., 2000; Kavan et al., 1996). On the other hand, many researchers have proven that rutile has one direct band gap of 3.05 eV and one indirect band gap of 3.10 eV (Valencia et al., 2010). No consensus has been achieved on whether direct or indirect transitions dominate the optical response in brookite (Koelsch et al., 2004; Li et al., 2007b).

Anatase and brookite are metastable whereas rutile is the most thermodynamically stable phase among three crystalline phase due to its lower free energy properties (Hanaor & Sorrell, 2011). Therefore anatase and brookite will be transformed to rutile under higher temperature and pressure condition (Lee & Yang, 2011; Wang et al., 2014). Such thermodynamic properties cause the TiO₂ mineral ore is mostly in rutile phase due to high pressure and temperature such as molten lava environment, which will transform the TiO₂ in mineral ore into rutile phase. In this study, the pre-treated ilmenite extracts from raw ilmenite also has rutile phase properties.

2.4 Ilmenite metallurgical process

2.4.1 Commercialised ilmenite conversion process

The conversion of ilmenite to synthetic rutile or high grade titanium slag has several commercialised or proposed processes in order to produce high purity of TiO_2 as ilmenite is the main mineral ore for TiO_2 . These commercialised processes are Becher process, Benelite process, Mursco process, Laporte process, Kataoka process (in Japan) and Dunn process. These processes are a combination of thermal oxidation and reduction through roasting, leaching and physical separation steps. In these steps, iron in ilmenite is reduced at high temperature (800 – 1200 °C), converting it from insoluble iron to soluble ferrous or elemental forms, followed by acid leaching to remove iron in ilmenite in order to obtain synthetic rutile TiO_2 products. The details and comparison of these commercialised processes characteristic are summarised in Table 2.5. Current commercialised processes require high amounts of energy to convert ilmenite to synthetic rutile and generate a huge amount of waste, thus direct leaching-purification processes have been developed to obtain TiO_2 .

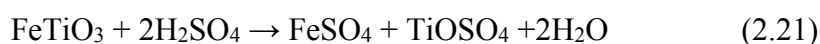
Table 2.5: Commercialised process of Ilmenite conversion to TiO₂ (Zhang et al., 2011).

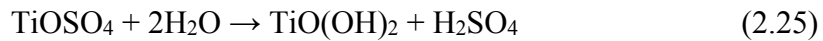
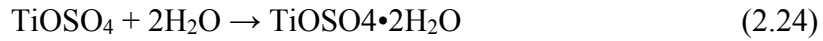
Process	Thermo-conversion treatment	Leaching	Advantage	Disadvantage
Becher	Iron oxidized to pseudobrookite and reduced to metallic Fe at 1200°C	(1) NH ₄ Cl/O ₂ (2) 0.5M H ₂ SO ₄	Diverse Ilmenite ores can be as feedstock	Require multiple steps for iron conversion and leaching, High emission of CO ₂ and energy demand.
Benelite	Iron convert into Fe(II) in carbon thermo-reduction	18-20% HCl	One step conversion of iron	A higher requirement for ilmenite as feedstock.
Murso	Equivalent to Becher process but fluidised beds are used entire process	20% HCl	Better efficiency and easier HCl recycle	Require multiple steps for iron conversion and leaching, High emission of CO ₂ and energy demand.
Laporte	The lower temperature required for iron conversion under controlled CO ₂ pressure.	18% HCl with a bed contractor.	No fine TiO ₂ particle formation. High FeO removal efficiency.	Require multiple steps for iron conversion and leaching. High emission of CO ₂ .
Kataoka (in Japan)	Iron to ferrous iron conversion	H ₂ SO ₄	Low leaching temperature and low corrosive of acid used.	Generate large quantity of iron sulphate wastes.
Austpac	Ilmenite magnetization at 800-1000°C	25% (w/w) HCl	Higher purity (>97%) synthetic rutile produced	Higher concentration of acid required for remove remaining magnetic iron form.

2.4.2 Sulphuric acid leaching processes

The sulphuric acid leaching process or sulphate leaching process was the first commercialised technology to convert ilmenite to TiO_2 . Natural ilmenite containing roughly 40-60 % of TiO_2 and/or titanium slag with roughly 72-87 % of TiO_2 content formed water soluble sulphates, titanyl sulphate (TiOSO_4) and iron sulphates (FeSO_4) when they were digested with sulphuric acid. Then, metallic iron scrap is used to convert the ferric iron to ferrous iron to prevent the co-precipitation of ferric iron with TiO_2 . The solution is cooled down for ferrous sulphate to crystallise followed by the hydrolysis of TiO_2 . Alternatively, Han et al. (1987) suggested the use of methyl alcohol to separate TiOSO_4 and FeSO_4 as TiOSO_4 is insoluble in methyl alcohol but not FeSO_4 . A similar process had been developed by BHP Billiton researchers by using a solvent extraction process to isolate crystals of TiOSO_4 , followed by hydrolysis and calcination to form titania (Roche et al., 2008a).

The typical conventional sulphate leaching process is widely described in the following reactions, the ilmenite reacts with sulphuric acid and Fe (II) sulphate and titanyl sulphate was formed (Eq. 2.21). On the other hand, Fe^{3+} in ilmenite formed Fe (III) sulphate in the solution and was reduced by iron powder for ferric reduction for easy separation from the system (Eq. 2.22). As Fe (II) sulphate and titanyl sulphate will crystalline in the presence of water (Eq 2.23, 2.24) thereby contaminate the final product, researchers had proposed alternative methods to improve the purity of TiO_2 in product such as selective solvent extraction and use of reductant such as metallic iron (Zhang et al., 2011).





Several researchers have investigated the optimum conditions to achieve high removal of Fe while preserving TiOSO_4 in solution through sulphate leaching process. Table 2.6 summarises the optimisation of sulphate leaching process by various researchers. The ilmenite content differs according to the source of ilmenite location, thus it is difficult to determine the exact optimum condition of each parameter for the sulphate leaching process but such an investigation provides an insight for research purpose. Based on Table 2.6, the optimum H_2SO_4 concentration is in the range of 13.5 -15.4 M, and the optimum time for the reaction was suggested to be within 2 h. On the other hand, there are disputes regarding the optimum temperature for the sulphate leaching process. Liang et al. (2005) and Li et al. (2016) proposed the optimum temperature should be around 160-200 °C whereas Han et al. (1987) suggested 88-100 °C was the optimum temperature. The difference of observation could link with different experimental design used in the respective experiments, therefore generating different results. Regardless the difference on the optimum temperature, it can conclude that high temperature promotes the leaching efficiency of ilmenite and speed up the sulphate leaching process. In contrast, Li et al. (2008) proposed a direct TiO_2 precipitation in the sulphate leaching process by using a low concentration of H_2SO_4 . In the experiment, ~100% of Fe in ilmenite has dissolved in 10 wt.% H_2SO_4 solution as well as 40% of Ti dissolution was observed but gradually decreased during the experiment duration. The product has 161.9 m^2/g surface area with an average pore size of 5.3 nm. Li et al. (2008) suggested dilute acid solution with high temperature conditions increased the rate of titanium hydrolysis since similar observations occurred in Li's previous work (2007), thus increase the recovery of TiO_2

Table 2.6: Various researches on optimisation of sulphate leaching process for direct leaching and purification.

Ilmenite composition [wt%]	Acid concentration	Temperature [°C]	Time [h]	Reductant	Final product [wt%]	References
43.6 TiO ₂ , 34.45 FeO, 3.11 Fe ₂ O ₃	13.5 M	160	2	-	-	(Li et al., 2016)
46.8 TiO ₂ , 37.6 FeO, 5.1 Fe ₂ O ₃	40 wt. %	150	3	FeSO ₄ salt	~ 85 Ti	(Jia et al., 2014)
47.25 TiO ₂ , 34.21 FeO, 5.58 Fe ₂ O ₃	10 wt. %	-	-	-	97.1 TiO ₂ , 0.6 Fe ₂ O ₃ , 2.3 SO ₃	(Li et al., 2008a)
47.25 TiO ₂ , 34.21 FeO, 5.58 Fe ₂ O ₃	10 wt. %	-	-	-	-	(Li et al., 2007a)
55.1 TiO ₂ , 20.3 FeO, 19.9 Fe ₂ O ₃	12.9 M	120 (9.2 M)	4	-	-	(Sasikumar et al., 2007)
47.5 TiO ₂ , 32.7 FeO, 5.5 Fe ₂ O ₃	15.4 M	180-200	-	-	-	(Liang et al., 2005)
51.06 TiO ₂ , 36.82 FeO, 4.97 Fe ₂ O ₃	14.1 M	88-100	-	-	-	(Han et al., 1987)

from sulphate leaching process. In addition, Jia et al. (2014) and Roche et al. (2008) highlighted that high concentration of H_2SO_4 (>40 wt.%) prevented premature TiO_2 hydrolysis and precipitation (Roche et al., 2008b).

Albeit the sulphate leaching process has been well-studied, the research on the conversion of ilmenite into photo-catalyst through the sulphate leaching process is still lacking. Smith et al. (2010) and Torres-Luna et al. (2016) had synthesised a photo-catalyst from ilmenite using the sulphate leaching process (Smith et al., 2010; Torres-Luna et al., 2016). The photo-catalyst from Torres-Luna et al. (2016) experiment had high concentration of TiO_2 with 2.85 eV band gap energy, $192 \text{ m}^2/\text{g}$ surface area and contained 0.24 wt.% of Fe. Similar result was reported by Smith et al. (2010) work with 2.73 eV band gap energy, $16 \text{ m}^2/\text{g}$ surface area and the photo-catalyst contained a mixture of FeTiO_3 , Fe_2O_3 and sulphated $\text{Fe}_2\text{O}_3\text{-TiO}_2$. It is clear that the presence of iron species in the structure has significantly reduced the band gap energy of TiO_2 . However, the photo-catalyst in the test for photo-degradation experiment was not conducted in their study whereas Smith et al. (2010) demonstrated the photo-catalyst underwent photo-catalytic decomposition of 4-chlorophenol under UV light irradiation.

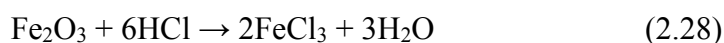
In the conversion of ilmenite to TiO_2 , the sulphate leaching process can process low grade ilmenite (>44% TiO_2) or Ti slag (78% TiO_2) with low energy consumption. The capital cost for sulphate leaching process is low as the technology set up requirement is not complex. However, this study would not focus on using sulphate leaching process to synthesise pre-treated ilmenite because the sulphate leaching process is known to consume a high amount of H_2SO_4 and generate large iron sulphate and dilute H_2SO_4 waste which requires additional cost for proper treatment before disposal (Zhang et al., 2011).

2.4.3 Hydrochloric acid (HCl) leaching process

The HCl leaching process or chloride leaching process employs more complicated technology to produce TiO_2 with higher purity. Similar to the sulphate leaching process, natural ilmenite can be used as feedstock for the conversion from ilmenite to TiO_2 . Titanyl chloride (TiOCl_2) and iron chloride (FeCl_2 or FeCl_3) formed when digestion of ilmenite with HCl solution. Berkovich et al. (1975) had developed a direct leaching process to dissolve around 80% of the titanium and iron in the ilmenite ore with concentrated HCl. In the study, Sulphur dioxide (SO_2) was used to reduce ferric ions to ferrous ions followed by the crystallisation and separation of FeCl_2 . The titanium chloride present in the solution was then hydrolysed, precipitated and calcined to produce TiO_2 . Berkovich pointed out that reduction of Fe(III) to Fe(II) is important due to the affinity between TiO_2 and Fe(III), causing difficulty in separation between Fe(III) and TiO_2 (Berkovich, 1975). Alternatively, Mahmoud et al. (2004) used iron powder as a reductant to accelerate the iron removal efficiency and avoid secondary contamination from foreign elements. Similar observations were reported in El-Hazek et al. (2007) and Lasheen et al. (2005) studies. In the chloride leaching process, two types of approaches were proposed to produce TiO_2 i.e. simultaneous hydrolysis and two-step hydrolysis. In simultaneous hydrolysis, Ti ions reacts with Cl^- to form TiOCl_2 , upon which TiOCl_2 hydrolyses and polymerises to TiO_2 . In two-step hydrolysis, after Ti and Fe have dissolved in the solution, a solvent is used to separate iron formed and Ti formed compounds, then the raffinate is hydrolysed to produce TiO_2 (Duyvesteyn et al., 2002a; Duyvesteyn et al., 2002b).

The mechanism of the chloride leaching process for the conversion of ilmenite is shown in eq. 27-29. Iron oxide species will react with HCl and formed FeCl_2 and FeCl_3 (Eq. 2.27 & 2.28). On the other hand, Ti ions that leached out from ilmenite formed titanyl chloride before precipitated to TiO_2 through hydrolysis (Eq 2.27 & 2.29). Chloride

leaching process can yield TiO₂ product with high purity due to FeCl₂ and FeCl₃ are highly soluble in water.



Various researches in the optimisation of Fe removal in chloride leaching process have been summarised in Table 2.7. HCl concentration has great influence in the dissolution of Fe and Ti as an increment of HCl concentration showed better Fe removal from ilmenite and promoted Ti ion polymerisation and precipitation to TiO₂ particle. The polymerisation of titanium would be triggered if the concentration of [Ti(IV)] and [H(I)] in the solution were more than 10⁻³ M and 0.5 M respectively (Nabivanets & Kudritskaya, 1967). In addition, Cservenyák et al. (1996) tabulated the relationship between the Ti (IV) species and Cl (-I) concentration where the Cl (-I) concentration in the solution was determined through the choice of initial acid strength and Ti (IV) concentration increased as the reduction reaction progresses. In addition, the research also suggested that Ti (IV) remains as complex titanyl chloride compounds when Cl (-I) concentration is high. These findings provide useful information for researchers to control the environment for either promoting or prohibiting the hydrolysis of TiO₂. Moreover, Mostafa et al. (2013) suggested that the process of extracting and purifying titanium as TiOCl₂ is favoured for low grade ilmenite mineral (high content of Fe).

In simultaneous hydrolysis, Mahmoud et al. (2004) yielded 90 wt.% of TiO₂ with 0.8 wt.% of Fe₂O₃ for final product whereas Tao et al. (2012) achieved 98.5 wt.% of TiO₂ with only 0.5 wt.% of Fe₂O₃ in the final product. The enhanced quality of the final product in Tao et al.'s work was because of an additional mechanical activation step on ilmenite before the chloride leaching process. The mechanical activation step by mixing active

Table 2.7: Various researches on optimisation of chloride leaching process for direct leaching and purification.

Ilmenite composition [wt%]	Acid concentration	Temperature [°C]	Time [h]	Reductant	Final product [wt%]	References
60.6 TiO ₂ , 30 FeO, 1.7 Fe ₂ O ₃	30 wt.%	70	-	Gypsum	-	(Gireesh et al., 2015)
49.6 TiO ₂ , 32.8 FeO, 13.7 Fe ₂ O ₃	4 M	90	4	Active carbon	98.5 TiO ₂ , 0.5 Fe ₂ O ₃	(Tao et al., 2012)
51.33 TiO ₂ , 40.87 FeO, 6.5 Fe ₂ O ₃	20 wt.%	160	10	-	94.72 TiO ₂ , 1.44 Fe ₂ O ₃	(Janssen & Putnis, 2011)
32.9 TiO ₂ , 44.6 Fe ₂ O ₃	20 wt.%	110	6	-	-	(Akhgar et al., 2010)
47.25 TiO ₂ , 34.21 FeO, 5.56 Fe ₂ O ₃	20 wt.%	100	8	-	92 TiO ₂ , 2.1 Fe ₂ O ₃	(Li et al., 2008b)
44.01 TiO ₂ , 28.5 FeO, 21.41 Fe ₂ O ₃	7 M	80	2.5	Fe powder	-	(El-Hazek et al., 2007)
39.5 TiO ₂ , 24.2 FeO, 33 Fe ₂ O ₃	15 wt.%	75	-	-	89.9 TiO ₂ , 2.5 Fe	(Sarker et al., 2006)
46.69 TiO ₂ , 27.5 FeO, 20.9 Fe ₂ O ₃	12 M	90	8	Fe powder	89 TiO ₂ , 6.7 Fe ₂ O ₃	(Lasheen, 2005)
41.1 TiO ₂ , 24.4 FeO, 28.6 Fe ₂ O ₃	20 wt.%	110	5	Fe powder	90 TiO ₂ , 0.8 Fe ₂ O ₃	(Mahmoud et al., 2004)
26.4 TiO ₂ , 35.2 FeO	9.6 M	70-90	-	-	-	(Olanipekun, 1999)

carbon with ilmenite and heated for 1 h in furnace at 1000 °C resulted in carbothermic reduction of ilmenite, causing most of Fe (III) reduced to Fe (II) which readily reacts with HCl, therefore it improved the iron removal efficiency by using dilute acid solution.

Compared with the sulphate leaching process, research on the potential of turning ilmenite into photo-catalyst using the chloride leaching process are far scarcer. Tao et al. (2013) produced TiO₂ nanorods through the chloride leaching process and the photo-catalyst has better photo-catalytic activity in the photo-degradation of oxalic acid compared with commercial rutile TiO₂. This is attributed to the presence of Fe impurities which reduce band gap energy and the good crystallinity of TiO₂ nanorods. The chloride leaching process is more environmental friendly as less waste is generated from the process. The recyclability of acid in the system is more complete than sulphate leaching process and yield higher purity products. However, the chloride leaching process requires higher capital cost for equipment management, sophisticated operation and maintenance skill. Albeit the mentioned disadvantages, the chloride leaching process was chosen in this study since the process generate less waste and produce TiO₂ with minima Fe impurities in the lattice and these impurities could reduce the recombination rates of TiO₂.

2.5 Potential application of doped TiO₂ photo-catalyst

Because of the versatility, high chemically and physically stability of titania based material, thereby this material has received considerable study for environmental catalytic application such as water purification and pollutant oxidation. Yet its own large band gap energy hinder the potential of TiO₂ application for sun light irradiation. Several recent studies have showed that doped TiO₂ photo-catalyst have better performance and properties over pure TiO₂ photo-catalyst for application in photo-catalytic oxidation of pollutant. This is because the addition of dopants reduce the band gap of the TiO₂, enable the doped TiO₂ to absorb visible light. The conduction band (CB) of the dopant has a

more negative reduction potential than TiO_2 , allowing the photo-induced electron from visible light region enter into the lower-energy CB of TiO_2 (Smith et al., 2010).

In this study, RB 5 dye (Fig 2.4) was selected because it is a well-known non-biodegradable disazo dye and it has relatively high consumption rate (Alaton & Balcioglu, 2001). Several researchers have studied the degradation of RB 5 for decolourisation and mineralisation. Wang et al. (2003) reported ozonation was effective in RB 5 decolourisation but this method yield low mineralisation efficiency. On the other hand, UV/ H_2O_2 and photo-catalytic treatment (UV/ TiO_2) was found to yield impressive result in both decolourisation and mineralisation of RB 5 (Alaton & Balcioglu, 2001; Mohey El-Dein et al., 2003; Neamtu et al., 2002). This is because ozone has short life span whereas photo-catalytic treatment can continuously generate $\bullet\text{OH}$ radical as long as sufficient light energy was supplied. Table 2.8 summarise the studies focus on photo-degradation of RB 5 by using TiO_2 and doped TiO_2 .

Reutergardh et al. (1997) compared TiO_2 and CdS in photo-catalytic decolourisation of RB 5 dye and found out that TiO_2 detoxified the RB 5 wastewater whereas CdS increased the toxicity of RB 5 wastewater because of its photo-corrosion. In addition, the photo-degradation efficiency of TiO_2 has no difference after recycled but the efficiency of recycled CdS was lower than for new CdS due to precipitation of $\text{Cd}(\text{OH})_2$ on the CdS active surface site. Similar result was reported in Alaton et al. (2001) work as 70% of TOC removal was achieved, indicated most of RB 5 and the intermediate products from RB 5 was mineralised by $\bullet\text{OH}$ radical. On the other hand, Chong et al. (2015) evaluated the use of TiO_2 in removal of RB 5 in synthetic and real greywater effluents. The RB 5 removal efficiency in synthetic greywater effluent was 97% in 150 min however the efficiency was dropped to 76% in real greywater effluent in 330 min of reaction. The

Table 2.8: Photo-degradation of RB 5 by using TiO₂ and doped TiO₂.

Catalyst	RB 5 concentration [ppm]	Experiment duration [min]	Removal Efficiency [%]	Light source	Reference
H-TiO ₂	3	120	99	Solar	(An et al., 2017)
Fe-TiO ₂	20	60	100	Solar	(Soo et al., 2016)
TiO ₂ – ZSM5	10	10	>95	UV	(Zhou et al., 2016)
TiO ₂	1	150	97	UV	(Chong et al., 2015a)
TiO ₂ – zeolite	1	100	100	UV	(Chong et al., 2015b)
N-Cu-TiO ₂	-	30	100	UV	(Kaur et al., 2015)
TiO ₂ – ZSM5	50	90	98	UV	(Mahadwad et al., 2011)
NZVI-TiO ₂	-	120	100	UV	(Satapanajaru et al., 2011)
P25 TiO ₂	75	60	-	UV	(Alaton & Balcioglu, 2001)
Anatase TiO ₂	-	-	-	UV	(Reutergådth and Iangphasuk, 1997)

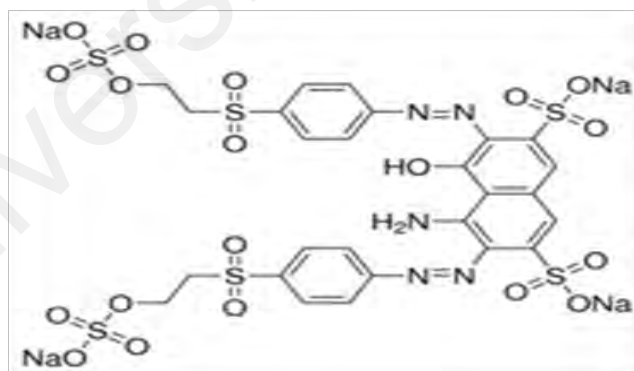


Figure 2.4: RB 5 structure

reduction of the efficiency because of the competition of TiO_2 active site between RB 5 and other pollutants present in the real greywater effluent.

Besides the use of pure TiO_2 in RB 5 removal, other researchers focus on the use of doped TiO_2 in RB 5 removal. For example, Chong et al. (2015) compared the photo-degradation efficiency of RB 5 dye between commercial TiO_2 and own synthesised TiO_2 – zeolite nano-composite and the study showed TiO_2 – zeolite nano-composite had higher kinetic pseudo-first order rate than commercial TiO_2 . In addition, the study showed the TiO_2 - zeolite achieved 100% degradation of dye in less than 100 min whereas commercial TiO_2 required 120 min to achieve similar degradation efficiency. On the other hand, Zhou et al. (2016) study where the TiO_2 – Zeolite Socony Mobil-5 (TiO_2 – ZSM-5) composite achieved > 95% of RB 5 degradation within 10 min. In addition, the study also focus on the toxicity of the intermediate product of RB 5 during degradation. The toxicity increased at first and then gradually decreased, indicating that the highly toxic intermediates gradually destroyed by further photo-catalytic degradation. Similar result reflect in Mahadwad et al. (2010) study which TiO_2 – ZSM 5 had the highest efficiency with 98% degradation of RB 5 solution in 90 min whereas commercial P 25 TiO_2 has only 80% degradation of RB 5.

RB 5 is an anionic dye thus the zeta potential of the catalyst will affect the efficiency of RB 5 degradation. Kaur et al. (2015) compared the photo-catalytic activity of RB 5 dye between nano-crystalline undoped, N-doped and N and metal co-doped titania. 100% of RB 5 degradation was observed in N,Cu co-doped TiO_2 whereas undoped TiO_2 has 52.4% of RB 5 degradation. However, complete mineralisation was not achieved in N,Cu codoped TiO_2 as a pink coloured residual solution was observed. Kaur et al. (2015) pointed out undoped TiO_2 and N,Cu co-doped TiO_2 has better degradation efficiency than N-doped and N,Fe co-doped TiO_2 due to the latter has highly negative zeta potential thus

lowers the adsorption of RB 5 dye. An et al. (2017) synthesised hydrogenated TiO₂ (H-TiO₂) using plasma treatment and the H-TiO₂ achieved >99% of RB 5 dye degradation under solar light irradiation whereas P 25 has only around 30% of degradation efficiency. This is because P 25 is a pure TiO₂ which it can only perform well under UV light region and UV light account 5% only in visible light spectrum.

Although the research of Fe doped TiO₂ (Fe-TiO₂) has been well studied however the use of Fe-TiO₂ on RB 5 degradation is still scarce. Satapanajaru et al. (2011) reported the nano zerovalent iron doped TiO₂ (NZVI-TiO₂) has the degradation kinetic rate constant of 0.59 h⁻¹ and the kinetic rate was enhanced about four-five times to 2.37 h⁻¹ when NZVI-TiO₂ was irradiated by UV. On the other hand, Soo et al. (2016) synthesised Fe doped anatase brookite TiO₂ (Fe-TiO₂) nano-composite and the Fe-TiO₂ have 100% of dye degradation efficiency whereas pristine TiO₂ accounted around 30% of dye degradation efficiency only. This is because Fe ions as the p-type dopant create acceptor centre which has trapping effect for photo-generated electron thus reduce the recombination rate for photo-generated electron-hole pairs.

Compare with pure TiO₂, doped TiO₂ provide better performance in photo-catalytic degradation of RB 5. However, the current focus is on the bottom up synthesis of doped TiO₂ rather than the top bottom synthesis. This is because of the dopant concentration can be controlled in the bottom up synthesis but the chemicals used in this synthesis are harmful to people. For example, titanium (IV) isopropoxide is used widely in sol-gel method to synthesise titania material catalyst, and the chemical can cause skin and eye irritation and it is acute toxic to human. Besides that, proper disposal treatment has to be in consideration for the waste generated in the bottom up synthesis. On the other hand, there are many benefits by using the top bottom synthesis method such as less harmful chemical in use and easy set up but the dopant concentration is hard to control in this

synthesis. In this study, top bottom synthesis method was used as it is more eco-friendly and less harmful chemical was used in this method.

Although there has been a study to produce TiO₂ nanorods from ilmenite through chloride leaching process and shown good photo-catalytic activity, there is a lack of study on the effect of Fe ion content in the pre-treated ilmenite for photo-degradation of RB 5.

University of Malaya

CHAPTER 3: METHODOLOGY

3.1 Introduction

Chapter 3 covers the explanation and discussion of three important sections to study the photo-catalytic activity of raw and pre-treated ilmenite. The first section provides information about the raw material selection and type of chemicals that were used in this study. The second section elaborates on the experimental procedure and design of experiment to form pre-treated ilmenite by considering the effect of acid concentration, time, temperature and calcination temperature. The third section emphasised on the photo-catalytic dye removal performance test with regards to raw and pre-treated ilmenite. These studies aim to determine the optimum processing parameters to obtain desired pre-treated ilmenite for the best photo-catalytic dye removal performance by improving the raw ilmenite. The last section of this chapter outlines the characterisation of structural, morphological, optical, electronic and electrochemical properties of the raw and pre-treated ilmenite using various techniques, such as FESEM, EDX, XRD, Raman, XPS, and PL analysis. This covers a brief explanation on the characterisation equipment, operating principles and sample preparation. In this research, pre-treated were synthesised via acid leaching technique. The outline of research methodology is presented in Figure 3.1.

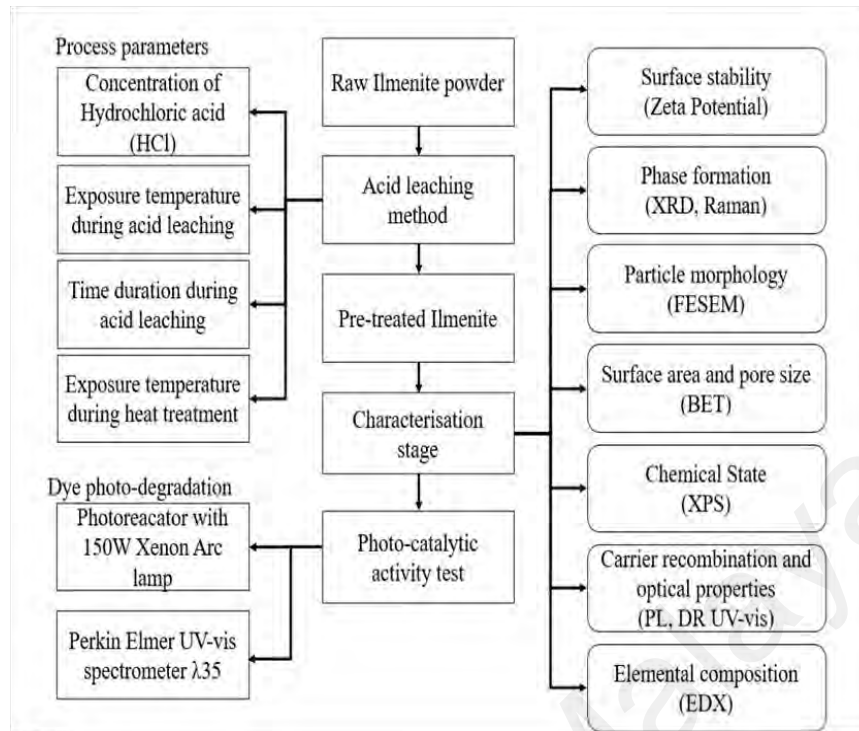


Figure 3.1: Overview of research methodology

3.2 Raw materials and chemical

All chemicals and material selection would be remaining under the same manufacturer throughout entire research in order to achieve standardised results. In this research study, pre-treated ilmenite was treated by using acid leaching method under different conditions, including acid concentration, exposure time, exposure temperature and calcination temperature. The general information and properties of the chemicals and raw materials used in this research are specified in Table 3.1.

Table 3.1: Raw materials and chemicals used for the synthesis of pre-treated ilmenite.

Material	Function	Manufacturer	Properties
Natural ilmenite sand	precursor	Tor Minerals Co., Ltd., Malaysia	Chemical formula: FeTiO_3 TiO ₂ min 58% wt Total Fe max 24% wt Al ₂ O ₃ max 0.8% wt SiO ₂ max 0.8% wt
Hydrochloric acid	Leaching agent and indicator of inorganic ion (Cl ⁻)	Merck	Chemical formula: HCl Purity: 37%, ACS,ISO Reagent
Nitric acid	Indicator of inorganic ion (NO ₃ ⁻)	Merck	Chemical formula: HNO ₃ Purity: 65%, ISO
Sulphuric acid	Indicator of inorganic ion (SO ₄ ²⁻)	Merck	Chemical formula: H ₂ SO ₄ Purity: 95-97%, ISO
Ortho-Phosphoric acid	Indicator of inorganic ion (PO ₄ ³⁻)	Merck	Chemical formula: H ₃ PO ₄ Purity: 85%, ACS,ISO Reagent
Reactive Black 5	Model pollutant compound	Sigma Aldrich	Chemical formula: C ₂₆ H ₂₁ N ₅ Na ₄ O ₁₉ S ₆ Dye content: ≥50%

3.3 Experimental procedures

Natural ilmenite mineral (Tor Minerals Co., Ltd., Malaysia) was used as the starting materials. The sample was crushed and ground by using an agate mortar. Then, the crushed sample was sieved by a sieve to ensure all sample is less than 45 μm and used for conducting in this research work. In the acid leaching experiments, the ilmenite powders, stirring rods, and their corresponding aqueous solution were placed in Schott bottles. The bottles then were immersed in silicon oil baths on the top of a hot plate. The solution was stirred at 450 rpm to ensure slurry suspended during the leaching experiment. Figure 3.2 displays the detailed flow chart of the catalyst synthesis.

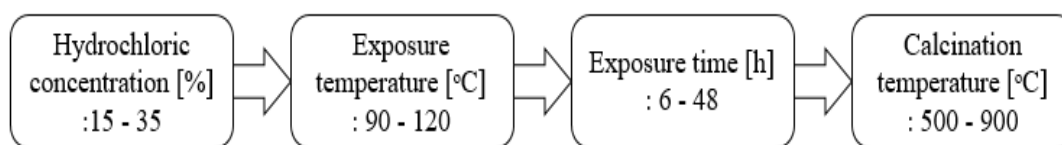


Figure 3.2: Detailed flow chart of pre-treated Ilmenite synthesis.

3.3.1 Acid leaching procedure

A 2.5g of ilmenite powder was treated with 250 ml of HCl solution. The HCl solution has respectively concentration of in term of v/v% (15, 20, 25, 30 and 35%) and the mixture was treated at 100 °C for 24 h. The samples were denoted as H-X, in which X represents the HCl concentration i.e. H-15 represent ilmenite has been pre-treated with 15% HCl. The suspension was centrifuged after leaching and the leached sample was washed and dried at 70 °C for 12 h. The sample then was tested its photo-catalytic activity by degrading 5 ppm of Reactive Black 5 dye at pH 3 to identify the optimum acid concentration used to produce pre-treated ilmenite with the highest photo-degradation efficiency.

After determination of the optimum acid concentration, a 2.5g of ilmenite powder and 250 ml of HCl solution was treated at different exposure temperature for 24 h. The samples were denoted as T-Y, in which Y represent the exposure temperature i.e. T-90 represent ilmenite has been pre-treated under 90 °C. Similar photo-degradation test was conducted to determine the optimum exposure temperature for pre-treated ilmenite.

At last, a 2.5g of ilmenite powder and 250 ml of HCl solution was treated under optimised acid concentration and exposure temperature for various exposure time. The samples were denoted as TI-Z, in which Z represents the exposure time i.e. TI-8 represent ilmenite has been pre-treated for 8 h.

3.3.2 Calcination temperature

In this experiment, different calcination temperatures were used to refine the crystalline phase of pre-treated ilmenite after acid leaching treatment. The calcination was done in the air atmosphere with the heating rate at $5\text{ }^{\circ}\text{C min}^{-1}$ for 4 h dwell time. The pre-treated ilmenite then was cooled down naturally until the room temperature was achieved. Figure 3.3 shows the annealing profile of the calcination of pre-treated ilmenite. The calcination temperature chosen was from 500 to 900 $^{\circ}\text{C}$ with 100 $^{\circ}\text{C}$ increments and then denoted as C-500, C-600, C-700, C-800 and C-900, respectively.

All the pre-treated samples then will be tested their photo-catalytic activity which mentioned in section 3.4. The sample with the best photo-catalytic activity will be selected and its physicochemical properties will be studied.

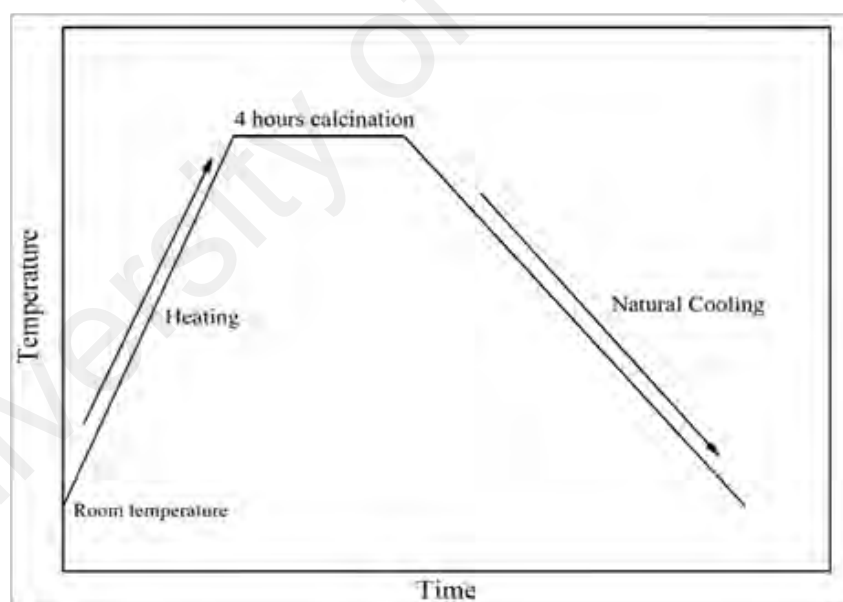


Figure 3.3: Annealing profile of the calcination of pre-treated Ilmenite.

3.4 Photo-catalytic activity testing of raw and pre-treated ilmenite

The photo-catalytic measurement of raw and pre-treated ilmenite was conducted as batch photo-catalytic reaction system. In this experiment, 5 ppm of RB 5 solution was prepared with deionised water using a volumetric flask. 1.0 g/L of pre-treated ilmenite

powder was dispersed in of 50 ml of RB 5 dye. The pH of RB 5 solution was adjusted to pH 3 by using 1M of nitric acid solution. A photo-reactor with a 150 W Xenon Arc lamp mimicking solar light (200-2500 nm, Newport), magnetic stirrer and air pump was installed as shown in Figure 3.4. The reaction was set for 30 minutes in the dark environment and then followed by 30 minutes light irradiation. The solution was then filtered and measured by UV-Vis spectrophotometer to determine the remaining absorbance of RB 5 at wavelength of 597 nm.



Figure 3.4: Schematic diagram of the photo-reactor set up for photo-degradation of RB 5 dye solution.

The parameters for the photo-catalytic activity of raw ilmenite are summarised in Table 3.2.

Table 3.2: The parameters investigated on the photo-catalytic activity of raw ilmenite

Parameters investigated	Constant value
Effect of pH	Concentration of dye, temperature, stirring speed, catalyst loading, acid used
Effect of different inorganic ions	Concentration of dye, temperature, stirring speed, catalyst loading, pH
Effect of catalyst loading	Concentration of dye, temperature, stirring speed, acid used, pH

For the pH study, RB 5 solution was initially adjusted to pH 2, 3, 4, 6, and 9. The pH of the RB 5 dye solution was adjusted with 1 M of HNO₃ and 1 M of NaOH.

For inorganic ion study, the pH of RB 5 dye solution was set based on the optimum photo-catalytic activity. 1M of HCl, HNO₃, H₂SO₄ and H₃PO₄ solution were used to adjusted pH value of RB 5 dye solution which is pH 6.

For catalyst loading study, the pH of RB 5 dye solution and the acid solution used were determined from the previous study. A 0.5, 1.0, 1.5, and 2.0 g/L of catalyst loading was used to determine the optimum photo-catalytic activity for RB 5 dye removal.

The kinetic rate of photo-catalytic activity of raw and pre-treated ilmenite was determined using Eq. (3.1); k' denote as pseudo-first order rate constant, C_0 the initial concentration of RB 5 and C is the concentration at time “ t ”.

$$\ln\left[\frac{C}{C_0}\right] = k't \quad (3.1)$$

3.5 Catalyst characterisations

The pre-treated ilmenite was characterised using various techniques to comprehend the properties of the material. The principles of the characterisation techniques and the parameters set to analyse the samples were described and indicated. The phase structure

analysis was examined by using X-ray diffraction (XRD) and Raman spectroscopy, photoluminescence spectroscopy (PL) for carrier recombination analysis. Field emission scanning electron microscopy (FESEM) was used for morphological studies, Energy-dispersive X-ray spectroscopy (EDX) for elemental composition analysis, X-ray photoelectron spectroscopy (XPS) for chemical state analysis and optical properties analysis was conducted by UV-Vis diffuse reflectance spectroscopy (UV-Vis DRS). The surface area and pore size of the pre-treated ilmenite were studied by nitrogen adsorption-desorption method. Zeta potential was conducted for electrochemical equilibrium on interfaces of the sample.

3.5.1 X-ray Diffraction

The information of phase structure of the raw and pre-treated ilmenite was obtained by using X-ray diffraction analysis. At first, the sample was grounded into fine powder in an agate mortar and then around 0.1 g of the fine powder was pressed using a glass slide evenly on the sample holder prior put it into the sample chamber of the diffractometer. In this research, XRD analysis was conducted using a D8 Discover Bruker diffractometer from 20 to 70° with Cu K α radiation $\lambda = 0.15406$ nm at step size of 0.02° s⁻¹.

XRD is a technique used for studying the atomic and molecular structure of a crystal and atomic spacing, in which the crystalline atom diffract a beam of incident X-ray into various specific directions. The incident rays interact with the sample and produce constructive interference when conditions obey Bragg's Law ($n\lambda = 2d \sin\theta$). Crystallographer can generate a three dimensional picture of the density of electrons within the crystal by measuring the angles and intensities of these diffracted beams. All possible diffraction directions of the lattice should be attained by scanning the sample through a range of 2θ angles even though the random orientation of the powdered

materials. The diffraction peaks covered to d -spacing, which provide a unique fingerprint of the materials present in the sample as each mineral has a set of unique d -spacing (Klug and Alexander, 1954; Skoog et al., 2007; Valcárcel, 2012; Warren, 2012). The reference pattern from International Centre of Diffraction Data (ICDD) database was used to compare with the generated XRD spectrum, the phases of the sample can be calculated and identified.

The crystalline size of crystallites can be calculated by using Scherrer equation (Warren, 2012). The Scherrer equation can be written as below:

$$\tau = \frac{K\lambda}{\beta \cos \theta} \quad (3.2)$$

In the Eq. 3.2, the τ is the mean size of the ordered crystalline domains, K is a shape factor with no dimension with a value of 0.9. The λ is the X-ray wavelength, β represents the line broadening at half the maximum intensity and θ is the Bragg angle.

3.5.2 Raman Spectroscopy

Raman spectroscopy is a spectroscopic technique used to provide information about molecular vibrations that can be used for sample identification and quantisation. Raman spectroscopy is commonly used for sample phase identification as every molecule has its unique fingerprint. The technique involves shining a monochromatic light source on a sample and detecting the scattered light. The majority of the scattered light is of the same frequency as the excitation source, this phenomenon is known as Rayleigh or elastic scattering. A small amount of scattered light is shifted in energy from the laser frequency because of the incident electromagnetic waves interact with the vibrational energy levels of the molecules in the sample. The intensity of the shifted light versus frequency plots result in a Raman spectrum, which showed the energy levels of different functional group vibrations (Bowley et al., 2012; Colthup, 2012; Long, 1977; McCreery, 2005; Skoog et

al., 2007; Valcárcel, 2012). The Raman analysis in this study was initiated with 0.1 g of the sample was grounded into fine powder in an agate mortar and the fine powder then was placed evenly on a new glass slide followed by placing the glass slide under the objective lens of Raman spectroscopy machine. In this research, the crystal structures of the samples were determined by using a Raman spectrometer (Renishaw in Via) and its Windows-based Raman Environment (Wire™) software. The Argon ion laser with 514.5 nm wavelength was used as an excitation source.

3.5.3 Photoluminescence Spectroscopy

All solids have energy gaps for the conducting electrons and some of the electrons in a solid are not firmly attached to the atoms. These loosely attached electrons are bound in the solid by differing amounts and thus have many different energies. Electrons having energies above a certain value are referred to as conduction electrons while electrons having energies below a certain value are referred to as valence electrons. Under normal conditions, electrons are forbidden to have energies between the valence and conduction bands. When a substance absorbs photons, its electrons have enough energy for them to excite from valence to conduction bands. The conduction electrons then emit photons and return to a lower energy state. The energy of the emitted photons also known as photoluminescence, which relates to the difference in energy levels between the electron states involved in the transition between the excited state and equilibrium state. Thus, photoluminescence is light emission from any form of matter after the absorption of photons. Defect or disorder in a substance can cause localisation of carriers and leading to a drastically increase of photoluminescence life time (Che & Védrine, 2012; Kumar, 2013; Lakowicz, 2013; Perkowitz, 2012; Skoog et al., 2007; Valcárcel, 2012). In this research, a small amount of sample in the fine powder form was placed evenly on the top of a new glass slide and then was put into microscope. The recombination in the samples was characterised using Raman Microscope (Renishaw in Via) with 325 nm wavelength

monochromatic beam. The photoluminescence was recorded in the range of 350 nm to 750 nm.

3.5.4 Field Emission Scanning Electron Microscopy

A Field Emission Scanning Electron microscopy (FESEM) is microscope that works with electrons, which are liberated by field emission source. A FESEM is used to visualize very small topographic details on the surface or entire or fractioned objects. Morphology and composition of the solid sample could also be studied by FESEM technique, providing a characteristic three-dimensional appearance for researchers easy to understand the surface structure of a sample. The working principle of FESEM is based on electrons are liberated from a field emission source and accelerated in a high electrical field gradient. Within the high vacuum column, these so called primary electrons are focused and deflected by electronic lenses to produce a narrow scan beam that bombards the solid sample. As a result, secondary electrons are emitted from each spot on the object. The angle and velocity of these secondary electrons relate to the surface structure of the object. A detector catches the secondary electrons and produces an electronic signal. This signal is amplified and transformed into a video scan image that can be seen, save and process further (Echlin, 2011; Echlin et al., 2013; Goldstein et al., 2012; Reimer, 2000). The sample preparation for FESEM analysis was begun by the sample was sprinkled evenly on the top of a carbon conductive tape which it was attached on the surface of an aluminium sample stub. In this research, raw and pre-treated ilmenite were examined using a JOEL JSM 7600-F field emission scanning electron microscope operate at 3kV and 5kV and magnifications of 10, 30, 50 and 100 kX were typically used for detailed characterisation.

3.5.5 X-ray Photoelectron Spectroscopy

X-ray Photoelectron spectroscopy (XPS) reveals the presence of chemical elements at the surface and the nature of the chemical bond that exists between these elements. In XPS experiment, sufficient energy input breaks the photoelectron away from an element core. The electron binding energies are related to the chemical environment of the atom, giving the XPS a significant tool to identify the chemical state and oxidation state of an atom (Carlson, 1978; Chastain et al., 1995; Van der Heide, 2011). In this research, small amount of sample in fine powder form was pressed into a pellet and was vacuumed in ultra-high vacuum (UHV) chamber before and during the measurement. The examination of chemical and oxidation states of raw and pre-treated ilmenite was executed on a PHI Quantera II scanning X-ray microprobe using an Al cathode ($h\nu = 1486.8$ eV) with 100 microns spot size and 280 eV pass energy. Survey scan was conducted in the range of 0-1200 eV whereas the determination of Fe 2p, O 1s and Ti 2p regions was conducted by narrow scan. The C 1s peak at 284 eV was used as a charge correction reference.

3.5.6 UV-vis Diffuse Reflectance Spectroscopy (DR-UV-Vis)

Beer-Lambert discovered the relationship between the attenuation of light and the properties of the material which the light is travelling through, thus Beer-Lambert law states that the absorbance of a solution is directly proportional to the concentration of the absorbing species in the solution and the path length. Therefore, UV-Vis spectroscopy can be used to determine the absorption values of liquid samples or concentration of the absorber in a solution through measuring the relative change of light transmittance as it passes through the solution for a fixed path length. The relative change of light transmittance due to absorbing species absorbs part of the light energy, results in a decrease in the amount of light at that particular energy level (Kumar, 2013).

DR-UV-Vis spectroscopy can be used to compute the energy band gap value of the material when the material interacts with light of various wavelengths. As the opaque solid sample prohibit light penetration, the light reflected on the surface of the sample and diffuse reflectance spectroscopy measures the relative change in the amount of reflected light off of the surface of the sample. A diffuse reflectance spectroscopy spectrum is produced, indicate the interaction of the sample with light of various wavelength, resulting electrons excite from the valence bands into the conduction band (Jackson & Hargreaves, 2009; Skoog et al., 2007; Valcárcel, 2012). In this research, the samples were grounded into fine powder in an agate mortar and then it placed in a quartz cell fairly before inserting into spectrophotometer. A barium sulphate standard was measured and used as a reference spectrum prior samples measurement. The optical properties of the raw and pre-treated ilmenite were examined using a Shimadzu UV-2700 UV-Vis Spectrophotometer and diffuse reflectance spectrum measurement was done in wavelength range of 240 to 800 nm using an integrating sphere.

3.5.7 Nitrogen adsorption-desorption measurement

The theory of physical adsorption of gas molecules on solid surfaces was explained by Brunauer, Emmett, and Teller (BET). The BET theory is according to the following hypotheses: (a) gas molecules adsorbed on a solid layer physically and infinitely; (b) each adsorption layer is no interacted with each other, and (c) formation of each layer obey Langmuir theory. Hence, the BET theory can be used for monolayer and multilayer molecular adsorption as long as they obey the hypotheses. The specific surface area of a powder is determined by physical adsorption of a gas on the surface of the solid and calculating the amount of adsorbate gas corresponding to a mono-molecular layer on the surface. Van der Waals forces hold the adsorbate gas molecules on the adsorbent surface area of the test powder. The determination is normally performed at the temperature of liquid nitrogen (Lowell & Shields, 2013). In this research, the surface area and pore size

distribution were investigated using Micromeritics ASAP 2020. Outgassing step was initiated to remove the gases and vapours before measurement of the specific surface area of the sample. 0.2 g of sample was degassed overnight at 300 °C under vacuum in order to ensure no previous adsorbed gas on the surface of the sample. Then the sample was shifted to the analysis station to cool down in liquid nitrogen.

3.5.8 Zeta Potential

Zeta potential is a magnitude measurement of the electrostatic or charge attraction/repulsion between particles, and it is one of the fundamental parameters to know affect stability. At the surface of particulate, there are a positive and negative charge separation components thus a region of varying electrical potential has created. When two different phases of particulate or molecules contacted each other, a difference in electric potential between them is developed. For example, water is a dipolar molecules and it orient into a certain direction at the interface of another surface, creating an electric potential difference between themselves. This difference is known as electro-kinetic and calculation of zeta potential can be measured based on data from electro-kinetic phenomena as electro-kinetic measurements are based on the electrostatic potential difference between the interior of the liquid phase and a certain plane or surface in the interfacial regions. The mechanisms behinds the development of zeta potential can be divided into four depends on the situation: (1) differences in the affinity of the two phases for electrons, (2) differences in the affinity of the two phases for ions of one charge or the other, (3) ionization of surface groups, and (4) physical entrapment of non-mobile charge in one phase (Hunter, 2013). In this research, 0.05 g of sample was soaked in deionised water and sonicated to prevent agglomeration. The mixture then was placed under an auto-titration machine where 1 M HCl and 1 M NaOH solution were prepared for pH adjustment. The zeta potential of raw and pre-treated ilmenite was measured by Malvern Zetasizer Nano Seires ZS.

3.5.9 Elementary analysis

The trace of elements in the solution can be detected and analysed by using inductively coupled plasma – optical emission spectroscopy (ICP-OES). During the analysis, the Argon plasma energy from outside is given to the component elements or atoms, causing the excitation occurred. The spectrum rays are released from component elements after the excitation process and the corresponded photon wavelength are measured. The position of the photon rays are used to determine the element type whereas the intensity of the rays can determine the content of the elements. In this study, 10 ml of samples was filtered and collected after the photo-degradation of dye by using raw ilmenite. The lines to be studied for specific element were selected. The standards and the anticipated working range for these specific elements were prepared before the analysis. The elementary test of the solution was measured by Perkin Elmer Optima 5300 DV.

CHAPTER 4: RESULTS AND DISCUSSION

4.1 Introduction

This chapter presents the results obtained from the experiments conducted and the discussion of the analyses. There are three main sections in this chapter, in which the results of the experiment work carried out by using raw ilmenite and pre-treated ilmenite as a catalyst as well as the discussion based on the experiment results are presented. In the first section, the physicochemical properties of raw ilmenite were characterised by conducting several characterisation methods to determine the chemical state, the crystalline phase, specific surface area and pore size, surface stability, particle morphology, carrier recombination and optical properties and element composition. The photo-catalytic activity of raw ilmenite was determined by the photo-degradation of RB 5 dye solution under artificial solar light irradiation. Several parameters were proposed and conducted in order to determine the optimum condition for raw ilmenite in photo-degradation of RB 5 dye solution. The physicochemical properties of pre-treated ilmenite at different HCl concentration were discussed in section 4.3. Section 4.4 focuses on the photo-catalytic activity of the pre-treated ilmenite by studying the photo-degradation of RB 5 dye solution.

4.2 Raw ilmenite

In this section, the physicochemical properties and the photo-catalytic activity of raw ilmenite are presented in subsequent sections respectively. The study of the photo-catalytic activity of raw ilmenite focused on the effects of RB 5 dye solution pH, the presence of inorganic ions and the catalyst loading.

4.2.1 Physiochemical properties of raw ilmenite

The quality and crystalline phase of raw ilmenite were characterised by XRD and Raman spectroscopy. Figure 4.1 displays the XRD patterns of the raw ilmenite. The existence of ilmenite in the XRD pattern was clearly shown from the presence of the (104) peak at $2\theta = 32.65^\circ$ (JCPDS: 29-0733 (raw ilmenite) and 96-900-8036 (rutile TiO_2)); whereas in the TiO_2 (rutile) spectrum, the (110), (101), (111), and (211) were observed. The intensity at (101), (111) and (211) is higher compare with that of pure rutile TiO_2 (Yan et al., 2013), indicated that the presence of Fe in the lattice structure enhanced the non-active site of rutile TiO_2 since previous studies suggested the (110) peak is rutile TiO_2 active site (Schaub et al., 2001; Zhao & Liu, 2014). Besides that, each rutile TiO_2 peak has an ilmenite peak next to it, suggesting the formation of Fe – TiO_2 bonding in the structure yet similar observation was not found in the Fe doped rutile (Abazović et al., 2009a). This may due to high Fe ions concentration in raw ilmenite which is more than 20% whereas synthesised Fe doped rutile has a maximum of 4.20% of Fe ions. Because of excessive Fe – TiO_2 bonding in raw ilmenite, this may probably reflect that the raw ilmenite has low photo-catalytic activity since overloaded Fe ions in the lattice structure might increase the recombination rate of photo-electron holes pairs. The composition of raw ilmenite contains 62.7% of rutile and 37.3% of ilmenite based on the XRD pattern in Fig 4.1. Rutile has the characteristics of a thermodynamically stable polymorph at all temperatures and pressures, therefore TiO_2 in the raw ilmenite normally are in rutile phase as the minerals typically found in igneous and metamorphic rock which had once experienced extreme temperature and pressure during geological formation (Li et al., 2008b; Mahmoud et al., 2004; Pataquiva-Mateus et al., 2016). The crystalline size of raw ilmenite and rutile TiO_2 were 6.39 nm and 2.96 nm respectively based on the Sherrer equation. The bigger crystalline size of raw ilmenite was due to the chemical bonding of Fe- TiO_2 . However, typical rutile TiO_2 peaks at 447 and 613 cm^{-1} was not shown in the

Raman diagram in Figure 4.2 while on the contrary the Raman peaks of natural Fe_2O_3 and FeO was observed. This is because the Raman peaks of rutile TiO_2 has been overlapped by the Raman peaks of Fe oxide species. The Raman peaks of Fe_2O_3 occur at 424 cm^{-1} , 1320 cm^{-1} and FeO occur at 154 cm^{-1} , 298 cm^{-1} , 546 cm^{-1} , corresponding with Faria et al.(de Faria et al., 1997) and Raman peaks for raw ilmenite are located at 680 cm^{-1} .

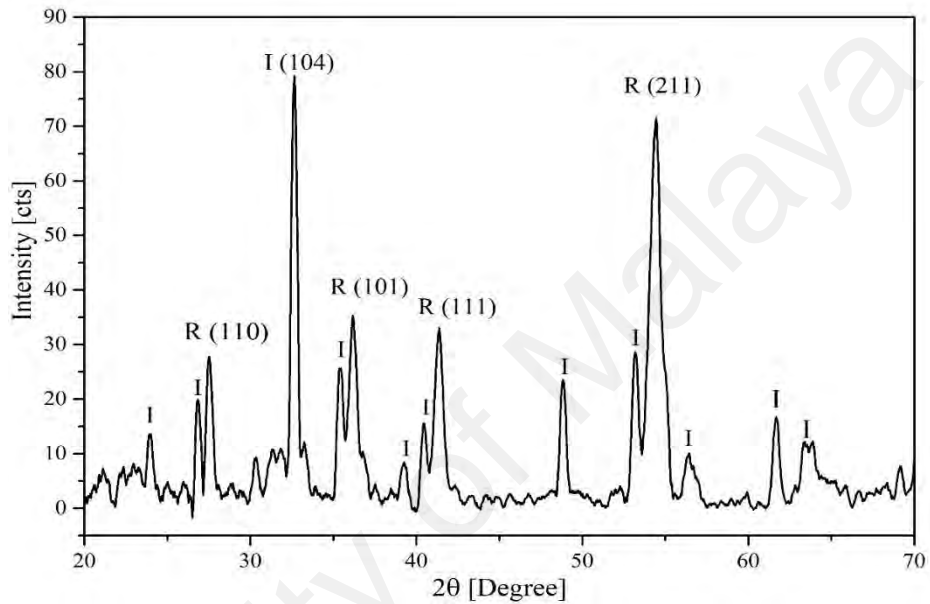


Figure 4.1: XRD pattern of raw ilmenite (R: rutile TiO_2 ; I: raw ilmenite)

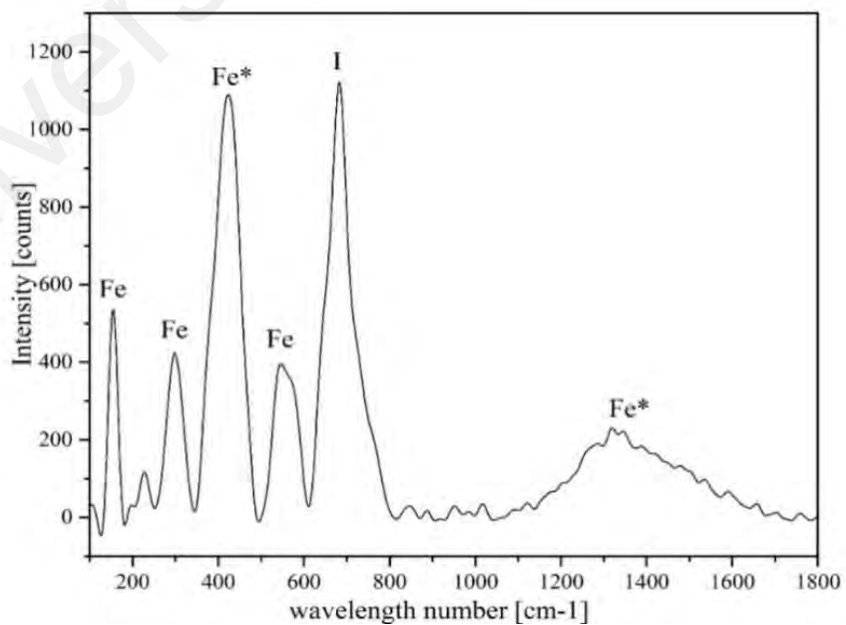


Figure 4.2: Raman plot of raw ilmenite. (Fe: FeO , Fe^* : Fe_2O_3 , I: raw ilmenite)

Next, the XPS analysis was conducted to identify the chemical composition and oxidation state of the raw ilmenite. Both Ti and Fe are transition elements; hence, they may exhibit different oxidation states. In this study, the three areas of the XPS spectrum of raw ilmenite was examined. The Ti 2p region between 450 to 470 eV (Fig. 4.3b), the O 1s regions between 520 and 535 eV (Fig. 4.3c) and the Fe 2p regions between 700 to 740 eV (Fig 4.3d). The presence of C at 284 eV, which is attributed to the adventitious hydrocarbon in the XPS instrument itself. In Figure 4.3b, the Ti 2p_{3/2} and Ti 2p_{1/2} spin-orbital splitting photo-electrons for raw ilmenite are observed at binding energies of 464.2 and 458.3 respectively. Similar observations was reported by previous studies (Abazović et al., 2009a; Zhu et al., 2006), thus the Ti binding energies are not affected by Fe ions. In addition, the absence of peak broadening of Ti 2p_{3/2} signal indicated no Ti³⁺ species were observed in raw ilmenite, thus this study may conclude that the presence of Ti⁴⁺ species only in raw ilmenite. The XPS spectrum of O 1s core level of raw ilmenite was displayed in Figure 4.3c with the E_g at 529.60 eV which is in contrast compared with previous studies on pure TiO₂ with the E_g at ~530 eV (Bharti et al., 2016; Ghafoor et al., 2017). The negative E_g shift of lattice O²⁻ may because of the high concentration of Fe-O-Ti bonds in raw ilmenite. The O 1s peak can be further separated into several contributions corresponding to the bonding with Fe and Ti. The main contribution is from Ti⁴⁺ by Ti-O bonding. The second contribution is from Fe³⁺ by Fe-O bonding and the remains are attributed by carbon bonding from adventitious hydrocarbon in XPS itself which are not displayed in Figure 4.3c. The oxidation state of Fe is shown in Figure 4.3d. The peak position of Fe 2p_{3/2}, Fe 2p_{1/2} and satellite peak are 710.8, 724.0 and 718.5 eV respectively, which experienced small shift compared to Fe₂O₃ (Yamashita & Hayes, 2008). This may due to the diffusion of Fe³⁺ ions into TiO₂ lattice structure (Glisenti, 2000). However, there is no peak from Fe²⁺ was observed because of the Fe²⁺ ions in low concentration thus beyond detection from the instrument. The formation of satellite peak

in the XPS is because of the ionisation of X-ray with slightly higher photon energy than the main Al K α line (Zhang et al., 2008).

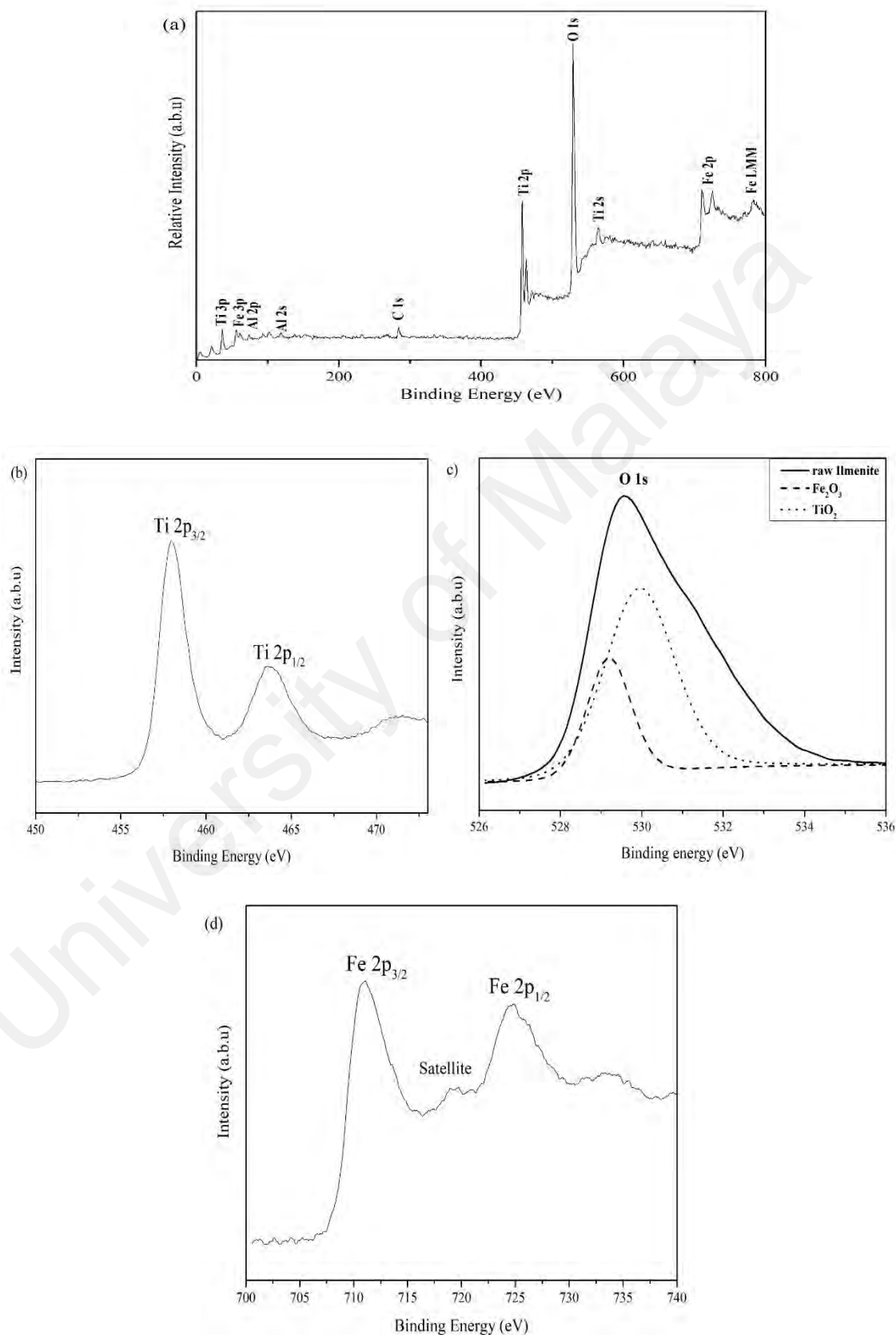


Figure 4.3: XPS survey (a) spectrum of raw ilmenite and XPS spectra of (b) Ti 2p (c) O 1s and (d) Fe 2p

The surface stability of raw ilmenite was identified by zeta potential and the result is shown in Figure 4.4. The point of zero charge (PZC) of raw ilmenite is located at pH 4.5 whereas the pure rutile TiO_2 is proposed to be at pH 5.4 (Kosmulski, 2002). Hence, the surface zeta potentials of raw ilmenite were more negative than pure rutile TiO_2 , suggesting that the surface of raw ilmenite are acidic. The OH group on the TiO_2 surface which located at terminal sites and bridging sites represent as basic and acidic sites respectively (Miyachi et al., 2004). The reported pK_a value for OH groups at the basic and acidic site are 12.7 and 2.9 with nearly identical amount of OH groups in both sites (Boehm, 1971). Hence, the TiO_2 has neutral value on IEP and exhibits amphoteric properties. Previous studies suggested the electronegativity of metal ions will affect the strength of the O-H bonding on it. For example, the strength between O-H bonding relies on the polarisation of covalent electron pairs (Misono et al., 1967; Tanaka & Ozaki, 1967). On the other hand, Zhou et al. (2006) reported that increase of dopant concentration in metal-doped TiO_2 will decrease the PZC value of the catalyst due to the surface enrichment of species with an acidic behaviour. Furthermore, the acidity of a metal ion increase with its electronegativity according to Lewis concept, and Fe (1.88) has higher electronegativity value than Ti (1.54), thus the shift of the PZC value suggested that the surface of raw ilmenite is enriched with Fe ions. Previous studies suggested that the PZC of the raw ilmenite ranged from pH 4 to 6.5. Hence, the PZC value of the raw ilmenite in this study is consistent with the literature (Mehdilo et al., 2013).

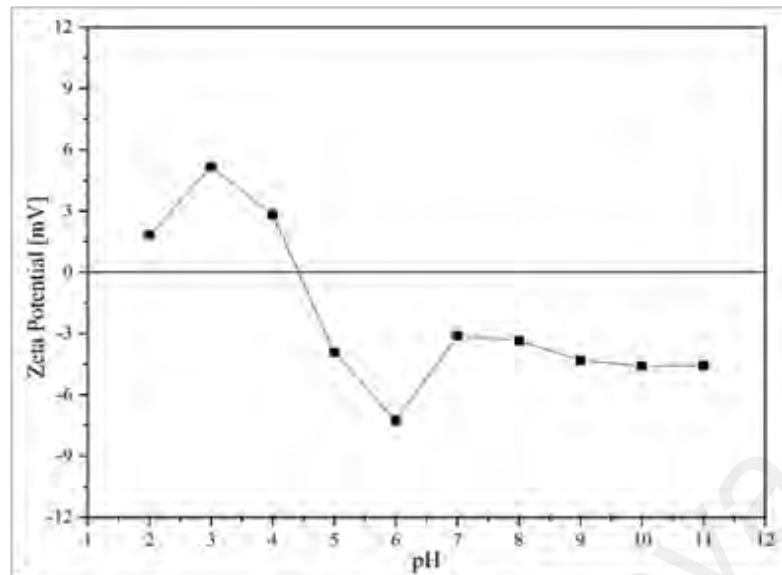


Figure 4.4: Zeta potential of raw ilmenite, PZC of raw ilmenite is at pH 4.5.

The surface area and the pore structure of the raw ilmenite were determined by N_2 physical adsorption-desorption studies. Figure 4.5a shows the BET isotherm and the relative Barret-Joyner-Halender (BJH) pore size distributions obtained from the desorption branch of the isotherms of the raw ilmenite. It was observed that the raw ilmenite had mesoporous surface as the isotherms are of Type IV. Based on the adsorption data in relative pressure (P/P_0) range (0.44 – 0.98), the BET specific surface area for raw ilmenite was found to be $16.2 \text{ m}^2/\text{g}$. From the BJH pore size distributions (Fig 4.5b), it was observed that the sample showed a narrow pore size distribution with pore width between 1.0 – 1.5 nm.

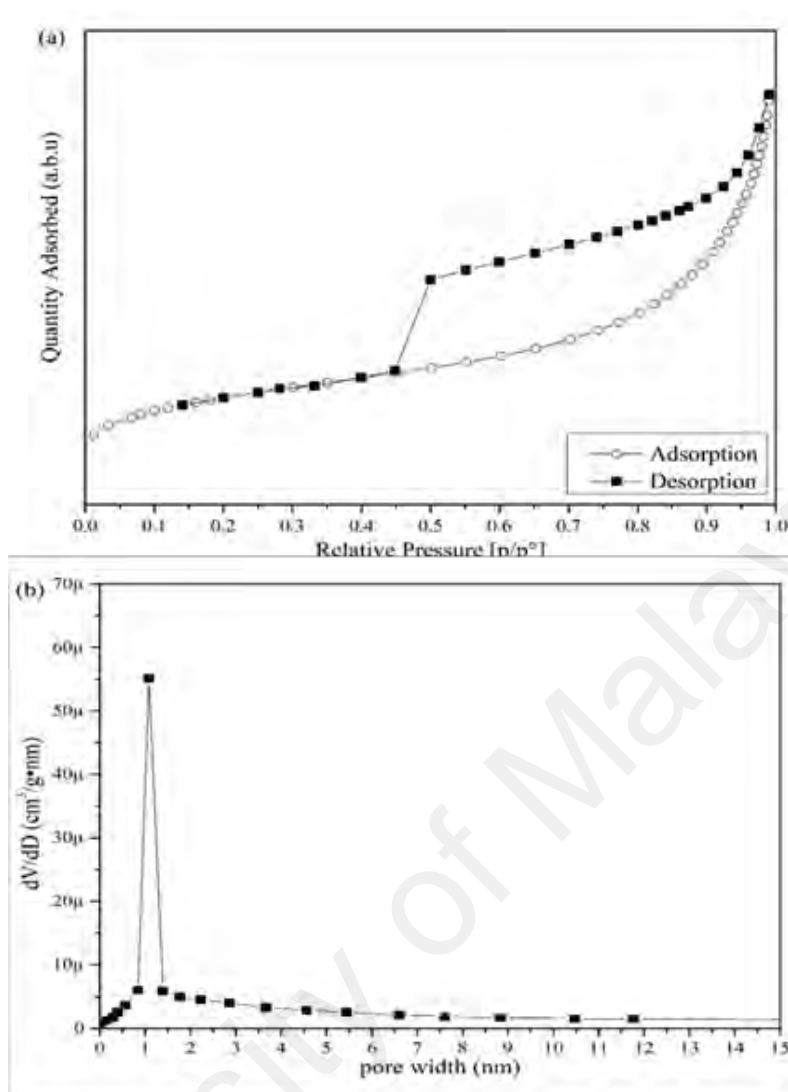


Figure 4.5: (a) N_2 adsorption-desorption BET isotherm for raw ilmenite (b) the BJH pore size distribution (from the desorption branch of the isotherms).

The micro morphology of raw ilmenite is illustrated in Figure 4.6 using FESEM. The figures revealed raw ilmenite had irregular shape overall. Besides that, some small size raw ilmenite formed agglomeration together and the agglomeration was scattered on the surface of bigger size raw ilmenite. This small raw ilmenite is beneficial for the catalytic activity of raw ilmenite as the RB 5 reaction takes place on the surface of the catalyst, prompting more RB 5 dye can be adsorbed on the surface of raw ilmenite prior photo-degradation reaction. Moreover, small size raw ilmenite has larger active surface area and a large number of active reaction sites for chemical reaction to occur which also enhances and allow more generation of photo-induced electron.

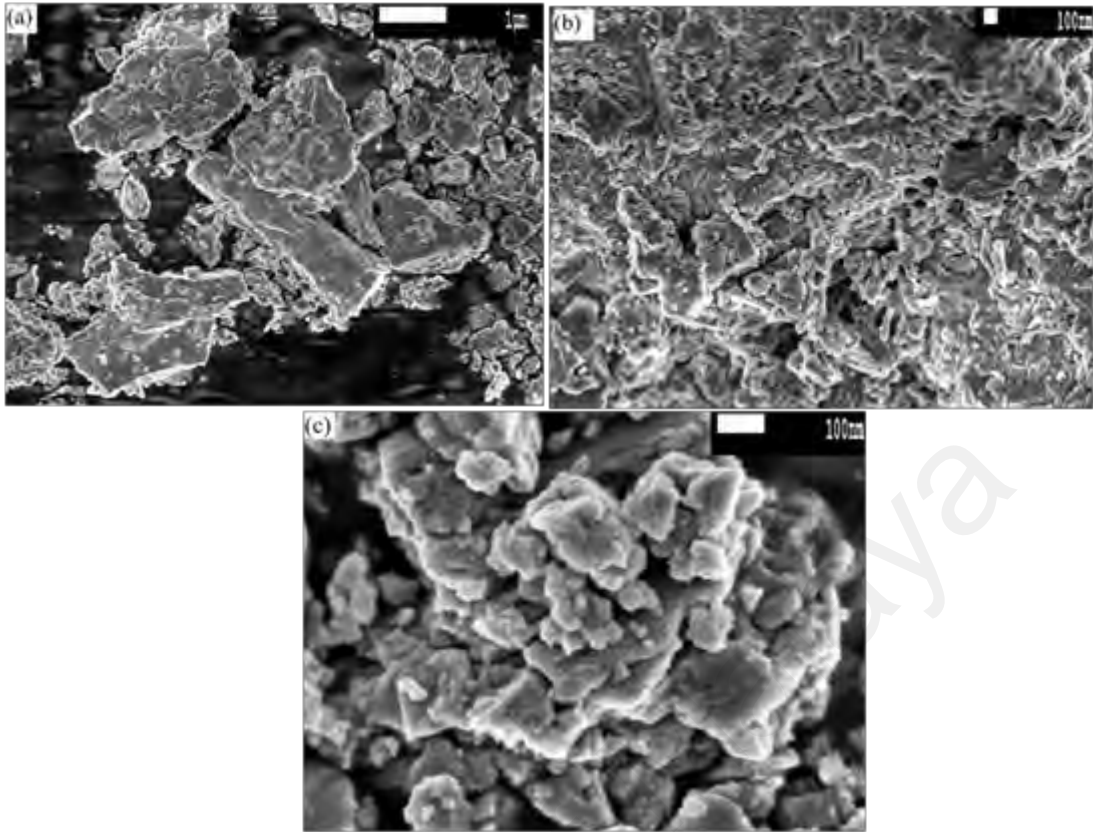


Figure 4.6: FESEM images of the raw ilmenite: a) raw ilmenite powder; b,c) a close up on the surface of raw ilmenite powder.

Based on the literature, it could be noticed that band gap energy of raw ilmenite is 2.5 eV which is lower than pure rutile TiO_2 (3.0 eV). The narrowed band gap of raw ilmenite is due to the occurrence of Fe that provides new dopant levels, thus lowering the charge transfer transition between valence band and conduction band. There are no studies regards the band level for Fe ion located in raw ilmenite because it formed naturally, but manmade Fe doped TiO_2 studies could provide some insights on the optical properties of raw ilmenite as shown in Figure 4.7. As Fe ions has *p*-type semi-conducting behaviour when it doped with TiO_2 with 1.72 – 2.7 eV band gap (Abazović et al., 2009a; Navio et al., 1992; Soo et al., 2016; Zaleska, 2008), therefore this study could proposed that the Fe ions may locate at conduction band region in raw ilmenite.

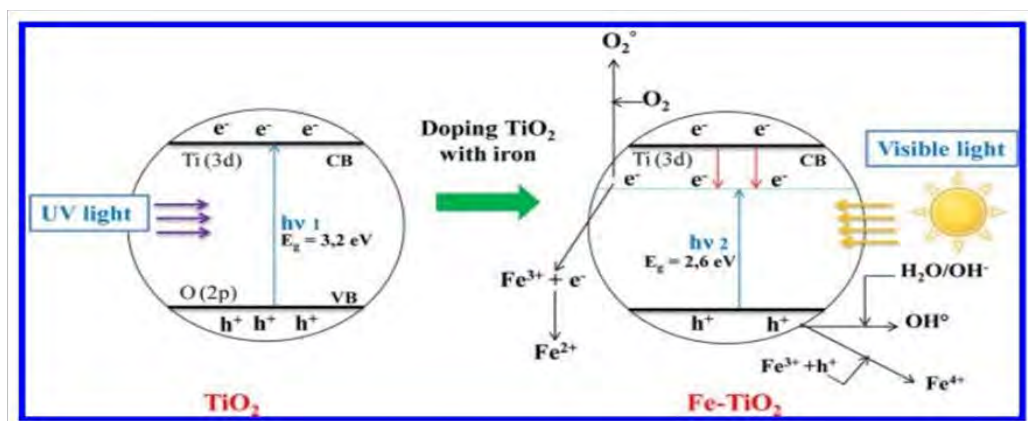


Figure 4.7: Proposed schematic energy level of manmade iron doping TiO_2 . (Daghrir et al., 2013)

Alternatively, Photoluminescence (PL) was carried out to examine the recombination rate of photo-induced charge carriers in raw ilmenite. The peaks/shoulders (Fig. 4.8) suggested that the defects are formed in/on the crystal lattice of raw ilmenite (Abazović et al., 2009b). The formation of defects occurred in raw ilmenite may due to bulk defects and oxygen vacancies in the lattice structure. Previous studies also suggested that the high energy peaks in photoluminescence diagram can be attributed to band edge luminescence of the catalyst particle while on the contrary oxygen vacancies in the lattice structure of the catalyst can cause lower energy peaks/shoulders (Abazović et al., 2006; Abazović et al., 2008). Since raw ilmenite formed naturally, it has naturally-occurring defects in the lattice structure, which may affect the photo-catalytic activity of raw ilmenite through the recombination of photo-generated charge carriers through oxygen vacancy-cascade processes.

Previous studies have been conducted by using raw ilmenite for pollutants photo-degradation and it seems like raw ilmenite has a large gap to be a better photo-catalyst (Moctezuma et al., 2011). However, several considerations should be taken into account for the removal of pollutants in wastewater through photo-degradation especially the chemical properties of wastewater. In the following section, some parameters were proposed to study the photo-catalytic activity of raw ilmenite.

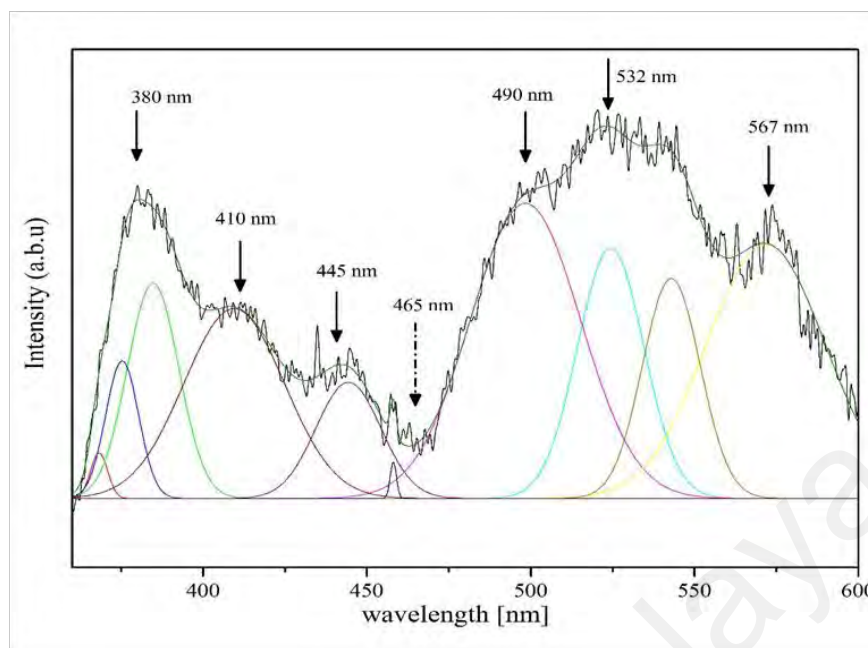


Figure 4.8: Photoluminescence data of raw Ilmenite.

4.2.2 Photo-degradation process of RB5 using raw ilmenite

4.2.2.1 Effect of pH

The pH of wastewater is known to play an important role in the photo-degradation (Chen et al., 1999; Yu et al., 2006). Therefore, pH of RB 5 dye solution was adjusted accordingly. The absence of raw ilmenite at different pH values is shown in Figure 4.9a. The highest photo-catalytic activity is under acidic condition at pH 2 (25%). The removal of RB 5 dye was negligible when the experiments were conducted at pH 4, 6 and 9, respectively. In the presence of raw ilmenite, the dye degradation (C_t/C_0) of RB 5 showed higher degradation rate at pH 2 ($C_t/C_0 = 0.4415$, 55%) but decreased gradually until total inhibition as the pH increased to 9. The kinetic constant rate of raw ilmenite dropped from 0.04047 min^{-1} at pH 2 to 0 at pH 9.

The pH of RB 5 solution plays a significant role in photo-catalytic degradation because pH affects the ionization state of the photo-catalyst surface as well as RB 5. The changes of pH can influence the adsorption of RB 5 onto the surface of ilmenite; hence increase the photo-degradation rate. As the PZC of raw ilmenite is 4.5 (Fig. 4.4), thus the surface of raw ilmenite is positively charged at $\text{pH} < 4.5$ and negatively charged at $\text{pH} > 4.5$. RB

5 is an anionic dye as the sodium ions react with water molecules and leave the dye molecule with negative charge at $\text{pH} < 4.5$. Therefore, at low pH ($\text{pH} < 4.5$) the electrostatic attraction between RB 5 dye molecules and surface of raw Ilmenite will favour the adsorption and subsequently leads to higher degradation. In addition, the RB 5 molecules with 0.9 nm can penetrate into the pore and be absorbed on the inner surface of raw ilmenite (Tze et al., 2015), thus more RB 5 molecules can be absorbed by raw ilmenite prior photo-catalytic activity. It is necessary to highlight that at lower pH, more amounts of Fe may leach out from raw ilmenite (Table 4.1), and the free Fe ions may increase the production of radical hydroxyl group through homogenous Fenton or Fenton-like reaction (Pataquiva-Mateus et al., 2016). Notably, as the $\bullet\text{OH}$ radicals can be formed into H_2O_2 , the H_2O_2 can be subsequently broken down by ferrous and ferric ions in the solution (Eq 4.1-4.3) (Kang et al., 2002a; Machulek et al., 2006). Thus, it corresponded to a drastic increase in dye degradation (C_t/C_0) from pH 3 to pH 2. Al, Mg and Si ions were detected as well, probably due to the impurities in ilmenite whereas Na was from RB 5 dye.



Table 4.1: Elementary analysis of RB 5 solution at pH 2 with catalyst loading 1.0 g/L under solar irradiation for 20 min.

Element	Concentration [mg/L]	Standard deviation	RSD [%]
Fe	0.088	0.004	3.92
Al	0.009	0.002	24.27
Na	0.773	0.009	1.15
Mg	0.034	0.002	8.70
Si	0.294	0.010	3.44

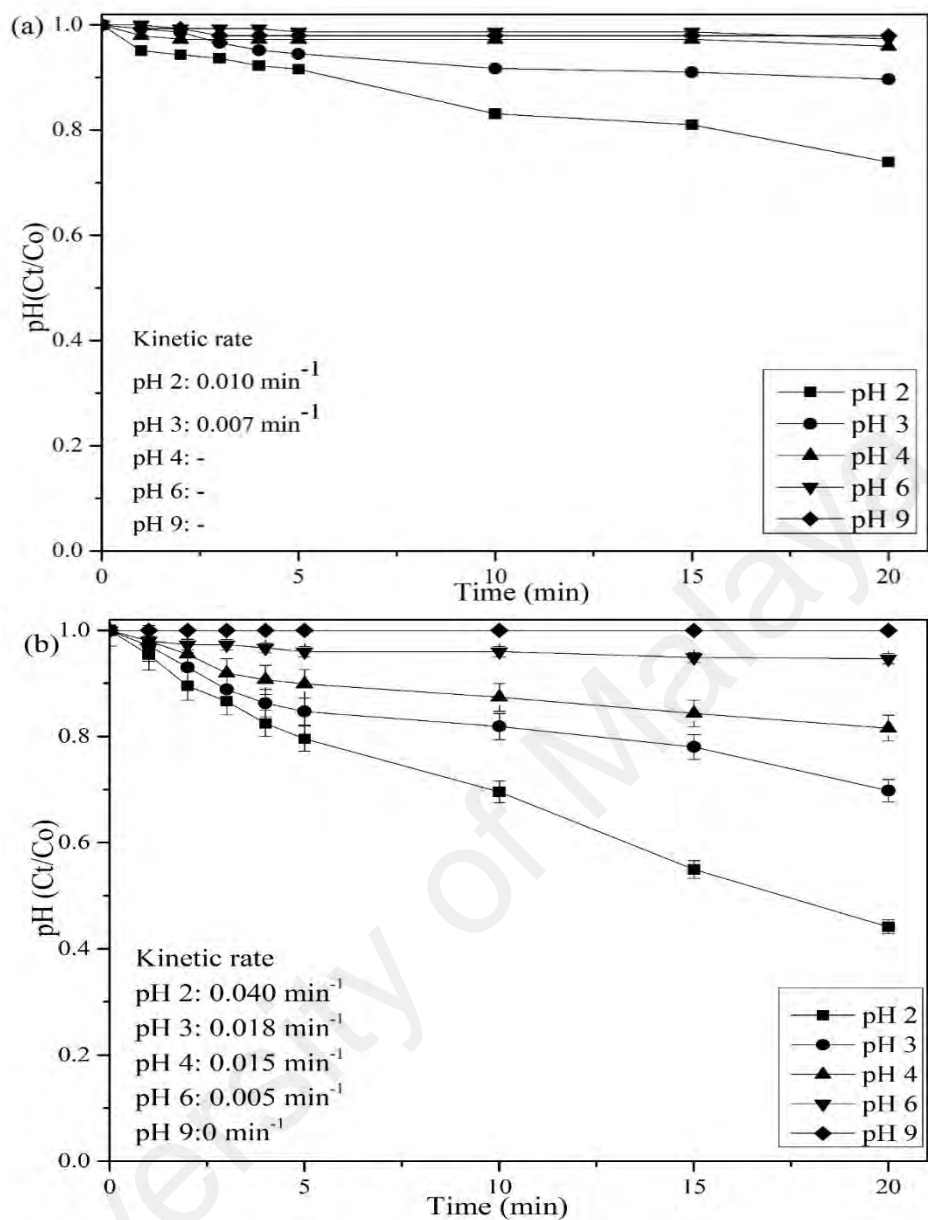


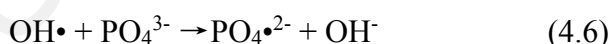
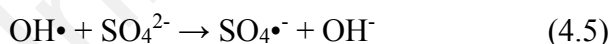
Figure 4.9: Effect of dye degradation at various pH value (a) absence of raw ilmenite (b) presence of raw ilmenite. (Dye concentration 5 ppm, catalyst loading 1g/L, 25°C)

4.2.2.2 Inorganic ions as hydroxyl radical scavengers

Based on afore mentioned discussion, pH 2 exhibited the best photo-degradation performance with maximum dye degradation of 55%. Therefore, in the following studies, different type of acids were introduced into RB 5 solution in such condition mentioned above to study the effect of inorganic ions presence. Several literature works have been

shown that the presence of optimum content of inorganic ions could affect the efficiency of photo-catalytic degradation of organic pollutants significantly due to the competition between pollutants and inorganic ions for $\bullet\text{OH}$ radicals (Akpan & Hameed, 2009; De Laat et al., 2004; C. Hu et al., 2003; Selvam et al., 2007). At pH 2, the kinetic rate of dye degradation was 0.04047, 0.01958, 0.00552 and 0.00299 min^{-1} in the presence of HNO_3 , HCl , H_2SO_4 and H_3PO_4 , respectively (Fig. 4.10). The presence of PO_4^{3-} demonstrated highest inhibition meanwhile NO_3^- has the lowest effect. Thus, the order of inhibition of these anions are $\text{PO}_4^{3-} > \text{SO}_4^{2-} > \text{Cl}^- > \text{NO}_3^-$.

On the whole, the presence of NO_3^- produced less effect because NO_3^- will not react with $\bullet\text{OH}$ and thus the photo-degradation rate of RB 5 dye was not inhibited (De Laat et al., 2004; Lu et al., 1997; Ratanatamskul et al., 2010). On the other hand, Cl^- , SO_4^{2-} and PO_4^{3-} anion are known to be $\bullet\text{OH}$ scavengers, which adsorbed on the surface of the catalyst then react with $\bullet\text{OH}$ generated and formed $\text{Cl}\bullet$, $\text{SO}_4^{\bullet-}$ and $\text{PO}_4^{\bullet 2-}$ (Eq 4.4 - 4.6), which are less effective in pollutant oxidation (De Laat et al., 2004; C. Hu et al., 2003). Below are the proposed reactions between $\bullet\text{OH}$, Cl^- , SO_4^{2-} and PO_4^{3-} (Akpan and Hameed, 2009; C. Hu et al., 2003; Riga et al., 2007; Selvam et al., 2007):



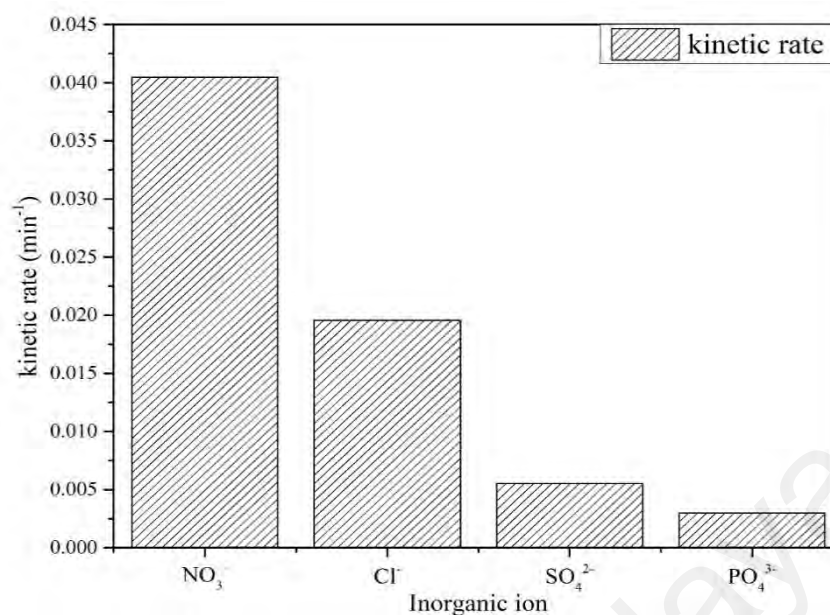


Figure 4.10: Kinetic rate of dye degradation of raw ilmenite in the presence of different inorganic ion at pH 2 (dye concentration 5ppm, catalyst loading 1g/L, 25 °C)

4.2.2.3 Catalyst loading in RB 5 solution

According to afore mentioned discussion, raw ilmenite has the best photo-degradation performance under acidic condition in the presence of NO₃⁻. In the following studies, the catalyst loading of raw ilmenite in RB 5 solution was studied in such condition mentioned previously. The amount of raw ilmenite was varied from 0.5 to 2.0 g/L. Figure 4.11 clearly shows that the catalyst loading affects the photo-degradation of RB 5. The result (Fig 4.11) showed that the overall dye degradation rate was directly proportional to the increment of catalyst loading. A significant increment in degradation efficiency was shown when the catalyst loading increased from 0.5 g/L ($C_t/C_0 = 0.4858$) to 2.0 g/L ($C_t/C_0 = 0.27$). The degradation of RB 5 using raw ilmenite obeyed pseudo-first order kinetic rate at all catalyst loadings and the kinetic rate constant of raw ilmenite increased from 0.03621 (0.5 g/L) to 0.07088 min⁻¹ (2.0 g/L). The increment of catalyst loading provides more active site of raw ilmenite for RB 5 to be adsorbed on the surface prior photo-degradation reaction, hence increase the kinetic rate of photo-catalytic activity of raw

ilmenite. The complete degradation of dye was observed after 120 minutes irradiation of artificial light with 2.0 g/L catalyst loading as shown in Appendix A.

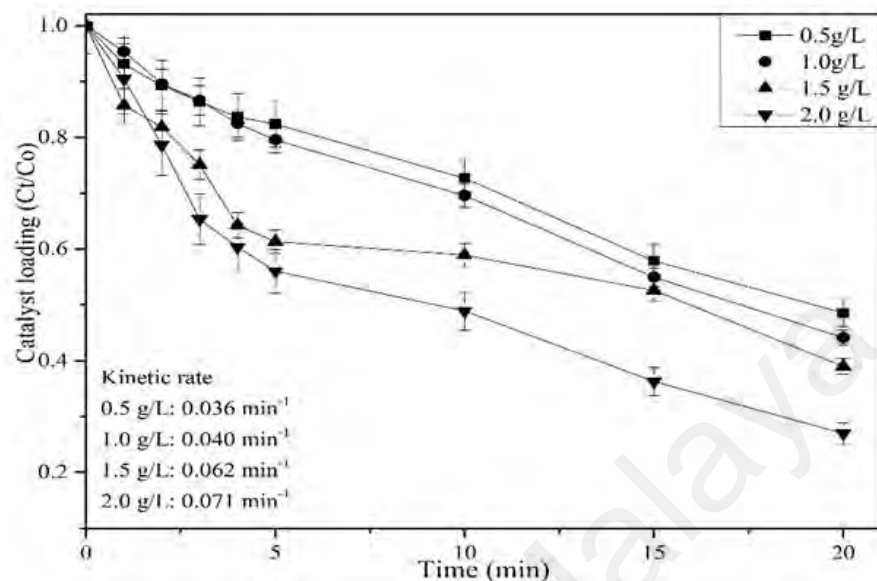


Figure 4.11: Effect of dye degradation at various catalyst loading at pH 2. (Dye concentration 5 ppm, temperature 25°C)

4.3 Physicochemical properties of pre-treated ilmenite at different HCl concentration

The photo-catalytic activity of pre-treated ilmenite at different HCl concentrations, exposure time, exposure temperature and calcination temperature had also been carried out (Appendix B). It is interesting to observe that the most significant parameters were HCl concentration and thus the physicochemical properties and photo-catalytic activity of pre-treated ilmenite at different HCl concentrations have been well studied.

4.3.1 EDX analysis

Table 4.2 shows the EDX of the pre-treated ilmenite which underwent treatment at different HCl concentrations at 110 °C. The increment of HCl concentration imposed a significant effect on Fe removal as nearly 0.77% of Fe content remained or 99.2% of Fe has been removed in the ilmenite sample pre-treated with 35% HCl as compared to 7.15% Fe content in the sample pre-treated with 15% HCl concentration (92.9% removal). It was

clearly indicated that low HCl concentration was not capable to fully dissolve Fe and Ti into solution, thus more Fe atom still exist in the lattice structure in H-15 and H-20.

The greatest influencing factor towards dye removal efficiency was the acid concentration. This is because of the relationship between the concentration of chloride, Fe and Ti ions. In general, Fe doping in TiO₂ had narrowed the band gap of TiO₂ but at high concentrations, Fe ions may become recombination centres through quantum tunnelling, which results in rapid recombination of charge carriers and reduction in the photo-catalytic activity of iron doped TiO₂ (Abazović et al., 2009a; Zhou et al., 2005). Hence, the acid concentration was the main factor to reduce Fe concentration in raw ilmenite in order to produce high photo-catalytic activity of pre-treated ilmenite.

Table 4.2: EDX of pre-treated ilmenite under different HCl concentration. (Temperature: 110 °C, reaction time: 24 h)

Sample	Fe [atomic%]	Ti [atomic%]	O [atomic%]
Raw ilmenite	18.54	23.57	57.89
H-15 (15 v/v% HCl)	7.15	21.63	71.22
H-20 (20 v/v% HCl)	5.73	33.54	60.73
H-25 (25 v/v% HCl)	1.62	47.37	51.00
H-30 (30 v/v% HCl)	1.18	38.88	59.94
H-35 (35 v/v% HCl)	0.77	24.12	75.12

4.3.2 Raman analysis

Figure 4.12 presents the Raman plot of pre-treated ilmenite under treatment of various HCl concentrations. Several works revealed the relationship about the Raman-active “lattice vibrations” with the bond length and covalence correlations (Balachandran & Eror, 1982; Hardcastle & Wachs, 1990, 1991). The distinct rutile TiO₂ peak can be observed at H-25, H-30 and H-35 samples. This is because more Ti atom dissolved into solution as TiOCl₂ as an intermediate product and the TiOCl₂ then precipitated and polymerised to form TiO₂. These distinct peaks corresponded to the pure rutile phase at

four active modes, which were 143(B_{1g}), 236, 447(E_g), and 613(A_{1g}) cm^{-1} (Balachandran & Eror, 1982; Bersani et al., 1998; Mazza et al., 2007; Ocaña et al., 1992). The Ti-O bonds were observed at 447 and 610 cm^{-1} , O-O interactions occurred at region from 250-394 cm^{-1} and Ti-Ti bonds gave a sharp peak at 143 cm^{-1} (Cromer & Herrington, 1955; Hardcastle, 2011). A dominant peak at 130 – 140 cm^{-1} range was observed at H-15 and H-20 samples. It is worthy to note that the significant Raman peak of raw ilmenite was not seen in the plot, which suggested that most of Fe-Ti bonds had been broken, leaving Ti in the lattice structure, thus the Ti-Ti bond peak intensity was high. The Raman peaks of pre-treated ilmenite were blue-shifted from 430 to 447 cm^{-1} with peak sharpening along with the increment of HCl concentration. Peak sharpening may indicate that the rutile TiO_2 produced using high acid concentration has better crystallinity whereas the blue-shift suggested the presence of defects such as oxygen vacancies (Samsudin et al., 2015).

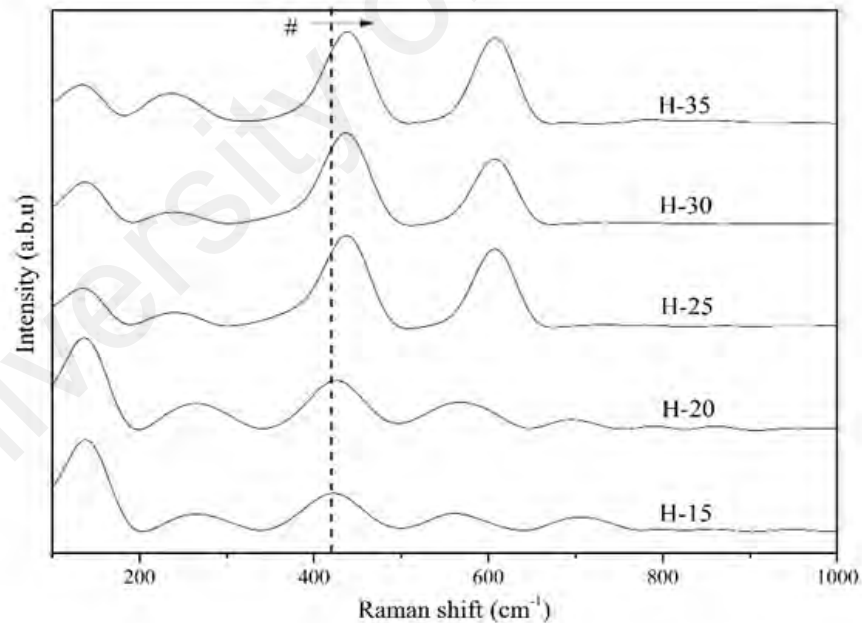


Figure 4.12: Raman plot of pre-treated ilmenite with different HCl concentration

4.3.3 XRD analysis

Figure 4.13 shows the XRD profile of the quality and crystalline phase of pre-treated ilmenite. In the XRD patterns, the rutile TiO_2 phase was clearly shown from the presence of the (110), (101), (111), (211) and (220) peak and they corresponded to these JCPDS references (JCPDS: 01-083-2242, 01-084-1284, 01-078-1510, 01-076-0649 and 01-089-0553). The XRD pattern of raw ilmenite in Figure 4.1 was not observed in Figure 4.19, which suggested the destruction of raw ilmenite lattice structure by acid leaching. It is worthy to point out that low concentration of acid promoted the growth of rutile TiO_2 in pre-treated ilmenite since the rutile TiO_2 peak was observed in XRD of H-15 sample. The increase of acid concentration promoted more dissolution of raw ilmenite thus more rutile TiO_2 formed in pre-treated ilmenite with low Fe content which reflected in EDX result (Table 4.2). However, all pre-treated ilmenite sample did not show any Fe related peaks. This is because the Fe ions may have been located in interstitial positions of the TiO_2 nano-crystal structure or the concentration is too low to be detected (El-Hazek et al., 2007). Based on the Scherrer equation, the crystalline size of rutile in pre-treated ilmenite was in the range of 52 – 69 nm (Table 4.4). The difference of the crystalline size of rutile between raw and pre-treated ilmenite due to the hydrolysis and polymerisation of TiO_2 during chloride leaching process and the absence of the foreign element in the structure, thus increase the crystalline size of rutile in pre-treated ilmenite (Soo et al., 2016; Yang et al., 2009).

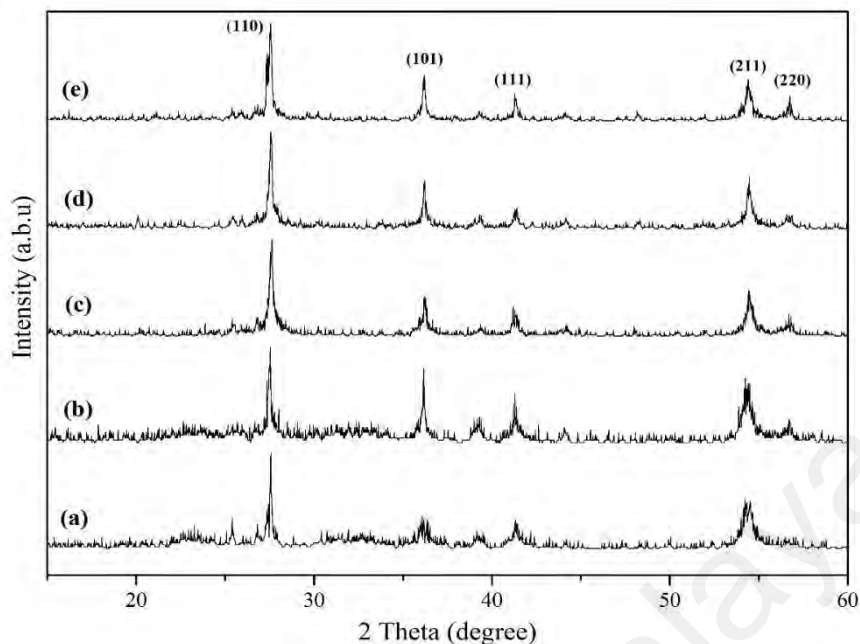


Figure 4.13: XRD pattern of pre-treated ilmenite prepared by chloride leaching process: (a) H-15, (b) H-20, (c) H-25, (d) H-30, (e) H-35.

4.3.4 XPS analysis

Figure 4.14 shows the broad XPS spectrum of the H-25 sample, which was selected to be investigated because of its excellent photo-catalytic activity which will be discussed in section 4.4. From the Figure 4.14, the Fe 2p peak was not observed, and therefore suggesting that the concentration of Fe was quite low in the H-25 sample. A similar observation was also reflected by Tao et al. (2013) in the production of rutile TiO₂ with low Fe impurities. In addition, the absence of Al 2p peak indicated the dissolution of impurities during chloride leaching process. Table 4.3 summarises the binding energies of Ti 2p and O 1s signals. The signals from both elements are similar to the reference XPS spectra of rutile TiO₂ (Diebold & Madey, 1996). Thus, these results confirmed that the production of high purity rutile TiO₂ in pre-treated ilmenite.

Table 4.3: The binding energy of Ti and O from H-25 pre-treated ilmenite sample

Element	Ti 2p _{3/2}	O 1s
Binding Energy (eV)	459.1	530.1

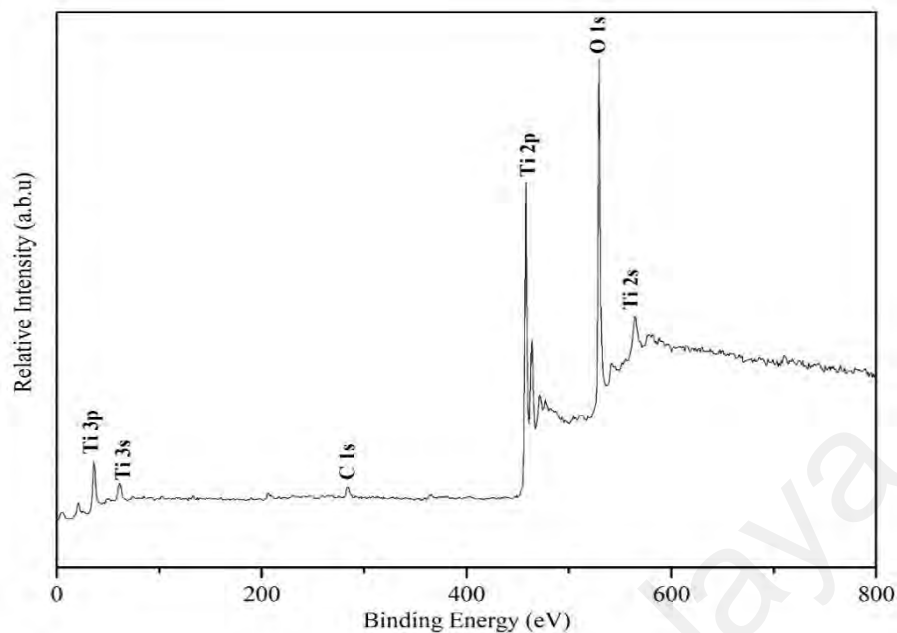


Figure 4.14: XPS survey spectrum of H-25 pre-treated Ilmenite sample

4.3.5 Nitrogen absorption-desorption analysis

The surface area of raw ilmenite was recorded as 16.2 m²/g and the chloride leaching process had changed the surface area of the ilmenite material. The changes of the surface area are mentioned in Table 4.4. The measured surface area of H-15 pre-treated ilmenite was 18.1 m²/g and gradually increased to 37.3 m²/g (H-25) along with acid concentration. However, a further increase in acid concentration beyond 25% resulted in a negative impact toward the surface area. The surface area of H-35 sample has reduced to 25.5 m²/g. The changes of the surface area could be probably due to the effect of the concentration of Cl⁻ and Ti⁴⁺ in the solution. At the beginning, the rise of surface area at lower acid concentrations was due to the dissolution of Fe from raw ilmenite, thus leaving a porous layer on the structure ilmenite. Ti ions were dissolved into the solution at the same time and its concentration in the solution increased proportionally with HCl concentration, then the Ti ions will be hydrolysed and precipitated into TiO₂. However, high HCl concentration (30 – 35% in this study) will also increase Cl⁻ concentration in the solution. In the environment of high Cl⁻ concentration will cause the Ti⁴⁺ remained in the formed of

complex titanyl chloride compounds in the solution, thus hinder the hydrolysis of TiO_2 (Cservenyák et al., 1996). Therefore this caused lesser recovery of Ti from the solution and leading to lower amount of TiO_2 formed in H-35 samples. Low Ti recovery rate in high acid concentration was reported in other literature (Mahmoud et al., 2004). The reduction of surface area in these pre-treated ilmenite samples affected their photo-catalytic activity by reducing a number of active surface sites for RB 5 molecules to be absorbed on the surface of photo-catalyst, thus reduced the kinetic rate of photo-degradation. This is well agreed with the other researchers found in which the reduction of surface area gives a significant effect on the photo-catalytic activity (Wantala et al., 2010). All sample remained as mesoporous with type IV nitrogen absorption-desorption linear isotherm (Fig. 4.15). Distinct changes observed in the linear isotherm curve implied morphological and structural changes. Based on Figure 4.15, all these curves conform to the IUPAC type H3 loops, indicated that the internal porosity is slit-shaped and panel-shaped. The pore size distribution in each pre-treated ilmenite sample has been summarised in Table 4.4 and Appendix C. The sample of H-15, H-20, H-25, and H-30 featured pore size of 3 – 4 nm which was bigger than raw ilmenite. This might be attributed to the loss of Fe in the lattice structure which contributed to the porous structure. But H-25 and H-30 featured another bigger pore size could probably indicate significant amount of TiO_2 was precipitated from the solution and agglomerated, thus H-25 and H-30 has bimodal pores. In addition, the pore size has significantly enlarged up to 20-40 nm and also lost of the surface area upon treatment with 35 v/v% HCl. As explained earlier, this was due to the reorganisation of rutile TiO_2 via hydrolysis instead of solely on the dissolution of Fe ions.

Table 4.4: pore size distribution of pre-treated ilmenite sample.

Sample	Surface area (m ² /g)	Pore size distribution (nm)	Crystallite size (nm) ^a
Raw ilmenite	16.2	1 - 2	2.96
H-15	18.1	3 - 4	69.3
H-20	22.1	3 - 4	35.6
H-25	37.3	3 - 4, 12 - 23	52.0
H-30	30.1	3 - 4, 15 - 33	69.2
H-35	25.5	20 - 40	69.3

^aBased on Sherrer equation from XRD peak at (110)

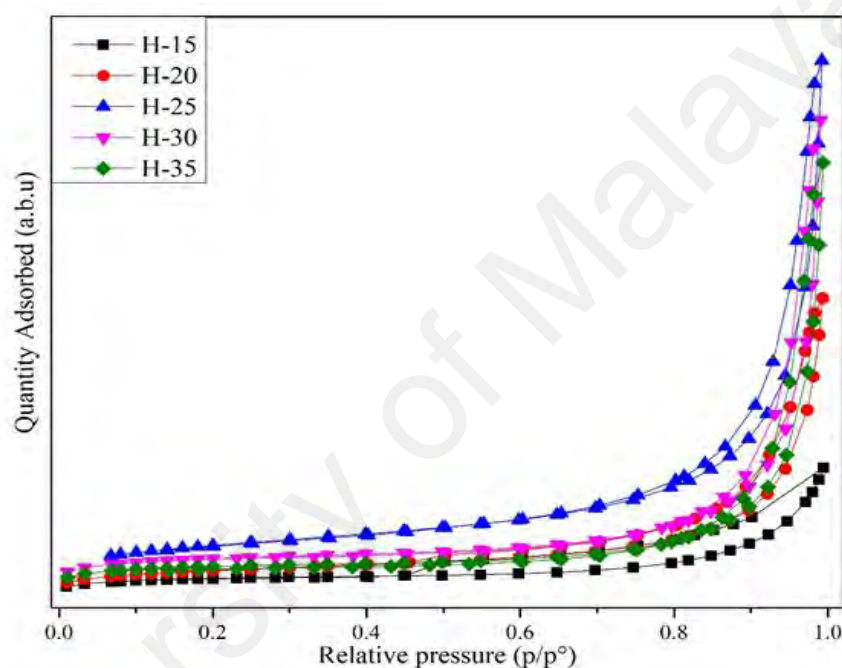


Figure 4.15: Nitrogen adsorption/desorption linear isotherm for all pre-treated ilmenite sample.

4.3.6 FESEM

The morphology of pre-treated ilmenite samples is observed under field emission scanning electron microscope (FESEM) are shown in Figure 4.16 (a-c). The morphology of pre-treated ilmenite sample has significant differences in terms of shape and size uniformity. Large quantities of small size of pre-treated ilmenite is observed in sample H-25 and H-35 (Fig. 4.16 b&c) whereas similar observation did not reflect in sample H-15, indicates an increase of acid concentration promoted hydrolysis of TiO₂. Thus, H-25

sample showed plenty of irregular tiny cluster of pre-treated ilmenite. On the other hand, a well distributed and uniform particle size of 20-40 nm is observed for H-35 with a mixture of small irregular and flat disc shape. Hence, the changes in the morphology in H-35 samples explained low surface area compared with H-25 sample reported in BET result.

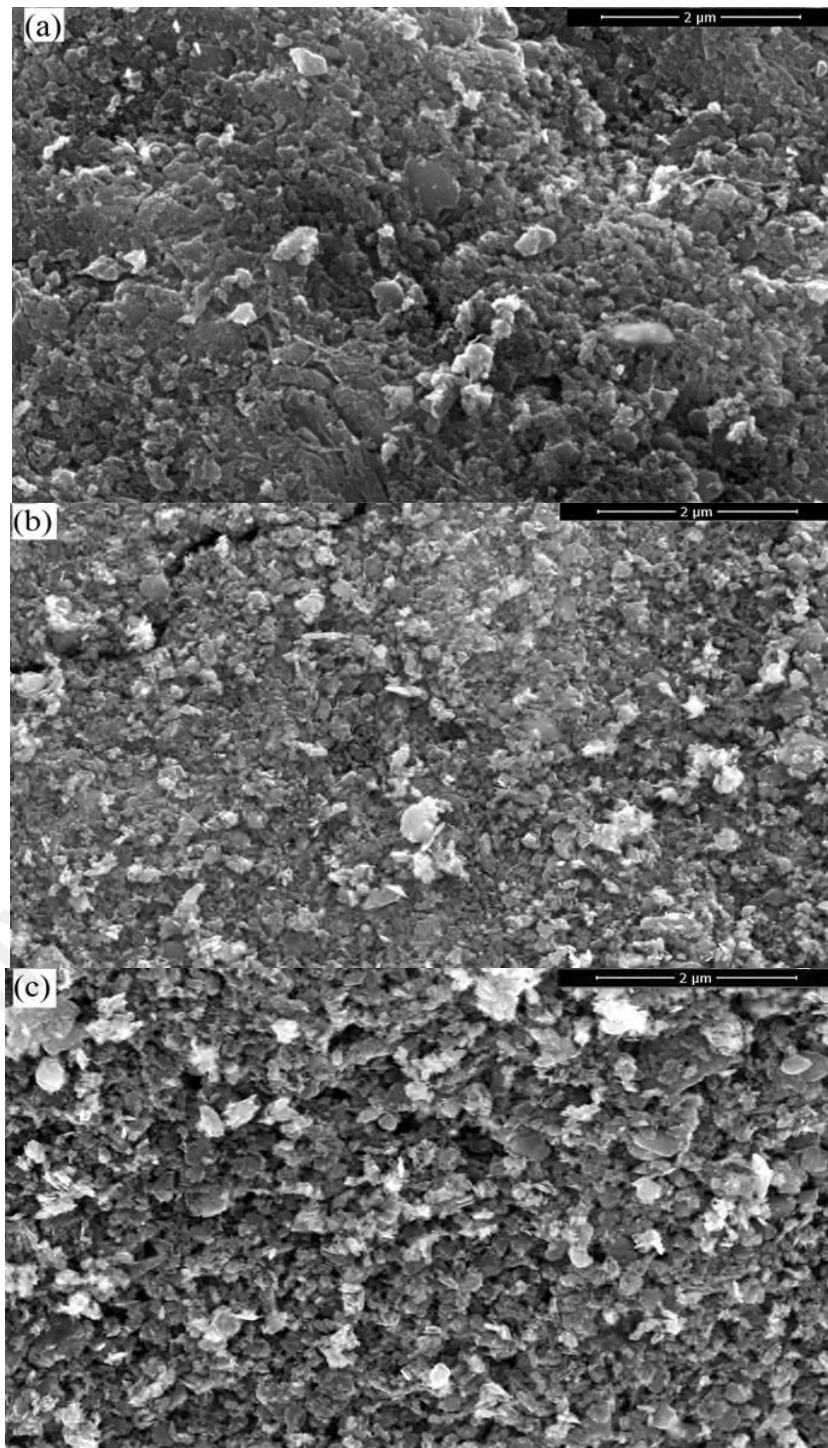


Figure 4.16: Surface morphology at magnification of 50,000× for (a) H-15, (b) H-25 and (c) H-35

4.3.7 DR UV-Vis analysis

All pre-treated ilmenite samples possessed rutile crystal phase with iron as a foreign element, readily promoting solar light absorption of UV and visible region. The rutile crystal phase can be activated under UV and visible light because of its smaller band gap compared with anatase crystal phase. It is widely reported that Fe-doped rutile TiO₂ possessed smaller band gap, increased light absorption ability and enhanced radical formation. In addition, the small amount of Fe inhibited carrier charge recombination which leads to good photo-catalytic response (Crişan et al., 2015; Wan et al., 2011; Zarazúa-Morín et al., 2016). Theoretically, raw ilmenite has the band gap energy of 2.5 eV, thus it has the ability to absorb light in both UV and visible region. The present study showed that an increase of band gap energy of pre-treated ilmenite was observed along with increasing the use of acid concentration (Fig. 4.17). The increment of band gap energy may indicate the reduction of Fe concentration and also the formation of rutile TiO₂ in pre-treated ilmenite. This is in well agreement with previous studies that reported lower band gap energies in TiO₂ with high Fe concentration (Abazović et al., 2009a). The authors attributed the lower band gap energy as a result of high Fe concentration as Fe ions can be either recombination centre or as charge transfer centre. H-25 has band gap energy of 2.84 eV which is lower as compared to that of pure rutile TiO₂ (3.0 eV) due to the contribution of Fe which can act as dopant. The interstitial impurities such Fe may attribute to the rise to locals states below the conduction edge (Tao et al., 2013). Similar results have been reported with similar band gap energy from Fe-doped TiO₂ (Abazović et al., 2009a; Raghavender et al., 2013; Tao et al., 2013).

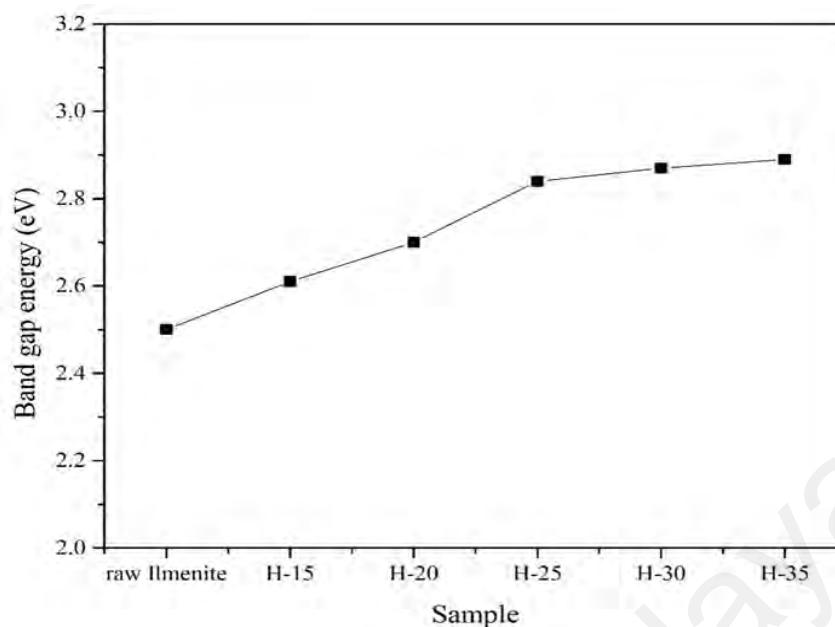


Figure 4.17: Changes in band gap energy of pre-treated ilmenite sample by leaching raw ilmenite with different concentration of HCl

4.3.8 Photoluminescence analysis

The photoluminescence (PL) spectrum in Figure 4.18 illustrates the efficiency of charge carrier trapping, migration, transfer and the fate of photo-generated electrons and holes. The H-25, H-30 and H-35 PL spectra show a broad peak near 430 nm which corresponds to the band-band transition photoluminescence of rutile TiO₂ (Yan et al., 2013). Alternatively, the similar peak was not observed in H-15 and H-20 PL spectra which may probably be due to high Fe concentration in the lattice and low rutile TiO₂ formed in the sample. Alternatively, multiple photoluminescence signals in the visible region can be observed in all samples. A visible region peak near 540 nm was observed in H-15, H-20 and H-25 samples whereas the peak for H-30 and H-35 were located near 525 nm. The detection of photoluminescence signal in the visible region is associated with the shallow traps on surface oxygen vacancies or defects (Yan et al., 2013). It is known that the introduction of element doping in pristine TiO₂ creates defect sites and a suitable amount of defects sites can improve the photo-catalytic activity of catalyst since the defects site has trapping effects to separate the photo-generated electrons and holes.

However, excess defects will become the new recombination centres for photo-generated electrons-hole pairs (Yan et al., 2015). Theoretically, the sample with lowest photoluminescence intensity is expected to demonstrate the best photo-catalytic activity because of slow recombination rate. The slow recombination from the electron will give more time for radical generation in the electron holes and electrons at the valence and conduction band which has been illustrated in Fig. 4.7. In this study, H-15 has the slowest recombination rate meanwhile H-35 has the fastest recombination rate.

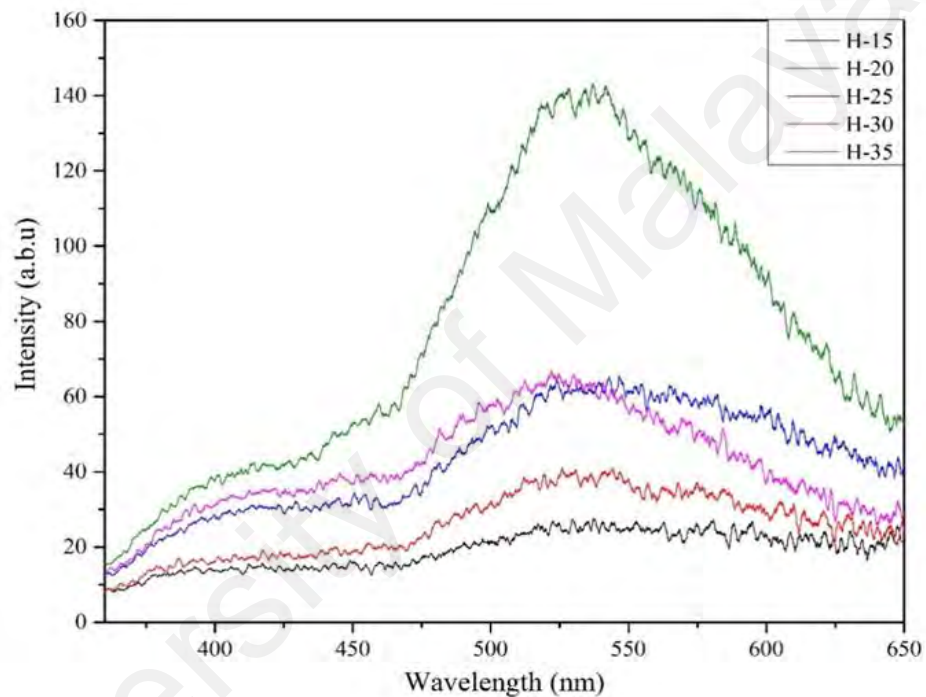


Figure 4.18: Photoluminescence spectrum of H-15, H-20, H-25, H-30 and H-35 pre-treated Ilmenite samples.

4.3.9 Zeta potential analysis

The zeta potential is used to measure the surface charge of a substance in a liquid through changing pH. The pH dependence of the zeta potential of pre-treated ilmenite sample in aqueous suspensions is illustrated in Figure 4.19. The iso-electric point (IEP) can be used to determine the colloidal stability of particle in different suspensions. The IEP of H-15, H-20, H-25, H-30 and H-35 samples were in the range of 3.1 to 3.3. The IEP of raw ilmenite was pH 4.5 and the shift in the IEP of pre-treated ilmenite samples

towards the acidic region (pH 3.1 – 3.3 for all pre-treated ilmenite sample) confirms the changes in the surface chemistry of raw ilmenite treated in acidic condition. The shift of IEP towards lower pH value due to the increment of surface area for pre-treated ilmenite thus increase H^+ adsorption hence reduce the IEP value of pre-treated ilmenite (Bae et al., 2003). The pre-treated ilmenite has better photo-degradation of RB 5 dye solution in acidic condition due to enhanced dye adsorption on the pre-treated ilmenite surface before photo-degradation. The high adsorption of RB 5 on pre-treated ilmenite is linked with strong attractive forces between the positively-charged pre-treated ilmenite surface at pH 3 and negatively-charged dye molecules, thus facilitating the adsorption process (Zielińska et al., 2001).

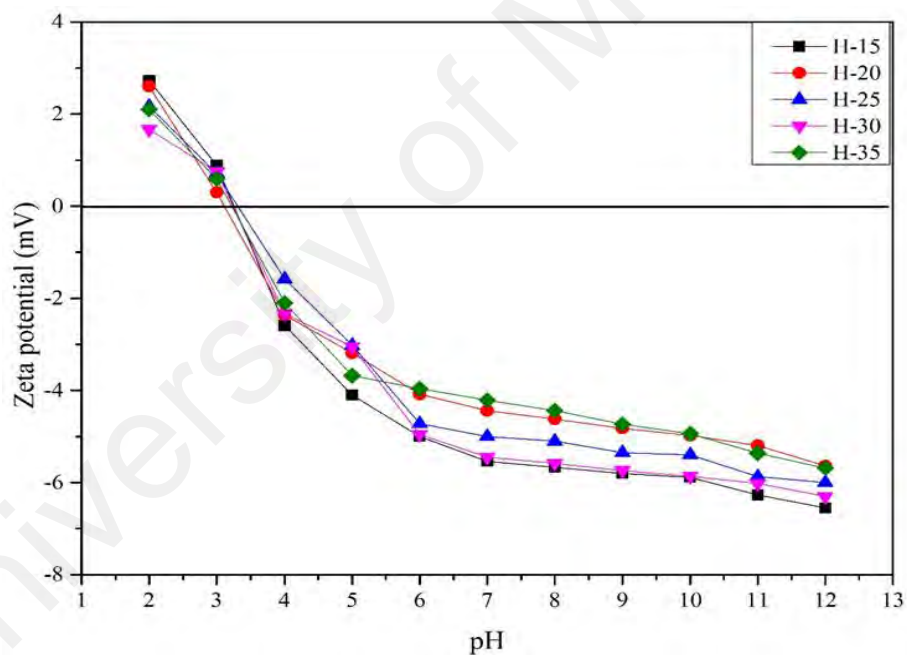


Figure 4.19: Zeta potential of the pre-treated ilmenite in various acid concentration.

4.4 Photo-catalytic activity of pre-treated ilmenite at different HCl concentration

Figure 4.20 illustrates the photo-catalytic activity of pre-treated ilmenite under different HCl concentration. The increment of HCl concentration has a positive effect on the photo-catalytic activity to pre-treated ilmenite when the percent removal ($(1-C_t/C_0 \times 100\%)$) of RB 5 has improved tremendously. For example, H-25 and H-30 managed to achieve up to 100% photo degradation as compared to that of raw ilmenite. The sequences of photo-catalytic activity is as follows $H-25 > H-30 > H-20 > H-15 > H-35 > \text{raw ilmenite}$. High concentration of impurities in TiO_2 normally will deteriorate the photo-catalytic activity of TiO_2 (Crişan et al., 2015; Wan et al., 2011; Zarazúa-Morín et al., 2016). The highest photo-catalytic rate (0.168 min^{-1}) for H-25 is due to the factor of high adsorption between ilmenite and RB 5 which can be clearly seen during the dark absorption. The high photo-catalytic activity of H-25 was due to various synergistic effects such as band gap, surface area, and recombination rate. The high surface area of H-25 ($37.31 \text{ m}^2/\text{g}$) with the relatively low band (2.84 eV) and relatively slow recombination rate (slower than H-35) has contributed to high photo-catalytic activity. The high surface area will provide more photo-catalytic active sites and adsorption sites. The low band gap also demonstrated that H-25 was activated under visible light and radicals were easily generated due to slow recombination rate. Although H-15 demonstrated slow recombination rate, the relatively high Fe ions concentration (Table 4.4) will give negative impact. This is because the excessive free Fe in H-15 might become recombination centres for photo-generated electrons and holes (Abazović et al., 2009a; Yan et al., 2015). In contrast, H-25 samples has higher surface area compared and relatively slow recombination rate which leads to higher absorption of dye on the catalyst surface area and photo-degradation. Therefore, ilmenite pre-treated with 25 v/v% of HCl demonstrated an appropriate amount of Fe dopant to give a best photo-catalytic activity.

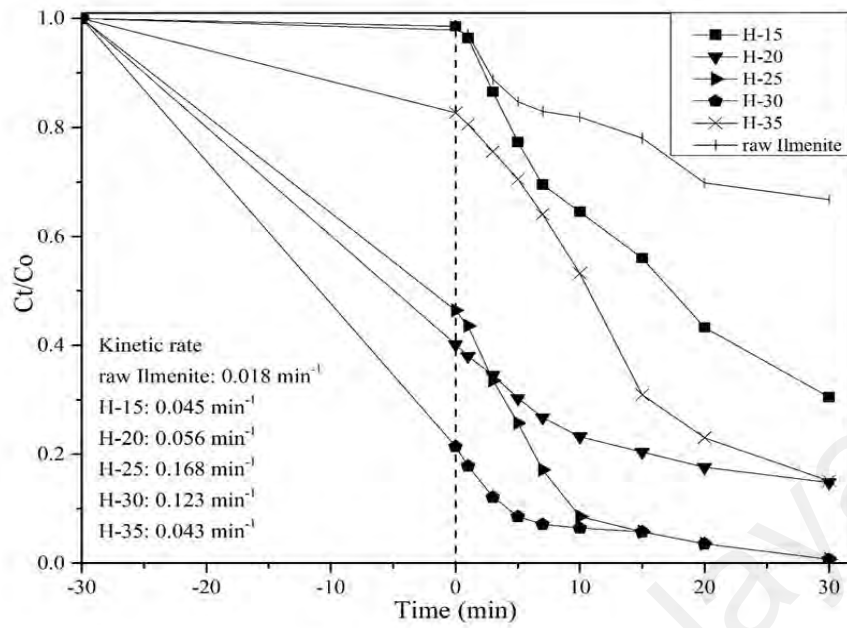


Figure 4.20: Dye degradation (C_t/C_0) of pre-treated ilmenite treated under different HCl concentration at pH 3. (Dye concentration 5 ppm, catalyst loading 1.0 g/L, 25°C)

University of Malaya

CHAPTER 5: CONCLUSION

5.1 Conclusion

This study have successfully understood the physicochemical properties and photo-catalytic activity of raw and pre-treated ilmenite. The photo-catalytic activity of the sequence follows H-25 > H-30 > H-20 > H-15 > H-35 > raw ilmenite. It was demonstrated that RB 5 has been fully degraded with H-25 within 30 minutes at pH 3 under artificial solar light irradiation (150 W Xenon Arc Lamp). However raw ilmenite needs to take 120 min at pH 2 to fully degrade RB 5 under artificial solar light irradiation. Therefore, the pre-treated ilmenite is highly potential to be used a photo-catalyst for textile wastewater treatment.

The conclusions attained in the research are as follows:

First, based on XRD and Raman results, the raw ilmenite composed of iron oxide species and rutile TiO₂. The PZC of raw ilmenite is at pH 4.5, therefore it has better photo-catalytic activity in acidic condition (pH 2). Raw ilmenite has an irregular shape with a rough surface and this was reflected in the nitrogen absorption desorption test with the record of 16.2m²/g. High Fe ion concentrations reduced the band gap energy of raw ilmenite (2.5 eV) compared with pure rutile TiO₂ (3.0 eV).

Second, raw ilmenite achieved the best photo-catalytic activity of photo-degradation of RB 5 dye solution under pH 2 whereas total photo-catalytic activity inhibition of raw ilmenite occurred at pH 9. Homogenous Fenton process may have attributed to the good photo-degradation performance under acidic conditions as some Fe ions may have dissolved into solution. Alternatively, the presence of NO₃⁻ had no negative effect on the photo-catalytic activity but PO₄³⁻ severely reduced the photo-catalytic activity due to its hydroxyl radical scavenger properties. Complete photo-degradation of RB 5 was

achieved by 2.0 g/L of catalyst loading of raw ilmenite after 2 h under artificial solar light irradiation.

The pre-treated ilmenite was synthesised by acid leaching through chloride leaching process. The acid concentration yielded the greatest influencing factor towards photo-catalytic activity, compared to other parameters. The best acid concentration for chloride leaching process is 25 v/v% HCl. The conclusions attained in the second stage of the research are as follows:

Firstly, the pre-treated ilmenite with different concentrations of HCl demonstrated better photo-catalytic dye degradation performance due to the increase of surface area which increased the interaction between adsorbate and adsorbent, hence increasing the amount of adsorbed dye compared to raw ilmenite. It is demonstrated the H-25 possessed the highest surface area as compared to that of other concentration of acid treatment.

Secondly, pre-treated ilmenite showed complete dye removal within 30 min at pH 3 under artificial solar light irradiation, whereas raw ilmenite achieved roughly 40% of dye removal at the same time frame and pH. This is because the appropriate low amount of Fe ion concentration in pre-treated ilmenite has the trapping effects to separate the photo-generated electrons and holes.

5.2 Suggestions and Recommendations

Pre-treated ilmenite has a great potential to be an ideal photo-catalyst synthesised through simple chloride leaching process, therefore further studies and development are required to enhance this process. A few suggestions for future studies are proposed:

First of all, the effect of other parameters such as use of reducing agent can be studied in order to optimise the properties of pre-treated ilmenite since the reducing agent can shorten the synthesis time of pre-treated ilmenite using chloride.

Secondly, since RB 5 dye as a model compound for dye removal was used in this work, other dye model compound can be used. RB 5 dye is an anionic dye with a negatively-charged surface in water, therefore other types of dye could be used in future studies such as basic dye (Methylene Blue) and acidic dyes (C.I. Acid Red 73).

The significant in this study is that this study has provided full details studies about raw and pre-treated ilmenite in their phase formation, morphology, chemical state, elemental composition, surface stability and its optical properties which haven't been studied before. Moreover, this study has provide some information about comparing the most influence factors for pre-treated ilmenite as photo-catalyst synthesis during chloride leaching process. In addition, studies on parameters in photo-catalytic activity of raw ilmenite could filled the gap in the potential application study of this mineral in future.

REFERENCES

- Abazović, N. D., Čomor, M. I., Dramićanin, M. D., Jovanović, D. J., Ahrenkiel, S. P., & Nedeljković, J. M. (2006). Photoluminescence of anatase and rutile TiO₂ particles. *The Journal of Physical Chemistry B*, 110(50), 25366-25370.
- Abazović, N. D., Mirengi, L., Janković, I. A., Bibić, N., Šojić, D. V., Abramović, B. F., & Čomor, M. I. (2009a). Synthesis and characterisation of rutile TiO₂ nanopowders doped with iron ions. *Nanoscale Research Letters*, 4(6), 518.
- Abazović, N. D., Mirengi, L., Janković, I. A., Bibić, N., Šojić, D. V., Abramović, B. F., & Čomor, M. I. (2009b). Synthesis and characterisation of rutile TiO₂ nanopowders doped with iron ions. *Nanoscale Research Letters*, 4(6), 518.
- Abazović, N. D., Ruvarac-Bugarčić, I. A., Čomor, M. I., Bibić, N., Ahrenkiel, S. P., & Nedeljković, J. M. (2008). Photon energy up-conversion in colloidal TiO₂ nanorods. *Optical Materials*, 30(7), 1139-1144.
- Adán, C., Bahamonde, A., Oller, I., Malato, S., & Martínez-Arias, A. (2014). Influence of iron leaching and oxidizing agent employed on solar photodegradation of phenol over nanostructured iron-doped titania catalysts. *Applied Catalysis B: Environmental*, 144, 269-276.
- Agustina, T. E., Ang, H., & Vareek, V. (2005). A review of synergistic effect of photocatalysis and ozonation on wastewater treatment. *Journal of Photochemistry and Photobiology C: Photochemistry Reviews*, 6(4), 264-273.
- Akbari, A., Desclaux, S., Rouch, J., Aptel, P., & Remigy, J. (2006). New UV-photografted nanofiltration membranes for the treatment of colored textile dye effluents. *Journal of Membrane Science*, 286(1), 342-350.
- Akhgar, B. N., Pazouki, M., Ranjbar, M., Hosseinnia, A., & Keyanpour-Rad, M. (2010). Preparation of nanosized synthetic rutile from ilmenite concentrate. *Minerals Engineering*, 23(7), 587-589.
- Akpan, U. G., & Hameed, B. H. (2009). Parameters affecting the photocatalytic degradation of dyes using TiO₂-based photocatalysts: a review. *Journal of Hazardous Materials*, 170(2-3), 520-529.
- Al-Kdasi, A., Idris, A., Saed, K., & Guan, C. T. (2004). Treatment of textile wastewater by advanced oxidation processes—a review. *Global Nest: the International Journal*, 6(3), 222-230.

- Alaton, I. A., & Balcioglu, I. A. (2001). Photochemical and heterogeneous photocatalytic degradation of waste vinylsulphone dyes: a case study with hydrolyzed Reactive Black 5. *Journal of Photochemistry and Photobiology A: Chemistry*, 141(2), 247-254.
- An, H.-R., Park, S. Y., Huh, J. Y., Kim, H., Lee, Y.-C., Lee, Y. B., Hong, Y. C., & Lee, H. U. (2017). Nanoporous hydrogenated TiO₂ photocatalysts generated by underwater discharge plasma treatment for solar photocatalytic applications. *Applied Catalysis B: Environmental*, 211, 126-136.
- Anjaneyulu, Y., Sreedhara Chary, N., & Samuel Suman Raj, D. (2005). Decolourisation of industrial effluents – available methods and emerging technologies – a review. *Reviews in Environmental Science and Bio/Technology*, 4(4), 245-273.
- Annadurai, G., Sung, S. S., & Lee, D.-J. (2004). Simultaneous removal of turbidity and humic acid from high turbidity stormwater. *Advances in Environmental Research*, 8(3–4), 713-725.
- Anpo, M., and Kamat, P. V. (2010). *Environmentally benign photocatalysts: applications of titanium oxide-based materials*: Springer Science & Business Media.
- Aouni, A., Fersi, C., Cuartas-Uribe, B., Bes-Pía, A., Alcaina-Miranda, M. I., & Dhahbi, M. (2012). Reactive dyes rejection and textile effluent treatment study using ultrafiltration and nanofiltration processes. *Desalination*, 297, 87-96.
- Aquino, J. M., Pereira, G. F., Rocha-Filho, R. C., Bocchi, N., & Biaggio, S. R. (2016). Combined coagulation and electrochemical process to treat and detoxify a real textile effluent. *Water, Air, & Soil Pollution*, 227(8), 266.
- Arumai Dhas, J. P. (2008). *Removal of cod and colour from textile wastewater using limestone and activated carbon*. Universiti Sains Malaysia.
- Asahi, R., Taga, Y., Mannstadt, W., & Freeman, A. J. (2000). Electronic and optical properties of anatase TiO₂. *Physical Review B*, 61(11), 7459-7465.
- Bae, H. S., Lee, M. K., Kim, W. W., & Rhee, C. K. (2003). Dispersion properties of TiO₂ nano-powder synthesized by homogeneous precipitation process at low temperatures. *Colloids and Surfaces A: Physicochemical and Engineering Aspects*, 220(1), 169-177.
- Balachandran, U., & Eror, N. G. (1982). Raman spectra of titanium dioxide. *Journal of Solid State Chemistry*, 42(3), 276-282.

- Balcioglu, I. A., Arslan, I., & Sacan, M. T. (2001). Homogenous and heterogenous advanced oxidation of two commercial reactive dyes. *Environmental Technology*, 22(7), 813-822.
- Barakat, T., Idakiev, V., Cousin, R., Shao, G. S., Yuan, Z. Y., Tabakova, T., & Siffert, S. (2014). Total oxidation of toluene over noble metal based Ce, Fe and Ni doped titanium oxides. *Applied Catalysis B: Environmental*, 146, 138-146.
- Bechtold, T., Burtscher, E., & Hung, Y.-T. (2004). Treatment of textile wastes. *Handbook of Industrial and hazardous waste treatment*, Marcel Dekker, 379-413.
- Berkovich, S. A. (1975). Recovery of titanium dioxide from ores: Google Patents.
- Bersani, D., Antonioli, G., Lottici, P. P., & Lopez, T. (1998). Raman study of nanosized titania prepared by sol-gel route. *Journal of Non-Crystalline Solids*, 232-234, 175-181.
- Bharti, B., Kumar, S., Lee, H.-N., & Kumar, R. (2016). Formation of oxygen vacancies and Ti³⁺ state in TiO₂ thin film and enhanced optical properties by air plasma treatment. *Scientific Report* 6, 32355.
- Bhatkhande, D. S., Pangarkar, V. G., & Beenackers, A. A. (2002a). Photocatalytic degradation for environmental applications—a review. *Journal of Chemical Technology and Biotechnology*, 77(1), 102-116.
- Bhatkhande, D. S., Pangarkar, V. G., & Beenackers, A. A. C. M. (2002b). Photocatalytic degradation for environmental applications – a review. *Journal of Chemical Technology & Biotechnology*, 77(1), 102-116.
- Bisschops, I., & Spanjers, H. (2003). Literature review on textile wastewater characterisation. *Environmental Technology*, 24(11), 1399-1411.
- Blanco, J., Torrades, F., De la Varga, M., & García-Montaña, J. (2012). Fenton and biological-Fenton coupled processes for textile wastewater treatment and reuse. *Desalination*, 286, 394-399.
- Boehm, H. P. (1971). Acidic and basic properties of hydroxylated metal oxide surfaces. *Discussions of the Faraday Society*, 52(0), 264-275.
- Bowley, H. J., Gerrard, D. L., Loudon, J. D., Turrell, G., Gardiner, D. J., & Graves, P. R. (2012). *Practical raman spectroscopy*: Springer Science & Business Media.

- Brik, M., Schoeberl, P., Chamam, B., Braun, R., & Fuchs, W. (2006). Advanced treatment of textile wastewater towards reuse using a membrane bioreactor. *Process Biochemistry*, 41(8), 1751-1757.
- Brillas, E., & Martínez-Huitle, C. A. (2015). Decontamination of wastewaters containing synthetic organic dyes by electrochemical methods. An updated review. *Applied Catalysis B: Environmental*, 166–167, 603-643.
- Brillas, E., Sirés, I., & Oturan, M. A. (2009). Electro-Fenton process and related electrochemical technologies based on Fenton's reaction chemistry. *Chemical Reviews*, 109(12), 6570-6631.
- Buehler, R. E., Staehelin, J., & Hoigné, J. (1984). Ozone decomposition in water studied by pulse radiolysis. 1. HO₂O₂ and HO₃O₃ as intermediates.[Electron beams]. *The Journal of Physical Chemistry.:(United States)*, 88(12), 2560-2564.
- Butler, M., & Ginley, D. (1977). Correlation of photosensitive electrode properties with electronegativity. *Chemical Physics Letters*, 47(2), 319-321.
- Carlson, T. A. (1978). *X-ray photoelectron spectroscopy* (Vol. 2): Dowden, Hutchinson & Ross.
- Chafi, M., Gourich, B., Essadki, A. H., Vial, C., & Fabregat, A. (2011). Comparison of electrocoagulation using iron and aluminium electrodes with chemical coagulation for the removal of a highly soluble acid dye. *Desalination*, 281, 285-292.
- Chan, S. H. S., Yeong Wu, T., Juan, J. C., & Teh, C. Y. (2011). Recent developments of metal oxide semiconductors as photocatalysts in advanced oxidation processes (AOPs) for treatment of dye waste-water. *Journal of Chemical Technology & Biotechnology*, 86(9), 1130-1158.
- Chastain, J., King, R. C., & Moulder, J. (1995). *Handbook of X-ray photoelectron spectroscopy: a reference book of standard spectra for identification and interpretation of XPS data*: Physical Electronics Eden Prairie, MN.
- Che, M., & Védrine, J. C. (2012). *Characterisation of solid materials and heterogeneous catalysts: from structure to surface reactivity*: John Wiley & Sons.

- Chen, J., Ollis, D. F., Rulkens, W. H., & Bruning, H. (1999). Photocatalysed oxidation of alcohols and organochlorides in the presence of native TiO₂ and metallized TiO₂ suspensions. Part (I): photocatalytic activity and pH influence. *Water Research*, 33(3), 661-668.
- Chen, S., Huang, M., Lin, P., Jeng, H., Lee, J., Haw, S., Chen, S., Lin, H., Lu, K., & Chen, D. (2013). Orbital structure of FeTiO₃ ilmenite investigated with polarisation-dependent X-ray absorption spectroscopy and band structure calculations. *Applied Physics Letters*, 102(4), 042107.
- Chen, X., & Mao, S. S. (2007). Titanium dioxide nanomaterials: synthesis, properties, modifications, and applications. *Chemical Reviews*, 107(7), 2891-2959.
- Chen, Y., Yang, S., Wang, K., & Lou, L. (2005). Role of primary active species and TiO₂ surface characteristic in UV-illuminated photodegradation of Acid Orange 7. *Journal of Photochemistry and Photobiology A: Chemistry*, 172(1), 47-54.
- Chong, M. N., Cho, Y. J., Poh, P. E., & Jin, B. (2015a). Evaluation of Titanium Dioxide photocatalytic technology for the treatment of Reactive Black 5 dye in synthetic and real greywater effluents. *Journal of Cleaner Production*, 89, 196-202.
- Chong, M. N., Jin, B., Chow, C. W. K., & Saint, C. (2010). Recent developments in photocatalytic water treatment technology: A review. *Water Research*, 44(10), 2997-3027.
- Chong, M. N., Tneu, Z. Y., Poh, P. E., Jin, B., & Aryal, R. (2015b). Synthesis, characterisation and application of TiO₂-zeolite nanocomposites for the advanced treatment of industrial dye wastewater. *Journal of the Taiwan Institute of Chemical Engineers*, 50, 288-296.
- Choo, K.-H., Choi, S.-J., & Hwang, E.-D. (2007). Effect of coagulant types on textile wastewater reclamation in a combined coagulation/ultrafiltration system. *Desalination*, 202(1), 262-270.
- Colthup, N. (2012). *Introduction to infrared and Raman spectroscopy*: Elsevier.
- Crişan, M., Răileanu, M., Drăgan, N., Crişan, D., Ianculescu, A., Niţoi, I., Oancea, P., Şomărescu, S., Stănică, N., Vasile, B., & Stan, C. (2015). Sol-gel iron-doped TiO₂ nanopowders with photocatalytic activity. *Applied Catalysis A: General*, 504, 130-142.

- Cromer, D. T., & Herrington, K. (1955). The structures of anatase and rutile. *Journal of the American Chemical Society*, 77(18), 4708-4709.
- Cservenyák, I., Kelsall, G. H., & Wang, W. (1996). Reduction of TiIV species in aqueous sulfuric and hydrochloric acids i. Titanium speciation. *Electrochimica Acta*, 41(4), 563-572.
- Ctibor, P., Pala, Z., Stengl, V., & Musalek, R. (2014). Photocatalytic activity of visible-light-active iron-doped coatings prepared by plasma spraying. *Ceramics International*, 40(1, Part B), 2365-2372.
- Daghrir, R., Drogui, P., & Robert, D. (2013). Modified TiO₂ for environmental photocatalytic applications: a review. *Industrial & Engineering Chemistry Research*, 52(10), 3581-3599.
- Dalvand, A., Gholami, M., Joneidi, A., & Mahmoodi, N. M. (2011). Dye removal, energy consumption and operating cost of electrocoagulation of textile wastewater as a clean process. *CLEAN – Soil, Air, Water*, 39(7), 665-672.
- Damodar, R. A., & You, S.-J. (2010). Performance of an integrated membrane photocatalytic reactor for the removal of Reactive Black 5. *Separation and Purification Technology*, 71(1), 44-49.
- de Faria, D. L. A., Venâncio Silva, S., & de Oliveira, M. T. (1997). Raman microspectroscopy of some iron oxides and oxyhydroxides. *Journal of Raman Spectroscopy*, 28(11), 873-878.
- De Laat, J., Truong Le, G., & Legube, B. (2004). A comparative study of the effects of chloride, sulfate and nitrate ions on the rates of decomposition of H₂O₂ and organic compounds by Fe(II)/H₂O₂ and Fe(III)/H₂O₂. *Chemosphere*, 55(5), 715-723.
- Deng, Y., & Englehardt, J. D. (2006). Treatment of landfill leachate by the Fenton process. *Water Research*, 40(20), 3683-3694.
- Deowan, S. A., Galiano, F., Hoinkis, J., Figoli, A., & Drioli, E. (2013). Submerged membrane bioreactor (SMBR) for treatment of textile dye wastewater towards developing novel MBR process. *APCBEE Procedia*, 5, 259-264.

Deowan, S. A., Galiano, F., Hoinkis, J., Johnson, D., Altinkaya, S. A., Gabriele, B., Hilal, N., Drioli, E., & Figoli, A. (2016). Novel low-fouling membrane bioreactor (MBR) for industrial wastewater treatment. *Journal of Membrane Science*, 510, 524-532.

Environmental Quality (Industrial Effluents) Regulations 2009, (2010).

Deveci, E. Ü., Dizge, N., Yatmaz, H. C., & Aytepe, Y. (2016). Integrated process of fungal membrane bioreactor and photocatalytic membrane reactor for the treatment of industrial textile wastewater. *Biochemical Engineering Journal*, 105, Part B, 420-427.

Diebold, U., & Madey, T. E. (1996). TiO₂ by XPS. *Surface Science Spectra*, 4(3), 227-231.

Duyvesteyn, W. P., Sabacky, B. J., Verhulst, D. E. V., West-Sells, P. G., Spitler, T. M., Vince, A., Burkholder, J. R., & Huls, B. J. P. M. (2002a). Processing titaniferous ore to titanium dioxide pigment: Google Patents.

Duyvesteyn, W. P., Spitler, T. M., Sabacky, B. J., & Prochazka, J. (2002b). Processing aqueous titanium chloride solutions to ultrafine titanium dioxide: Google Patents.

Echlin, P. (2011). *Handbook of sample preparation for scanning electron microscopy and X-ray microanalysis*: Springer Science & Business Media.

Echlin, P., Fiori, C., Goldstein, J., Joy, D. C., & Newbury, D. E. (2013). *Advanced scanning electron microscopy and X-ray microanalysis*: Springer Science & Business Media.

El-Gohary, F., & Tawfik, A. (2009). Decolourisation and COD reduction of disperse and reactive dyes wastewater using chemical-coagulation followed by sequential batch reactor (SBR) process. *Desalination*, 249(3), 1159-1164.

El-Hazek, N., Lasheen, T. A., El-Sheikh, R., & Zaki, S. A. (2007). Hydrometallurgical criteria for TiO₂ leaching from Rosetta ilmenite by hydrochloric acid. *Hydrometallurgy*, 87(1-2), 45-50.

Esch, T. R., Gadaczek, I., & Bredow, T. (2014). Surface structures and thermodynamics of low-index of rutile, brookite and anatase – a comparative DFT study. *Applied Surface Science*, 288, 275-287.

- Esplugas, S., Giménez, J., Contreras, S., Pascual, E., & Rodríguez, M. (2002). Comparison of different advanced oxidation processes for phenol degradation. *Water Research*, 36(4), 1034-1042.
- Foo, K., & Hameed, B. (2010). Decontamination of textile wastewater via TiO₂/activated carbon composite materials. *Advances in Colloid and Interface Science*, 159(2), 130-143.
- Freedonia. (2009). New Industry Forecasts for 2013 and 2018. *World Dyes & Organic Pigments*, (May 2009).
- Gao, B.-Y., Yue, Q.-Y., Wang, Y., & Zhou, W.-Z. (2007). Color removal from dye-containing wastewater by magnesium chloride. *Journal of Environmental Management*, 82(2), 167-172.
- García-Montaña, J., Ruiz, N., Muñoz, I., Domènech, X., García-Hortal, J. A., Torrades, F., & Peral, J. (2006). Environmental assessment of different photo-Fenton approaches for commercial reactive dye removal. *Journal of Hazardous Materials*, 138(2), 218-225.
- García-Ripoll, A., Arques, A., Vicente, R., Domenech, A., & Amat, A. M. (2008). Treatment of aqueous solutions containing four commercial pesticides by means of TiO₂ solar photocatalysis. *Journal of Solar Energy Engineering*, 130(4), 041011-041011.
- García, A., Amat, A. M., Arques, A., Sanchís, R., Gernjak, W., Maldonado, M. I., Oller, I., & Malato, S. (2006). Detoxification of aqueous solutions of the pesticide "SevnoI" by solar photocatalysis. *Environmental Chemistry Letters*, 3(4), 169-172.
- García, M. T., Ribosa, I., Guindulain, T., Sánchez-Leal, J., & Vives-Rego, J. (2001). Fate and effect of monoalkyl quaternary ammonium surfactants in the aquatic environment. *Environmental Pollution*, 111(1), 169-175.
- Gaya, U. I., & Abdullah, A. H. (2008). Heterogeneous photocatalytic degradation of organic contaminants over titanium dioxide: A review of fundamentals, progress and problems. *Journal of Photochemistry and Photobiology C: Photochemistry Reviews*, 9(1), 1-12.
- Georgiou, D., Aivazidis, A., Hatiras, J., & Gimouhopoulos, K. (2003). Treatment of cotton textile wastewater using lime and ferrous sulfate. *Water Research*, 37(9), 2248-2250.

- Ghafoor, S., Ata, S., Mahmood, N., & Arshad, S. N. (2017). Photosensitization of TiO₂ nanofibers by Ag₂S with the synergistic effect of excess surface Ti³⁺ states for enhanced photocatalytic activity under simulated sunlight. *Scientific Reports*, 7(1), 255.
- Giaquinta, D. M., & zur Loye, H.-C. (1994). Structural predictions in the ABO₃ phase diagram. *Chemistry of Materials*, 6(4), 365-372.
- GilPavas, E., Dobrosz-Gómez, I., & Gómez-García, M. Á. (2017). Coagulation-flocculation sequential with Fenton or Photo-Fenton processes as an alternative for the industrial textile wastewater treatment. *Journal of Environmental Management*, 191, 189-197.
- Ginley, D., & Butler, M. (1977). The photoelectrolysis of water using iron titanate anodes. *Journal of Applied Physics*, 48(5), 2019-2021.
- Gireesh, V. S., Vinod, V. P., Krishnan Nair, S., & Ninan, G. (2015). Catalytic leaching of ilmenite using hydrochloric acid: A kinetic approach. *International Journal of Mineral Processing*, 134, 36-40.
- Glisenti, A. (2000). The reactivity of a Fe–Ti–O mixed oxide under different atmospheres: study of the interaction with simple alcohol molecules. *Journal of Molecular Catalysis A: Chemical*, 153(1), 169-190.
- Goldstein, J., Newbury, D. E., Echlin, P., Joy, D. C., Romig Jr, A. D., Lyman, C. E., Fiori, C., & Lifshin, E. (2012). *Scanning electron microscopy and X-ray microanalysis: a text for biologists, materials scientists, and geologists*: Springer Science & Business Media.
- Gregory, J., & Rossi, L. (2001). Dynamic testing of water treatment coagulants. *Water Science and Technology: Water Supply*, 1(4), 65-72.
- Gupta, V. (2009). Application of low-cost adsorbents for dye removal—a review. *Journal of environmental management*, 90(8), 2313-2342.
- Haber, F., & Weiss, J. (1934). The catalytic decomposition of hydrogen peroxide by iron salts. *Proceedings of the Royal Society of London A: Mathematical, Physical and Engineering Sciences*, 147(861), 332-351.
- Haberl, R., Urban, W., Gehringer, P., & Szinovatz, W. (1991). Treatment of pulp-bleaching effluents by activated sludge, precipitation, ozonation and irradiation. *Water Science and Technology*, 24(3-4), 229-239.

- Habisreutinger, S. N., Schmidt-Mende, L., & Stolarczyk, J. K. (2013). Photocatalytic reduction of CO₂ on TiO₂ and other semiconductors. *Angewandte Chemie International Edition*, 52(29), 7372-7408.
- Hameed, B., Ahmad, A., & Aziz, N. (2007). Isotherms, kinetics and thermodynamics of acid dye adsorption on activated palm ash. *Chemical Engineering Journal*, 133(1), 195-203.
- Hameed, B., & El-Khaiary, M. (2008). Kinetics and equilibrium studies of malachite green adsorption on rice straw-derived char. *Journal of Hazardous Materials*, 153(1), 701-708.
- Han, G., Liang, C.-Z., Chung, T.-S., Weber, M., Staudt, C., & Maletzko, C. (2016). Combination of forward osmosis (FO) process with coagulation/flocculation (CF) for potential treatment of textile wastewater. *Water Research*, 91, 361-370.
- Han, K. N., Rubcumintara, T., & Fuerstenau, M. C. (1987). Leaching behavior of ilmenite with sulfuric acid. *Metallurgical Transactions B*, 18(2), 325-330.
- Hanaor, D. A., & Sorrell, C. C. (2011). Review of the anatase to rutile phase transformation. *Journal of Materials science*, 46(4), 855-874.
- Hardcastle, F. (2011). Raman spectroscopy of titania (TiO₂) nanotubular water-splitting catalysts. *Journal of the Arkansas Academy of Science*, 65(1), 43-48.
- Hardcastle, F. D., & Wachs, I. E. (1990). Determination of molybdenum–oxygen bond distances and bond orders by Raman spectroscopy. *Journal of Raman Spectroscopy*, 21(10), 683-691.
- Hardcastle, F. D., & Wachs, I. E. (1991). Determination of vanadium-oxygen bond distances and bond orders by Raman spectroscopy. *The Journal of Physical Chemistry*, 95(13), 5031-5041.
- Hayat, H., Mahmood, Q., Pervez, A., Bhatti, Z. A., & Baig, S. A. (2015). Comparative decolourisation of dyes in textile wastewater using biological and chemical treatment. *Separation and Purification Technology*, 154, 149-153.
- Herrmann, J.-M. (2010). Fundamentals and misconceptions in photocatalysis. *Journal of Photochemistry and Photobiology A: Chemistry*, 216(2–3), 85-93.

- Hoffmann, M. R., Martin, S. T., Choi, W., & Bahnemann, D. W. (1995). Environmental applications of semiconductor photocatalysis. *Chemical reviews*, 95(1), 69-96.
- Hoigne, J., & Bader, H. (1975). Ozonation of water: role of hydroxyl radicals as oxidizing intermediates. *Science*, 190, 782-784.
- Hoigne, J., & Bader, H. (1979). Ozonation of water: selectivity and rate of oxidation of solutes. *Ozone: Science and Engineering* 1(1), 73-85.
- Hu, C., Yu, J. C., Hao, Z., & Wong, P. K. (2003). Effects of acidity and inorganic ions on the photocatalytic degradation of different azo dyes. *Applied Catalysis B: Environmental*, 46(1), 35-47.
- Hu, S.-T., & Yu, Y.-H. (1994). Preozonation of Chlorophenolic wastewater for subsequent biological treatment. *Ozone: Science & Engineering*, 16(1), 13-28.
- Huang, R.-R., Hoinkis, J., Hu, Q., & Koch, F. (2009). Treatment of dyeing wastewater by hollow fiber membrane biological reactor. *Desalination and Water treatment*, 11(1-3), 288-293.
- Hunter, R. J. (2013). *Zeta potential in colloid science: principles and applications* (Vol. 2): Academic press.
- Idris, A., Hashim, R., Rahman, R. A., Ahmad, W., Ibrahim, Z., Razak, P. A., Zin, H. M., & Bakar, I. (2007). Application of bioremediation process for textile wastewater treatment using pilot plant. *International Journal of Engineering and Technology*, 4(2), 228-234.
- Jackson, S. D., & Hargreaves, J. S. (2009). *Metal oxide catalysis* (Vol. 1): Wiley Online Library.
- Jadhav, S. B., Yedurkar, S. M., Phugare, S. S., & Jadhav, J. P. (2012). Biodegradation studies on acid violet 19, a triphenylmethane dye, by *Pseudomonas aeruginosa* BCH. *CLEAN–Soil, Air, Water*, 40(5), 551-558.
- Janssen, A., & Putnis, A. (2011). Processes of oxidation and HCl-leaching of Tellnes ilmenite. *Hydrometallurgy*, 109(3–4), 194-201.
- Jia, L., Liang, B., Lü, L., Yuan, S., Zheng, L., Wang, X., & Li, C. (2014). Beneficiation of titania by sulfuric acid pressure leaching of Panzhihua ilmenite. *Hydrometallurgy*, 150, 92-98.

- Jiang, J.-Q., & Graham, N. J. (1998). Pre-polymerised inorganic coagulants and phosphorus removal by coagulation- a review. *Water Sa*, 24(3), 237-244.
- Kadam, A. A., Lade, H. S., Lee, D. S., & Govindwar, S. P. (2015). Zinc chloride as a coagulant for textile dyes and treatment of generated dye sludge under the solid state fermentation: Hybrid treatment strategy. *Bioresource Technology*, 176, 38-46.
- Kang, N., Lee, D. S., & Yoon, J. (2002a). Kinetic modeling of Fenton oxidation of phenol and monochlorophenols. *Chemosphere*, 47(9), 915-924.
- Kang, S.-F., Liao, C.-H., & Chen, M.-C. (2002b). Pre-oxidation and coagulation of textile wastewater by the Fenton process. *Chemosphere*, 46(6), 923-928.
- Karthikeyan, S., Titus, A., Gnanamani, A., Mandal, A. B., & Sekaran, G. (2011). Treatment of textile wastewater by homogeneous and heterogeneous Fenton oxidation processes. *Desalination*, 281, 438-445.
- Kaur, N., Shahi, S. K., & Singh, V. (2015). Anomalous behavior of visible light active TiO₂ for the photocatalytic degradation of different Reactive dyes. *Photochemical & Photobiological Sciences*, 14(11), 2024-2034.
- Kavan, L., Grätzel, M., Gilbert, S. E., Klemenz, C., & Scheel, H. J. (1996). Electrochemical and photoelectrochemical investigation of single-crystal anatase. *Journal of the American Chemical Society*, 118(28), 6716-6723.
- Kearney, P. C., Muldoon, M. T., Somich, C. J., Ruth, J. M., & Voaden, D. J. (1988). Biodegradation of ozonated atrazine as a wastewater disposal system. *Journal of Agricultural and Food Chemistry*, 36(6), 1301-1306.
- Klug, H. P., & Alexander, L. E. (1954). *X-ray diffraction procedures* (Vol. 2). Wiley-Interscience
- Koelsch, M., Cassaignon, S., Ta Thanh Minh, C., Guillemoles, J. F., & Jolivet, J. P. (2004). Electrochemical comparative study of titania (anatase, brookite and rutile) nanoparticles synthesized in aqueous medium. *Thin Solid Films*, 451-452, 86-92.
- Kosmulski, M. (2002). The significance of the difference in the point of zero charge between rutile and anatase. *Advances in Colloid and Interface Science*, 99(3), 255-264.

- Kumar, C. S. (2013). *UV-VIS and photoluminescence spectroscopy for nanomaterials characterisation*: Springer.
- Lai, C. W., Juan, J. C., Ko, W. B., & Bee Abd Hamid, S. (2014). An overview: recent development of Titanium Oxide nanotubes as photocatalyst for dye degradation. *International Journal of Photoenergy*, 2014, 14.
- Lakowicz, J. R. (2013). *Principles of fluorescence spectroscopy*: Springer Science & Business Media.
- Landmann, M., Rauls, E., & Schmidt, W. G. (2012). The electronic structure and optical response of rutile, anatase and brookite TiO₂. *Journal of Physics: Condensed Matter*, 24(19), 195503.
- Lapertot, M., Pulgarín, C., Fernández-Ibáñez, P., Maldonado, M. I., Pérez-Estrada, L., Oller, I., Gernjak, W., & Malato, S. (2006). Enhancing biodegradability of priority substances (pesticides) by solar photo-Fenton. *Water Research*, 40(5), 1086-1094.
- Lasheen, T. A. I. (2005). Chemical beneficiation of Rosetta ilmenite by direct reduction leaching. *Hydrometallurgy*, 76(1–2), 123-129.
- Leanne, T. (2016, 30 May 2016). Asia buyers may switch to non-China TiO₂ after price surge. *ICIS* Retrieved from <https://www.icis.com/press-releases/focus-story-tio2-price-surge/#>
- Ledakowicz, S., Solecka, M., & Zylla, R. (2001). Biodegradation, decolourisation and detoxification of textile wastewater enhanced by advanced oxidation processes. *Journal of Biotechnology*, 89(2–3), 175-184.
- Lee, J.-K., & Yang, M. (2011). Progress in light harvesting and charge injection of dye-sensitized solar cells. *Materials Science and Engineering: B*, 176(15), 1142-1160.
- Lee, K. M., Lai, C. W., Ngai, K. S., & Juan, J. C. (2016). Recent developments of zinc oxide based photocatalyst in water treatment technology: A review. *Water Research*, 88, 428-448.
- Li, C., Liang, B., & Guo, L.-h. (2007a). Dissolution of mechanically activated Panzhihua ilmenites in dilute solutions of sulphuric acid. *Hydrometallurgy*, 89(1–2), 1-10.

- Li, C., Liang, B., Song, H., Xu, J.-q., & Wang, X.-q. (2008a). Preparation of porous rutile titania from ilmenite by mechanical activation and subsequent sulfuric acid leaching. *Microporous and Mesoporous Materials*, 115(3), 293-300.
- Li, C., Liang, B., & Wang, H. (2008b). Preparation of synthetic rutile by hydrochloric acid leaching of mechanically activated Panzhihua ilmenite. *Hydrometallurgy*, 91(1-4), 121-129.
- Li, J.-G., Ishigaki, T., & Sun, X. (2007b). Anatase, brookite, and rutile nanocrystals via redox reactions under mild hydrothermal conditions: phase-selective synthesis and physicochemical properties. *The Journal of Physical Chemistry C*, 111(13), 4969-4976.
- Li, Z., Wang, Z., & Li, G. (2016). Preparation of nano-titanium dioxide from ilmenite using sulfuric acid-decomposition by liquid phase method. *Powder Technology*, 287, 256-263.
- Liang, B., Li, C., Zhang, C., & Zhang, Y. (2005). Leaching kinetics of Panzhihua ilmenite in sulfuric acid. *Hydrometallurgy*, 76(3-4), 173-179.
- Liang, C.-Z., Sun, S.-P., Li, F.-Y., Ong, Y.-K., & Chung, T.-S. (2014). Treatment of highly concentrated wastewater containing multiple synthetic dyes by a combined process of coagulation/flocculation and nanofiltration. *Journal of Membrane Science*, 469, 306-315.
- Liu, H.-L., & Chiou, Y.-R. (2005). Optimal decolourisation efficiency of Reactive Red 239 by UV/TiO₂ photocatalytic process coupled with response surface methodology. *Chemical Engineering Journal*, 112(1-3), 173-179.
- Liu, M., Lü, Z., Chen, Z., Yu, S., & Gao, C. (2011). Comparison of reverse osmosis and nanofiltration membranes in the treatment of biologically treated textile effluent for water reuse. *Desalination*, 281, 372-378.
- Long, D. A. (1977). *Raman spectroscopy*: McGraw-Hill International Book Company.
- López-López, C., Martín-Pascual, J., Leyva-Díaz, J. C., Martínez-Toledo, M. V., Muñío, M. M., & Poyatos, J. M. (2016). Combined treatment of textile wastewater by coagulation-flocculation and advanced oxidation processes. *Desalination and Water Treatment*, 57(30), 13987-13994.

- Low, F. C. F., Wu, T. Y., Teh, C. Y., Juan, J. C., & Balasubramanian, N. (2012). Investigation into photocatalytic decolourisation of CI Reactive Black 5 using titanium dioxide nanopowder. *Coloration Technology*, 128(1), 44-50.
- Lowell, S., & Shields, J. E. (2013). *Powder surface area and porosity* (Vol. 2): Springer Science & Business Media.
- Lu, M.-C., Chen, J.-N., & Chang, C.-P. (1997). Effect of inorganic ions on the oxidation of dichlorvos insecticide with Fenton's reagent. *Chemosphere*, 35(10), 2285-2293.
- Machulek, A., Vautier-Giongo, C., Moraes, J. E. F., Nascimento, C. A. O., & Quina, F. H. (2006). Laser flash photolysis study of the photocatalytic step of the photo-Fenton reaction in saline solution†. *Photochemistry and Photobiology*, 82(1), 208-212.
- Macwan, D. P., Dave, P. N., & Chaturvedi, S. (2011). A review on nano-TiO₂ sol-gel type syntheses and its applications. *Journal of Materials Science*, 46(11), 3669-3686.
- Mahadwad, O., Parikh, P., Jasra, R., & Patil, C. (2011). Photocatalytic degradation of Reactive Black-5 dye using TiO₂ impregnated ZSM-5. *Bulletin of Materials Science*, 34(3), 551-556.
- Mahmoud, M. H. H., Afifi, A. A. I., & Ibrahim, I. A. (2004). Reductive leaching of ilmenite ore in hydrochloric acid for preparation of synthetic rutile. *Hydrometallurgy*, 73(1-2), 99-109.
- Maldonado, M. I., Passarinho, P. C., Oller, I., Gernjak, W., Fernández, P., Blanco, J., & Malato, S. (2007). Photocatalytic degradation of EU priority substances: a comparison between TiO₂ and Fenton plus photo-Fenton in a solar pilot plant. *Journal of Photochemistry and Photobiology A: Chemistry*, 185(2-3), 354-363.
- Mantzavinos, D., Sahibzada, M., Livingston, A. G., Metcalfe, I. S., & Hellgardt, K. (1999). Wastewater treatment: wet air oxidation as a precursor to biological treatment. *Catalysis Today*, 53(1), 93-106.
- Mazza, T., Barborini, E., Piseri, P., Milani, P., Cattaneo, D., Bassi, A. L., Bottani, C., & Ducati, C. (2007). Raman spectroscopy characterisation of TiO₂ rutile nanocrystals. *Physical Review B*, 75(4), 045416.
- McCreery, R. L. (2005). *Raman spectroscopy for chemical analysis* (Vol. 225): John Wiley & Sons.

- Meenatchisundaram, S., Devaraj, M., Lajapathi Rai, C., & Nadarajan, K. M. (2014). An integrated approach for enhanced textile dye degradation by pre-treatment combined biodegradation. *Clean Technologies and Environmental Policy*, 16(3), 501-511.
- Mehdilo, A., Irannajad, M., & Rezai, B. (2013). Effect of chemical composition and crystal chemistry on the zeta potential of ilmenite. *Colloids and Surfaces A: Physicochemical and Engineering Aspects*, 428, 111-119.
- Merzouk, B., Madani, K., & Sekki, A. (2010). Using electrocoagulation–electroflotation technology to treat synthetic solution and textile wastewater, two case studies. *Desalination*, 250(2), 573-577.
- Merzouk, B., Yakoubi, M., Zongo, I., Leclerc, J. P., Paternotte, G., Pontvianne, S., & Lapique, F. (2011). Effect of modification of textile wastewater composition on electrocoagulation efficiency. *Desalination*, 275(1–3), 181-186.
- Mezzanotte, V., Fornaroli, R., Canobbio, S., Zoia, L., & Orlandi, M. (2013). Colour removal and carbonyl by-production in high dose ozonation for effluent polishing. *Chemosphere*, 91(5), 629-634.
- MIDA. (2015). *Annual Report 2015 - Leading by Fundamentals*. Retrieved from Kuala Lumpur:
[http://www.mida.gov.my/home/administrator/system_files/modules/photo/uploads/20170302190157_MIDA%20AR%202015%20EN%20\(Final\).pdf](http://www.mida.gov.my/home/administrator/system_files/modules/photo/uploads/20170302190157_MIDA%20AR%202015%20EN%20(Final).pdf)
- Misono, M., Ochiai, E. i., Saito, Y., & Yoneda, Y. (1967). A new dual parameter scale for the strength of lewis acids and bases with the evaluation of their softness. *Journal of Inorganic and Nuclear Chemistry*, 29(11), 2685-2691.
- Miyauchi, M., Ikezawa, A., Tobimatsu, H., Irie, H., & Hashimoto, K. (2004). Zeta potential and photocatalytic activity of nitrogen doped TiO₂ thin films. *Physical Chemistry Chemical Physics*, 6(4), 865-870.
- Mo, S.-D., & Ching, W. Y. (1995). Electronic and optical properties of three phases of titanium dioxide: rutile, anatase, and brookite. *Physical Review B*, 51(19), 13023-13032.
- Moctezuma, E., Zermeño, B., Zarazua, E., Torres-Martínez, L., & García, R. (2011). Photocatalytic degradation of phenol with Fe-Titania catalysts. *Topics in Catalysis*, 54(8-9), 496-503.

- Mohey El-Dein, A., Libra, J. A., & Wiesmann, U. (2003). Mechanism and kinetic model for the decolourisation of the azo dye Reactive Black 5 by hydrogen peroxide and UV radiation. *Chemosphere*, 52(6), 1069-1077.
- Nabivanets, B., & Kudritskaya, L. (1967). A study on the polymerization of titanium (IV) in hydrochloric acid solutions. *Russian Journal of Inorganic Chemistry*, 12(5), 616.
- Nagaraj, J., & Couucil, N. S. (1992). *Industrial Safety & Pollution Control Handbook*: National Safety Council.
- Namasivayam, C., & Sumithra, S. (2005). Removal of direct red 12B and methylene blue from water by adsorption onto Fe (III)/Cr (III) hydroxide, an industrial solid waste. *Journal of environmental management*, 74(3), 207-215.
- National Water Services Commission, S. (2009). *Malaysian Sewerage Industry Guidelines* (3 ed.). Suruhanjaya Perkhidmatan Air Negara.
- Navio, J. A., Macias, M., Gonzalez-Catalan, M., & Justo, A. (1992). Bulk and surface characterisation of powder iron-doped titania photocatalysts. *Journal of Materials Science*, 27(11), 3036-3042.
- Neamtu, M., Siminiceanu, I., Yediler, A., & Kettrup, A. (2002). Kinetics of decolourisation and mineralization of reactive azo dyes in aqueous solution by the UV/H₂O₂ oxidation. *Dyes and Pigments*, 53(2), 93-99.
- Nemes, A., Fábíán, I., & Gordon, G. (2000). Experimental aspects of mechanistic studies on aqueous ozone decomposition in alkaline solution. *Ozone: Science & Engineering*, 22, 287-304.
- Neyens, E., & Baeyens, J. (2003). A review of classic Fenton's peroxidation as an advanced oxidation technique. *Journal of Hazardous Materials*, 98(1-3), 33-50.
- Ni, M., Leung, M. K. H., Leung, D. Y. C., & Sumathy, K. (2007). A review and recent developments in photocatalytic water-splitting using for hydrogen production. *Renewable and Sustainable Energy Reviews*, 11(3), 401-425.
- Nidheesh, P. V. (2015). Heterogeneous Fenton catalysts for the abatement of organic pollutants from aqueous solution: a review. *RSC Advances*, 5(51), 40552-40577.

- Ocaña, M., Garcia-Ramos, J. V., & Serna, C. J. (1992). Low-temperature nucleation of rutile observed by Raman spectroscopy during crystallization of TiO₂. *Journal of the American Ceramic Society*, 75(7), 2010-2012.
- Olanipekun, E. (1999). A kinetic study of the leaching of a Nigerian ilmenite ore by hydrochloric acid. *Hydrometallurgy*, 53(1), 1-10.
- Ong, Y. K., Li, F. Y., Sun, S.-P., Zhao, B.-W., Liang, C.-Z., & Chung, T.-S. (2014). Nanofiltration hollow fiber membranes for textile wastewater treatment: lab-scale and pilot-scale studies. *Chemical Engineering Science*, 114, 51-57.
- Pang, Y. L., & Abdullah, A. Z. (2013). Current status of textile industry wastewater management and research progress in Malaysia: a review. *Clean–Soil, Air, Water*, 41(8), 751-764.
- Parra, S., Sarria, V., Malato, S., Péringer, P., & Pulgarin, C. (2000). Photochemical versus coupled photochemical–biological flow system for the treatment of two biorecalcitrant herbicides: metobromuron and isoproturon. *Applied Catalysis B: Environmental*, 27(3), 153-168.
- Pataquiva-Mateus, A. Y., Zea, H. R., & Ramirez, J. H. (2016). Degradation of Orange II by Fenton reaction using ilmenite as catalyst. *Environmental Science and Pollution Research*, 1-8.
- Patel, T. M., Chheda, H., Baheti, A., Patel, P., & Nath, K. (2012). Comparative performance of flat sheet and spiral wound modules in the nanofiltration of reactive dye solution. *Environmental Science and Pollution Research*, 19(7), 2994-3004.
- Pera-Titus, M., García-Molina, V., Baños, M. A., Giménez, J., & Esplugas, S. (2004). Degradation of chlorophenols by means of advanced oxidation processes: a general review. *Applied Catalysis B: Environmental*, 47(4), 219-256.
- Perkowitz, S. (2012). *Optical characterisation of semiconductors: infrared, Raman, and photoluminescence spectroscopy*: Elsevier.
- Pulgarin, C., & Kiwi, J. (1996). Overview on photocatalytic and electrocatalytic pretreatment of industrial non-biodegradable pollutants and pesticides. *CHIMIA International Journal for Chemistry*, 50(3), 50-55.

- Qi, L., Wang, X., & Xu, Q. (2011). Coupling of biological methods with membrane filtration using ozone as pre-treatment for water reuse. *Desalination*, 270(1–3), 264-268.
- Raghavender, A. T., Hoa Hong, N., Joon Lee, K., Jung, M.-H., Skoko, Z., Vasilevskiy, M., Cerqueira, M. F., & Samantilleke, A. P. (2013). Nano-ilmenite FeTiO₃: synthesis and characterisation. *Journal of Magnetism and Magnetic Materials*, 331, 129-132.
- Rao, N. N., Chaturvedi, V., & Li Puma, G. (2012). Novel pebble bed photocatalytic reactor for solar treatment of textile wastewater. *Chemical Engineering Journal*, 184, 90-97.
- Ratanatamskul, C., Chintitanun, S., Masomboon, N., & Lu, M.-C. (2010). Inhibitory effect of inorganic ions on nitrobenzene oxidation by fluidized-bed Fenton process. *Journal of Molecular Catalysis A: Chemical*, 331(1–2), 101-105.
- Reddy, P. V. L., & Kim, K.-H. (2015). A review of photochemical approaches for the treatment of a wide range of pesticides. *Journal of Hazardous Materials*, 285, 325-335.
- Reddy, S. S., & Kotaiah, B. (2005). Decolourisation of simulated spent reactive dye bath using solar / TiO₂ / H₂O₂. *International Journal of Environmental Science & Technology*, 2(3), 245-251.
- Reimer, L. (2000). *Scanning electron microscopy: physics of image formation and microanalysis*: IOP Publishing.
- Reutergårdh, L. B., & Iangphasuk, M. (1997). Photocatalytic decolourization of reactive azo dye: a comparison between TiO₂ and us photocatalysis. *Chemosphere*, 35(3), 585-596.
- Reyes-Coronado, D., Rodríguez-Gattorno, G., Espinosa-Pesqueira, M. E., Cab, C., Coss, R. d., & Oskam, G. (2008). Phase-pure TiO₂ nanoparticles: anatase, brookite and rutile. *Nanotechnology*, 19(14), 145605.
- Riga, A., Soutsas, K., Ntampeglitis, K., Karayannis, V., & Papapolymerou, G. (2007). Effect of system parameters and of inorganic salts on the decolourisation and degradation of Procion H-ex1 dyes. Comparison of H₂O₂/UV, Fenton, UV/Fenton, TiO₂/UV and TiO₂/UV/H₂O₂ processes. *Desalination*, 211(1–3), 72-86.

- Robinson, P., Harrison, R. J., McEnroe, S. A., & Hargraves, R. B. (2002). Lamellar magnetism in the haematite-ilmenite series as an explanation for strong remanent magnetization. *Nature*, *418*(6897), 517-520.
- Robinson, T., McMullan, G., Marchant, R., & Nigam, P. (2001). Remediation of dyes in textile effluent: a critical review on current treatment technologies with a proposed alternative. *Bioresource Technology*, *77*(3), 247-255.
- Roche, E. G., Stuart, A. D., & Grazier, P. E. (2008a). Production of Titania: Google Patents.
- Roche, E. G., Stuart, A. D., Grazier, P. E., & Nicholson, S. (2008b). Production of Titania: Google Patents.
- Rodrigues, C. S. D., Madeira, L. M., & Boaventura, R. A. R. (2013). Treatment of textile dye wastewaters using ferrous sulphate in a chemical coagulation/flocculation process. *Environmental Technology*, *34*(6), 719-729.
- Samsudin, E. M., Hamid, S. B. A., Juan, J. C., Basirun, W. J., & Kandjani, A. E. (2015). Surface modification of mixed-phase hydrogenated TiO₂ and corresponding photocatalytic response. *Applied Surface Science*, *359*, 883-896.
- Sarker, M. K., Rashid, A. K. M. B., & Kurny, A. S. W. (2006). Kinetics of leaching of oxidized and reduced ilmenite in dilute hydrochloric acid solutions. *International Journal of Mineral Processing*, *80*(2-4), 223-228.
- Sarria, V., Deront, M., Péringer, P., & Pulgarin, C. (2003). Degradation of a biorecalcitrant dye precursor present in industrial wastewaters by a new integrated Iron(III) photoassisted-biological treatment. *Applied Catalysis B: Environmental*, *40*(3), 231-246.
- Sasikumar, C., Rao, D. S., Srikanth, S., Mukhopadhyay, N. K., & Mehrotra, S. P. (2007). Dissolution studies of mechanically activated Manavalakurichi ilmenite with HCl and H₂SO₄. *Hydrometallurgy*, *88*(1-4), 154-169.
- Satapanajaru, T., Chompuchan, C., Suntornchot, P., & Pengthamkeerati, P. (2011). Enhancing decolourisation of Reactive Black 5 and Reactive Red 198 during nano zerovalent iron treatment. *Desalination*, *266*(1), 218-230.
- Savin, I.-I., & Butnaru, R. (2008). Wastewater characteristics in textile finishing mills. *Environmental Engineering and Management Journal*, *7*(6), 859-864.

- Schaub, R., Thostrup, P., Lopez, N., Lægsgaard, E., Stensgaard, I., Nørskov, J. K., & Besenbacher, F. (2001). Oxygen vacancies as active sites for water dissociation on rutile TiO₂. *Physical Review Letters*, 87(26), 266104.
- Schoeberl, P., Brik, M., Bertoni, M., Braun, R., & Fuchs, W. (2005). Optimisation of operational parameters for a submerged membrane bioreactor treating dyehouse wastewater. *Separation and Purification Technology*, 44(1), 61-68.
- Selvam, K., Muruganandham, M., Muthuvel, I., & Swaminathan, M. (2007). The influence of inorganic oxidants and metal ions on semiconductor sensitized photodegradation of 4-fluorophenol. *Chemical Engineering Journal*, 128(1), 51-57.
- Semerjian, L., & Ayoub, G. M. (2003). High-pH–magnesium coagulation–flocculation in wastewater treatment. *Advances in Environmental Research*, 7(2), 389-403.
- Sheffield. (2017). *Mineral Sand Market*. Retrieved from <http://www.sheffieldresources.com.au/irm/content/mineral-sand-market.aspx?RID=385>
- Sherman, D. M. (1987). Molecular orbital (SCF-X α -SW) theory of metal-metal charge transfer processes in minerals. *Physics and Chemistry of Minerals*, 14(4), 355-363.
- Skoog, D., Holler, F., & Crouch, S. (2007). *Principles of instrumental analysis*. Brooks Cole
- Smith, Y. R., Joseph Antony Raj, K., Subramanian, V., & Viswanathan, B. (2010). Sulfated Fe₂O₃–TiO₂ synthesized from ilmenite ore: a visible light active photocatalyst. *Colloids and Surfaces A: Physicochemical and Engineering Aspects*, 367(1–3), 140-147.
- Soo, C. W., Juan, J. C., Lai, C. W., Hamid, S. B. A., & Yusop, R. M. (2016). Fe-doped mesoporous anatase-brookite titania in the solar-light-induced photodegradation of Reactive Black 5 dye. *Journal of the Taiwan Institute of Chemical Engineers*, 68, 153-161.
- Souza, R. P., Freitas, T. K. F. S., Domingues, F. S., Pezoti, O., Ambrosio, E., Ferrari-Lima, A. M., & Garcia, J. C. (2016). Photocatalytic activity of TiO₂, ZnO and Nb₂O₅ applied to degradation of textile wastewater. *Journal of Photochemistry and Photobiology A: Chemistry*, 329, 9-17.

- Stahelin, J., & Hoigne, J. (1985). Decomposition of ozone in water in the presence of organic solutes acting as promoters and inhibitors of radical chain reactions. *Environmental Science and Technology*; (United States), 19(12), 1206-1213.
- Steber, J., & Wierich, P. (1986). Properties of hydroxyethane diphosphonate affecting its environmental fate: degradability, sludge adsorption, mobility in soils, and bioconcentration. *Chemosphere*, 15(7), 929-945.
- Strens, R., & Wood, B. (1979). Diffuse reflectance spectra and optical properties of some iron and titanium oxides and oxyhydroxides. *Mineral Magazine*, 43(327), 347-354.
- Survey, U. S. G. (2015). *Mineral Commodity Summaries 2015*. Retrieved from <http://minerals.usgs.gov/minerals/pubs/mcs/2015/mcs2015.pdf>.
- Tan, B. H., Teng, T. T., & Omar, A. K. M. (2000). Removal of dyes and industrial dye wastes by magnesium chloride. *Water Research*, 34(2), 597-601.
- Tanaka, K.-I., & Ozaki, A. (1967). Acid-base properties and catalytic activity of solid surfaces. *Journal of Catalysis*, 8(1), 1-7.
- Tao, T., Chen, Q.-Y., Hu, H.-P., Yin, Z.-L., & Chen, Y. (2012). TiO₂ nanoparticles prepared by hydrochloric acid leaching of mechanically activated and carbothermic reduced ilmenite. *Transactions of Nonferrous Metals Society of China*, 22(5), 1232-1238.
- Tao, T., Chen, Y., Zhou, D., Zhang, H., Liu, S., Amal, R., Sharma, N., & Glushenkov, A. M. (2013). Expanding the applications of the ilmenite mineral to the preparation of nanostructures: TiO₂ nanorods and their photocatalytic properties in the degradation of oxalic acid. *Chemistry – A European Journal*, 19(3), 1091-1096.
- Tao, T., Glushenkov, A. M., Liu, H., Liu, Z., Dai, X. J., Chen, H., Ringer, S. P., & Chen, Y. (2011). Ilmenite FeTiO₃ nanoflowers and their pseudocapacitance. *The Journal of Physical Chemistry C*, 115(35), 17297-17302.
- Tehrani-Bagha, A. R., Mahmoodi, N. M., & Menger, F. M. (2010). Degradation of a persistent organic dye from colored textile wastewater by ozonation. *Desalination*, 260(1-3), 34-38.
- Thuy, N. M., Van, D. Q., & Hai, L. T. H. (2012). The visible light activity of the TiO₂ and TiO₂: V⁴⁺ photocatalyst. *Nanomaterials and Nanotechnology*, 2(Godište 2012), 2-14.

- Torres-Luna, J. A., Sanabria, N. R., & Carriazo, J. G. (2016). Powders of Iron(III)-doped titanium dioxide obtained by direct way from a natural ilmenite. *Powder Technology*, 302, 254-260.
- Turhan, K., Durukan, I., Ozturkcan, S. A., & Turgut, Z. (2012). Decolourisation of textile basic dye in aqueous solution by ozone. *Dyes and Pigments*, 92(3), 897-901.
- Tze, M. W., Aroua, M. K., & Szlachta, M. (2015). Palm shell-based activated carbon for removing Reactive Black 5 dye: equilibrium and kinetics studies. *BioResources*, 11(1), 1432-1447.
- Üstün, G. E., Solmaz, S. K. A., & Birgül, A. (2007). Regeneration of industrial district wastewater using a combination of Fenton process and ion exchange—a case study. *Resources, Conservation and Recycling*, 52(2), 425-440.
- Valcárcel, M. (2012). *Principles of analytical chemistry: a textbook*: Springer Science & Business Media.
- Valencia, S., Marín, J. M., & Restrepo, G. (2010). Study of the bandgap of synthesized titanium dioxide nanoparticles using the sol-gel method and a hydrothermal treatment. *Open Materials Science Journal*, 4(1), 9-14.
- Van der Heide, P. (2011). *X-ray photoelectron spectroscopy: an introduction to principles and practices*: John Wiley & Sons.
- Verma, A. K., Dash, R. R., & Bhunia, P. (2012). A review on chemical coagulation/flocculation technologies for removal of colour from textile wastewaters. *Journal of Environmental Management*, 93(1), 154-168.
- W Lai, C., W Low, F., W Chong, S., PP Wong, C., Siddick, B. M., Siti, Z., C Juan, J., & B Abdul Hamid, S. (2015). An overview: recent development of titanium dioxide loaded graphene nanocomposite film for solar application. *Current Organic Chemistry*, 19(19), 1882-1895.
- Wan, L., Gao, Y., Xia, X.-H., Deng, Q.-R., & Shao, G. (2011). Phase selection and visible light photo-catalytic activity of Fe-doped TiO₂ prepared by the hydrothermal method. *Materials Research Bulletin*, 46(3), 442-446.
- Wang, J. L., & Xu, L. J. (2012). Advanced oxidation processes for wastewater treatment: formation of hydroxyl radical and application. *Critical Reviews in Environmental Science and Technology*, 42(3), 251-325.

- Wang, Y., He, Y., Lai, Q., & Fan, M. (2014). Review of the progress in preparing nano TiO₂: an important environmental engineering material. *Journal of Environmental Sciences*, 26(11), 2139-2177.
- Wantala, K., Laokiat, L., Khemthong, P., Grisdanurak, N., & Fukaya, K. (2010). Calcination temperature effect on solvothermal Fe-TiO₂ and its performance under visible light irradiation. *Journal of the Taiwan Institute of Chemical Engineers*, 41(5), 612-616.
- Warren, B. (2012). *X-Ray Diffraction*: Courier Corporation.
- Wilson, N. C., Muscat, J., Mkhonto, D., Ngoepe, P. E., & Harrison, N. M. (2005). Structure and properties of ilmenite from first principles. *Physical Review B*, 71(7), 075202.
- Wold, A. (1993). Photocatalytic properties of titanium dioxide (TiO₂). *Chemistry of Materials*, 5(3), 280-283.
- WTO. (2016). World Trade Statistical Review 2016. Retrieved 5/4/2017, from World Trade Organisation
https://www.wto.org/english/res_e/statis_e/wts2016_e/wts16_toc_e.htm
- Yamashita, T., & Hayes, P. (2008). Analysis of XPS spectra of Fe²⁺ and Fe³⁺ ions in oxide materials. *Applied Surface Science*, 254(8), 2441-2449.
- Yan, J., Wu, G., Guan, N., Li, L., Li, Z., & Cao, X. (2013). Understanding the effect of surface/bulk defects on the photocatalytic activity of TiO₂: anatase versus rutile. *Physical Chemistry Chemical Physics*, 15(26), 10978-10988.
- Yan, J., Zhang, Y., Liu, S., Wu, G., Li, L., & Guan, N. (2015). Facile synthesis of an iron doped rutile TiO₂ photocatalyst for enhanced visible-light-driven water oxidation. *Journal of Materials Chemistry A*, 3(43), 21434-21438.
- Yang, L., Liya, E. Y., & Ray, M. B. (2008). Degradation of paracetamol in aqueous solutions by TiO₂ photocatalysis. *Water Research*, 42(13), 3480-3488.
- Yang, X., Cao, C., Erickson, L., Hohn, K., Maghirang, R., & Klabunde, K. (2009). Photocatalytic degradation of Rhodamine B on C-, S-, N-, and Fe-doped TiO₂ under visible-light irradiation. *Applied Catalysis B: Environmental*, 91(3-4), 657-662.

- Yigit, N. O., Uzal, N., Koseoglu, H., Harman, I., Yukseler, H., Yetis, U., Civelekoglu, G., & Kitis, M. (2009). Treatment of a denim producing textile industry wastewater using pilot-scale membrane bioreactor. *Desalination*, 240(1–3), 143-150.
- You, S.-J., Damodar, R. A., & Hou, S.-C. (2010). Degradation of Reactive Black 5 dye using anaerobic/aerobic membrane bioreactor (MBR) and photochemical membrane reactor. *Journal of Hazardous Materials*, 177(1–3), 1112-1118.
- Yu, H., Irie, H., Shimodaira, Y., Hosogi, Y., Kuroda, Y., Miyauchi, M., & Hashimoto, K. (2010). An efficient visible-light-sensitive Fe(III)-grafted TiO₂ photocatalyst. *The Journal of Physical Chemistry C*, 114(39), 16481-16487.
- Yu, J., Low, J., Xiao, W., Zhou, P., & Jaroniec, M. (2014). Enhanced photocatalytic CO₂-reduction activity of anatase TiO₂ by coexposed {001} and {101} facets. *Journal of the American Chemical Society*, 136(25), 8839-8842.
- Yu, J., Su, Y., Cheng, B., & Zhou, M. (2006). Effects of pH on the microstructures and photocatalytic activity of mesoporous nanocrystalline titania powders prepared via hydrothermal method. *Journal of Molecular Catalysis A: Chemical*, 258(1), 104-112.
- Yu, J., Xiang, Q., & Zhou, M. (2009). Preparation, characterisation and visible-light-driven photocatalytic activity of Fe-doped titania nanorods and first-principles study for electronic structures. *Applied Catalysis B: Environmental*, 90(3), 595-602.
- Yurtsever, A., Çınar, Ö., & Sahinkaya, E. (2016). Treatment of textile wastewater using sequential sulfate-reducing anaerobic and sulfide-oxidizing aerobic membrane bioreactors. *Journal of Membrane Science*, 511, 228-237.
- Yurtsever, A., Sahinkaya, E., Aktaş, Ö., Uçar, D., Çınar, Ö., & Wang, Z. (2015). Performances of anaerobic and aerobic membrane bioreactors for the treatment of synthetic textile wastewater. *Bioresource Technology*, 192, 564-573.
- Zaleska, A. (2008). Doped-TiO₂: a review. *Recent Patents on Engineering*, 2(3), 157-164.
- Zallen, R., & Moret, M. (2006). The optical absorption edge of brookite TiO₂. *Solid State Communications*, 137(3), 154-157.

- Zarazúa-Morín, M. E., Torres-Martínez, L. M., Moctezuma, E., Juárez-Ramírez, I., & Zermeño, B. B. (2016). Synthesis, characterisation, and catalytic activity of FeTiO₃/TiO₂ for photodegradation of organic pollutants with visible light. *Research on Chemical Intermediates*, 42(2), 1029-1043.
- Zhang, S., Li, L., & Kumar, A. (2008). *Materials characterisation techniques*: CRC Press.
- Zhang, W., Zhu, Z., & Cheng, C. Y. (2011). A literature review of titanium metallurgical processes. *Hydrometallurgy*, 108(3-4), 177-188.
- Zhao, W.-N., & Liu, Z.-P. (2014). Mechanism and active site of photocatalytic water splitting on titania in aqueous surroundings. *Chemical Science*, 5(6), 2256-2264.
- Zhou, F., Kotru, S., & Pandey, R. K. (2003). Nonlinear current-voltage characteristics of ilmenite-hematite ceramic. *Materials Letters*, 57(13-14), 2104-2109.
- Zhou, K., Hu, X.-Y., Chen, B.-Y., Hsueh, C.-C., Zhang, Q., Wang, J., Lin, Y.-J., & Chang, C.-T. (2016). Synthesized TiO₂/ZSM-5 composites used for the photocatalytic degradation of azo dye: intermediates, reaction pathway, mechanism and biotoxicity. *Applied Surface Science*, 383, 300-309.
- Zhou, M., Yu, J., Cheng, B., & Yu, H. (2005). Preparation and photocatalytic activity of Fe-doped mesoporous titanium dioxide nanocrystalline photocatalysts. *Materials Chemistry and Physics*, 93(1), 159-163.
- Zhu, J., Chen, F., Zhang, J., Chen, H., & Anpo, M. (2006). Fe³⁺-TiO₂ photocatalysts prepared by combining sol-gel method with hydrothermal treatment and their characterisation. *Journal of Photochemistry and Photobiology A: Chemistry*, 180(1), 196-204.
- Zielińska, B., Grzechulska, J., Grzmil, B., & Morawski, A. W. (2001). Photocatalytic degradation of Reactive Black 5: a comparison between TiO₂-Tytanpol A11 and TiO₂-Degussa P25 photocatalysts. *Applied Catalysis B: Environmental*, 35(1), L1-L7.

LIST OF PUBLICATIONS AND PAPERS PRESENTED

ISI-Cited Publications:

1. **Ru Bin Lee**, Joon Ching Juan, Chin Wei Lai, Kian Mun Lee (2017). Ilmenite: Properties and photodegradation kinetic on Reactive Black 5 dye. *Chinese Chemical Letters*, 28, 1613-1618
2. **Ru Bin Lee**, Joon Ching Juan, Chin Wei Lai (2017). Pre-treated Ilmenite: the relationship of iron and Ilmenite for photocatalyst degradation. (Submitted)

Conference Proceeding:

1. **Ru Bin Lee**, Chin Wei Lai, Hwe Voon Lee, Joon Ching Juan. Characterisation and Photodegradation Acitivity of Ilmenite. *2nd International Conference on the Science & Engineering of Materials*. 16th – 18th November 2015. Kuala Lumpur, Malaysia.